https://theses.gla.ac.uk/

Theses Digitisation:

https://www.gla.ac.uk/myglasgow/research/enlighten/theses/digitisation/

This is a digitised version of the original print thesis.

Copyright and moral rights for this work are retained by the author

A copy can be downloaded for personal non-commercial research or study, without prior permission or charge

This work cannot be reproduced or quoted extensively from without first obtaining permission in writing from the author

The content must not be changed in any way or sold commercially in any format or medium without the formal permission of the author

When referring to this work, full bibliographic details including the author, title, awarding institution and date of the thesis must be given

Enlighten: Theses
https://theses.gla.ac.uk/
research-enlighten@glasgow.ac.uk

THERMAL PROBLEMS IN SEMICONDUCTOR RING LASER

by

CHEN Wei, B.Sc

A thesis submitted to the faculty of Engineering

of the University of Glasgow

for the degree of Master of Science

May, 1989

© CHEN Wei 1989

ProQuest Number: 10999336

All rights reserved

INFORMATION TO ALL USERS
The quality of this reproduction is dependent upon the quality of the copy submitted.

In the unlikely event that the author did not send a complete manuscript
and there are missing pages, these will be noted. Also, if material had to be removed,
a note will indicate the deletion.

ProQuest 10999336

Published by ProQuest LLC (2018). Copyright of the Dissertation is held by the Author.

All rights reserved.
This work is protected against unauthorized copying under Title 17, United States Code
Microform Edition © ProQuest LLC.

ProQuest LLC.
789 East Eisenhower Parkway
P.O. Box 1346
Ann Arbor, MI 48106 – 1346

ACKNOWLEDGEMENT

I would like to thank Professor John Lamb for the provision of excellent research facilities in the Department of Electronics and Electrical Enginnering during this project.

I would like also to express my sincere thanks to my supervisor, Professor P.J.R.Laybourn, for his constant guidance and encouragement throughout this work and the non–trivial task of proof reading and correcting this thesis. This work would hardly have been possible without his help.

My special appreciation would be addressed to my friend and colleague, A.F.Jezierski, for his invaluable advice, patience and many enlightening and helpful discussions. I thank him sincerely.

Thanks are also due to all the technical staff who provided assistance throughout this work. In particilar, R.Hutchins, J.Young, D.Clifton, L.Hobbs, L.Bradley, D.Gourlay, H.Anderson, T.Cormack and G.Thornton. And special thanks go to G.Boyle for printing all photos in this thesis and helpful technical assistance.

I am greatly indebted to Dr.P.W.Webb of Depatment of Electronics and Electrical Engineering, University of Birmingham, for allowing me to use the infrared thermal imaging facility there and for his kind assistances and useful discussions during my experimental work there. I gratefully acknowledge theinvaluable help of Dr.A.Chan of Department of Civil Enginnering , University of Glasgow in computing modelling work.

I have enjoyed the support of all my friends, especially Su Yongjie, Ge Yanchoa, Fang Weigi, Huang Xu, D.K.Lau and A.P.Ansbro for their useful discussion in computing and certain particular subject.

Appreciation is expressed to Professor H.Y.Wong of Department of Aeronautics and Fluid Mechanics, University of Glasgow, and the Higher Education Bureau of Guanhdong Province, China, for the organization of this special trainning programme for two master degrees, and also to Mr.Li Jiacheng (Geoffrey Lee) and University of Shantou, China, for the financial support, which provide me an opportunity to study at the University of Glasgow.

Finally, I should thank my parents for their incessant support and encouragement to seek higher education and most of all my wife for her patience and understanding over the past years, without whose support and help, this work would not have been possible, either.

SUMMARY

Semiconductor ring lasers with a output waveguide have been produced and have attracted considerable attention in integrated optics. Owing to its extremely small size, the increase in temperature within the structure is expected to be higher. This thesis is concerned with the thermal effects of the ring laser and it consists of three parts: (1) theoretical numerical modelling: the temperature distribution within the ring laser structure has been simulated by using finite difference technique and its thermal resistance has also been calculated. The results obtained show that the temperature rise in the laser is more severe for small rings or narrow width ribs; (2) infrared imaging technique: thermal maps of the surface of the ring laser have been obtained by using a RM−20 infrared image scanner and have shown a good assessment of their thermal behaviour which can be used to compare qualitatively with the theoretical results; (3) improvement of the laser temperature control system and the investigation of its temperature sensing system have been successfuly achieved.

CONTENTS

ACKNOWLEDGEMENTS

SUMMARY

page

CHAPTER 1. INTRODUCTION

1.1. General introduction 1

1.2. Purpose of the project 3

1.3. Previous work on thermal problem of semiconductor laser 4

CHAPTER 2. THEORY OF SEMICONDUCTOR LASER DEVICE

2.1. Semiconductor injection laser operation

2.1.1. Introduction 5

2.1.2. Laser structure 6

2.1.3. Population inversion 6

2.1.4. Carrier and optical confinements 7

2.1.5. Temperature dependence of threshold current density 8

2.1.6. Temperature dependence of lasing wavelength 10

2.2. Semiconductor ring laser

2.2.1. Introduction 11

2.2.2. Bending loss in ring resonant waveguide 11

2.2.3. Optimum bend radius in ring resonant waveguide 12

CHAPTER 3. THEORY OF HEAT TRANSFER IN SOLIDS

3.1. Introduction 14

3.2. Heat conduction 14

3.3. Heat convection 15
3.4. Heat radiation 16
3.5. Heat distribution equation in solids 18

CHAPTER 4. NUMERICAL MODELING OF TEMPERATURE DISTRIBUTION IN SEMICONDUCTOR RING LASER

4.1. Introduction 22
4.2. Theory for finite difference 23
4.3. Theoretical model description 24
4.4. Program implementation
4.4.1. Solution by interation 27
4.4.2. Rate of convergence 28
4.5. Error in the numerical methods 29
4.6. Temperature distribution in ring laser substrate 30
4.7. Temperature distribution in lasing rib 32
4.8. Summary 33

CHAPTER 5. TEMPERATURE MEASUREMENT BY THERMAL IMAGING

5.1. Introduction 35
5.2. Principle of infrared thermal imaging 35
5.3. Experimental equipment 37
5.4. Description of the sample 38
5.5. Results and discussions 39
5.6. Summary 41

CHAPTER 6. SEMICONDUCTOR LASER TEMPERATURE CONTROL SYSTEM

6.1. Introduction 42
6.2. Temperature control system
6.2.1. Peltier effect and Peltier cooler 43
6.2.2. Laser temperature control system 43

6.3. Temperature dependence experiment
of semiconductor stripe laser
6.3.1. Temperature dependence of threshold current 44
6.3.2. Temperature dependence of emission wavelength 45
6.3. Summary 46

CHPATER 7. TEMPERATURE SENSING SYSTEM

7.1. Introduction 47
7.2. Investigation of Al-Au thermocouple 48
7.3. Fabrication of laser device with thermocouple pad 49
7.4. Temperature measurement system 53
7.5. Measurement and result discussion 54
7.6. Summary 55

CHAPTER 8. CONCLUSION 56

REFERENCE 59

CHAPTER 1

INTRODUCTION

1.1. General introduction

It is well known that the semiconductor laser emits a highly monochromatic and directional beam of light like ruby laser and heliumneon gas laser. Also, the semiconductor laser has its distinctive features. It is extremely small in size compared to other lasers and easily modulated at high frequencies simply by modulating the bias current. Because made of semicondutor material, there is the possibility of integration with other optical and electronic device. It is the most important source in optical– fibre communications.

A semiconductor laser was proposed by Basov et al [1] in 1961. He suggested that stimulated emission due to recombination of carriers injected across a p– n junction was possible. But it was not till 1962 that the laser was first demonstrated, in pulsed operation at low temperature[2,3,4,5]. These first injection lasers were generally chips of single material GaAs, called homostructure lasers, in the form of a parallelpiped, with a planar diffused p– n junction perpendicular to the two opposite cleaved ends of the crystal. They require a very high current through the p– n junction (approximately 35– 100kA/cm^2) at room temperature in order to reach the threshold for lasing. This is because the recombination region is too thick due to minority carrier diffusion. Besides, the optical field is in an inefficient waveguide of uncertain region and the efficiency with which injected electrons are utilized for lasing transition is low. In about 1968, Alferow et al [1] suggested that the injection

laser could be improved by the use of heterostructures, in which a thin layer of semiconductor (e.g.GaAs) is sandwiched between layers of a different semiconductor (e.g.$Al_xGa_{1-x}As$). On comparing GaAs with $Al_xGa_{1-x}As$, it was found that the band−gap energy of AlGaAs is greater than that of GaAs, and the refractive index is smaller. Such structures can provide carrier confinement in a thin active region due to the wider band−gap on the both sides of GaAs which provides a potential barrier to carriers. Besides, light can be confined in the GaAs active layer due to the optics waveguide formed by the high refractive index material (GaAs) cladded by low refractive index material (AlGaAs). As a result, the threshold of laser oscillation is appreciably reduced. The threshold current density for a GaAs−AlGaAs heterostructure laser is below 1 kA/cm^2 even at room temperature. This can result in continuous running of a semiconductor laser at room temperature.

Since then, GaAs−AlGaAs double heterostructure lasers have shown promise as convenient optical source. However, the optical Fabry−Perot resonator formed by cleaved facets is impractical for monolithic integration and optical coupling with other optical elements is not easy.

Monolithic integration of semiconductor optical devices requires the development of laser sources with feedback mechanisms other than cleaved cavities and with little influence of the output termination on the lasing action. The ring resonant waveguide structure to be used as laser cavities has been investigated by A.H.Liao and S.Wong, et.al [6], recently by A.Jezierski and P.J.R.Laybourn [7] (Fig.(1.1)). A variety of ring configurations between 10 and 100um in diameter have been successfully formed in GaAs−AlGaAs material, coupling to output stripe waveguide via a Y−junction. They have attracted considerable attention because high quality mirrors are not needed, the output termination has little influence on oscillation conditions and the small dimensions make the longitudinal mode spacing increase so that single−mode operation is possible. A rib waveguide configuration was used to

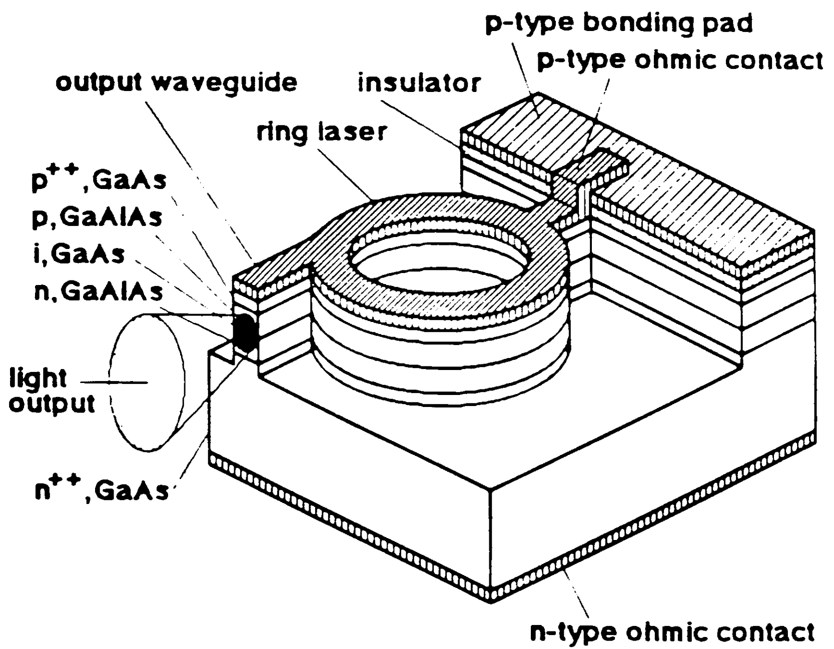

Fig.1.1 Semiconductor ring laser device [7].

maximise light confinement and minimise bending loss at small cavity circumferences [8,9]. Because of the simplicity of fabrication of the structure by planar processing, it can be more easily integrated with other optical elements in a monolithic optical circuit.

It is well known that the operating characteristics and life time of semiconductor lasers are strongly affected by the operating temperature. The supplied power mainly dissipates on the active layer and results in a temperature rise due to the nonradiative recombination process and absorption of generated light. The temperature increase may degrade the laser device performance:

(1) reduce its life time [10,11];

(2) increase threshold current [12,13,14];

(3) shift output wavelength [15,16];

(4) decrease the output power [17,18].

The temperature rises within the ring laser structures are expected to be larger, as the heat is more concentrated and difficult to dissipate due to their extremely small size. This extra thermal problem makes it difficult to obtain lasing under CW operation.

1.2. The purpose of the project

The purpose of the project is to characterize the temperature behaviour of the semiconductor ring laser. It is hoped that calculation and measurement of temperature profiles of various structures will be discussed with the aim of understanding their thermal characteristics and improving heat dissipation so that CW operation may be possible.

1.3. Previous work on thermal problem of semiconductor laser

The analysis of thermal problem in semiconductor laser devices has been demonstrated by many authors. The uniform generation of heat in a plane– stripe source embedded in a rectangular layered structure of GaAs– AlGaAs with contacts was analyzed by Joyce and Dixon [19]. They presented an analytical expression for the steady state heat distribution. The radiation transfer of energy of spontaneous radiation has been taken into account by Newman et al [20]. The relative influence of various heat sources including Joule heating has been investigated by Duda et al [21]. Better approximation of the distribution of heat sources, taking into account the current spreading effect, has been investigated by Buus [22]. The analysis of thermal resistance for a complex light source package has been carried out by Laff [23]. Both steady state heat distribution and dynamical thermal properties of various semiconductor laser structures have been investigated by Nakwaski [24,25]. The analysis and practical work on the heat removal from the laser device using a thermoelectric Peltier effect cooler were presented by Cortes and Laff [26,23]. The monolithically integrated laser and thermoelectric cooler were discussed in [27].

All work above was investigated by using analytical methods. This work is concerned with theoretical analysis, which uses numerial simulation technique, thermal measurement in both ring and stripe laser and improvement of the heat dissipation system and investigation of temperature sensing system.

CHAPTER 2

THEORY OF SEMICONDUCTOR LASER DEVICE

2.1. Semiconductor injection laser operation

2.1.1. Introduction

The laser (Light Amplication by Stimulated Emission of Radiation) is an oscillator similar to a radio transmitter. It consists of an amplifier of light waves through population inversion (Section 2.1.2) and stimulated emission with positive Feedback supplied by an optical resonator.

The possibility of lasing comes from the quantum mechanical principle, which states that when a photon interacts with an electron, it is equally probable that the photon will be absorbed and the electron become excited, or if the electron is already excited, the emission of a second photon will be stimulated with the electron "dropping" from its excited state to a lower–energy one. This second photon has the same wavelength (λ), phase, polarization and direction of propagation as the first. Thus the first photon can be amplified. Both absorption and light–stimulation processes are shown schematically in Fig.(2.1)

For lasing to occur, the number of electrons in the higher energy states must exceed the number of electrons in the lower energy states. This is called population inversion. Electrons are excited or "pumped" to higher energy states by special

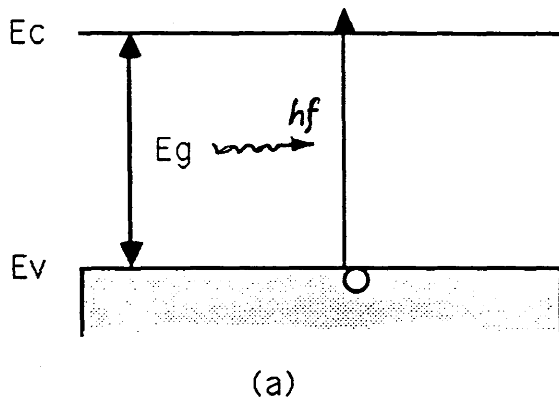

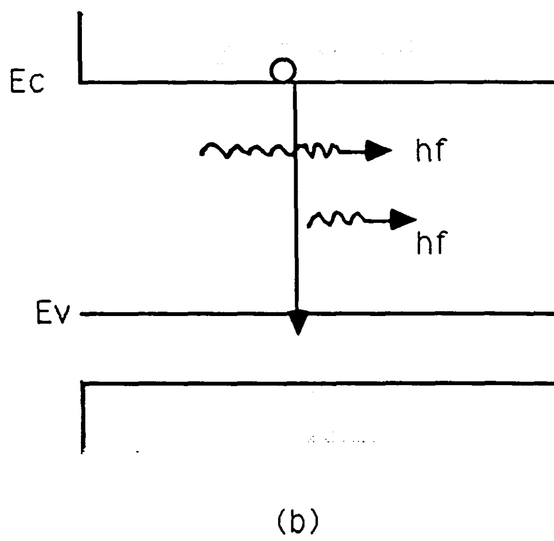

Fig.2.1 The two basic transition processes between two energy levels, (a)absorbtion; (b)stimulated emission.

means. Population inversion in semiconductor laser can be achieved near a p–n junction by the use of high doping densities and forward bias current.

2.1.2. Laser structure

Fig.(2.2) shows two laser structures. The first structure, Fig.(2.2a), is a basic p–n junction laser, called a homojunction laser as it has the same semiconductor material (e.g.GaAs) on both sides of the junction. A pair of parallel planes are cleaved perpendicularly to the <110> axis. Laser light will be emitted from these planes when it is biased appropriately. The two remaining sides of the diode are roughened to eliminate lasing in the directions other than the selected ones. This structure is called a Fabry–Perot cavity with a typical cavity length L of about 300um. The Fabry–Perot cavity configuation is extensively used for modern semiconductor lasers.

The second structure, Fig.(2.2b), is a double–heterostructure (DH) laser,in which a thin layer of semiconductor (e.g. GaAs) is sandwiched between layers of a different semiconductor (e.g. $Al_xGa_{1-x}As$). This laser can be fabricated using epitaxial crystal growth techniques. A DH laser requires much less current to operate than a homojunction laser with identical device geometry.

2.1.3. Population inversion

As disscussed above, population inversion is required in order to achieve stimulated emission for laser operation. Consider a p–n junction formed between degenerate semiconductors, that is, one in which the doping levels on both sides of the junction are high enough so that the Fermi–levels are below the valence band

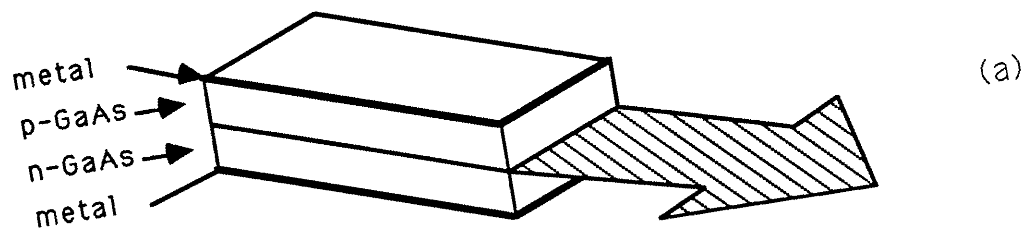

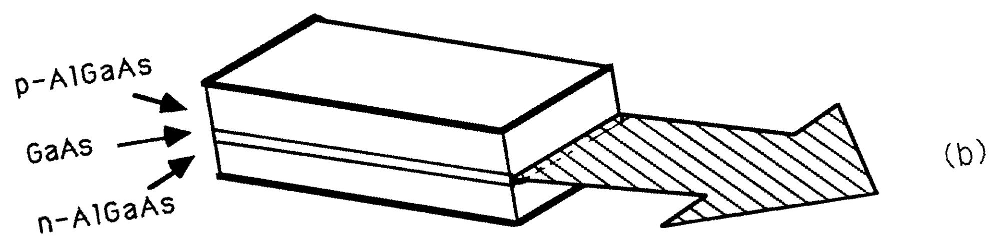

Fig.2.2 Semiconductor laser structure, a)homostructure;

b)double heterostructure laser.

edge on the p− side and above the conduction band edge on the n− side. Fig.(2.3) shows the band diagram of such a device at thermal equilibrium. When forward bias is applied to the diode (Fig.(2.3b)), electrons are injected from the n− side and holes are injected from the p− side into the junction. When a sufficiently large bias is applied (Fig.(2.3c)), high injection occurs,that is, large concentrations of electrons and holes are injected into the transition region. As a result, the region d contains a large concentration of electrons in the conduction band and a large concentration of holes in the valence band . This is the condition of population inversion.

The minimum energy required for band− to− band transition is the band gap energy E_g. Therefore, the condition necessary for population inversion can be written as (fig.(2.3c)): $(E_{fc} - E_{fv}) > E_g$.

2.1.4. Carrier and optical confinement

Schematic representations of the band diagram under a forward− bias condition, the refractive index profile and the optical− field distribution of light generated at the junction of a homojunction laser and a DH laser are shown in Fig(2.4a) and (2.4b) respectively. In the case of a DH laser, the carriers are confined on both sides of the active region by the heterojunction barriers. On the other hand, the carriers in the homojunction laser can move from the active region where radiative recombination occurs.

Since there is an abrupt reduction of the refractive index outside the active region, confinement of optical field within the active layer can be achieved. The optical confinement can be explained by Fig.(2.5), which shows a three− layer dielectric waveguide with refractive indices n_1, n_2 and n_3, where an active layer is sandwiched between two confining layers (Fig.(2.5a)). Under the condition

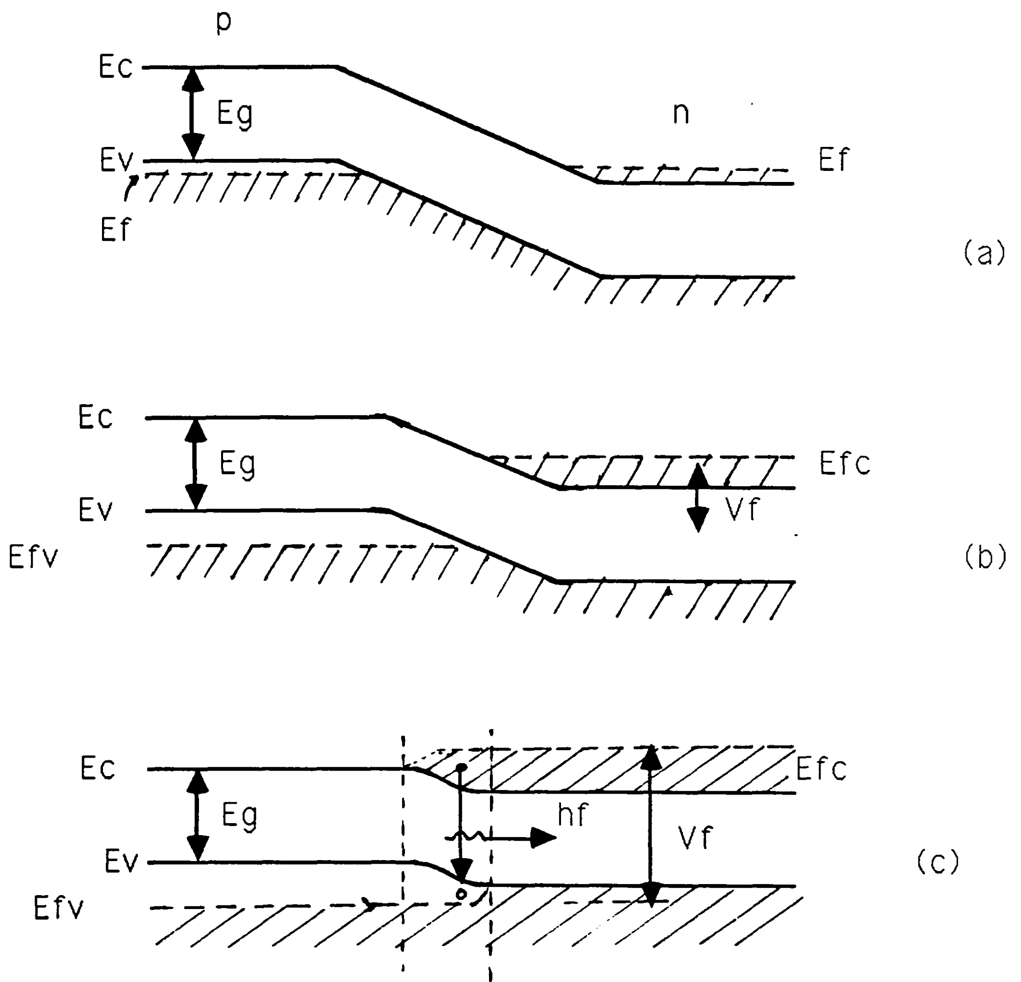

Fig.2.3 Energy band diagram of a degenerate p-n junction (a)at thermal equilibrium;(b)under forward bias; (c)under high-injection condition.

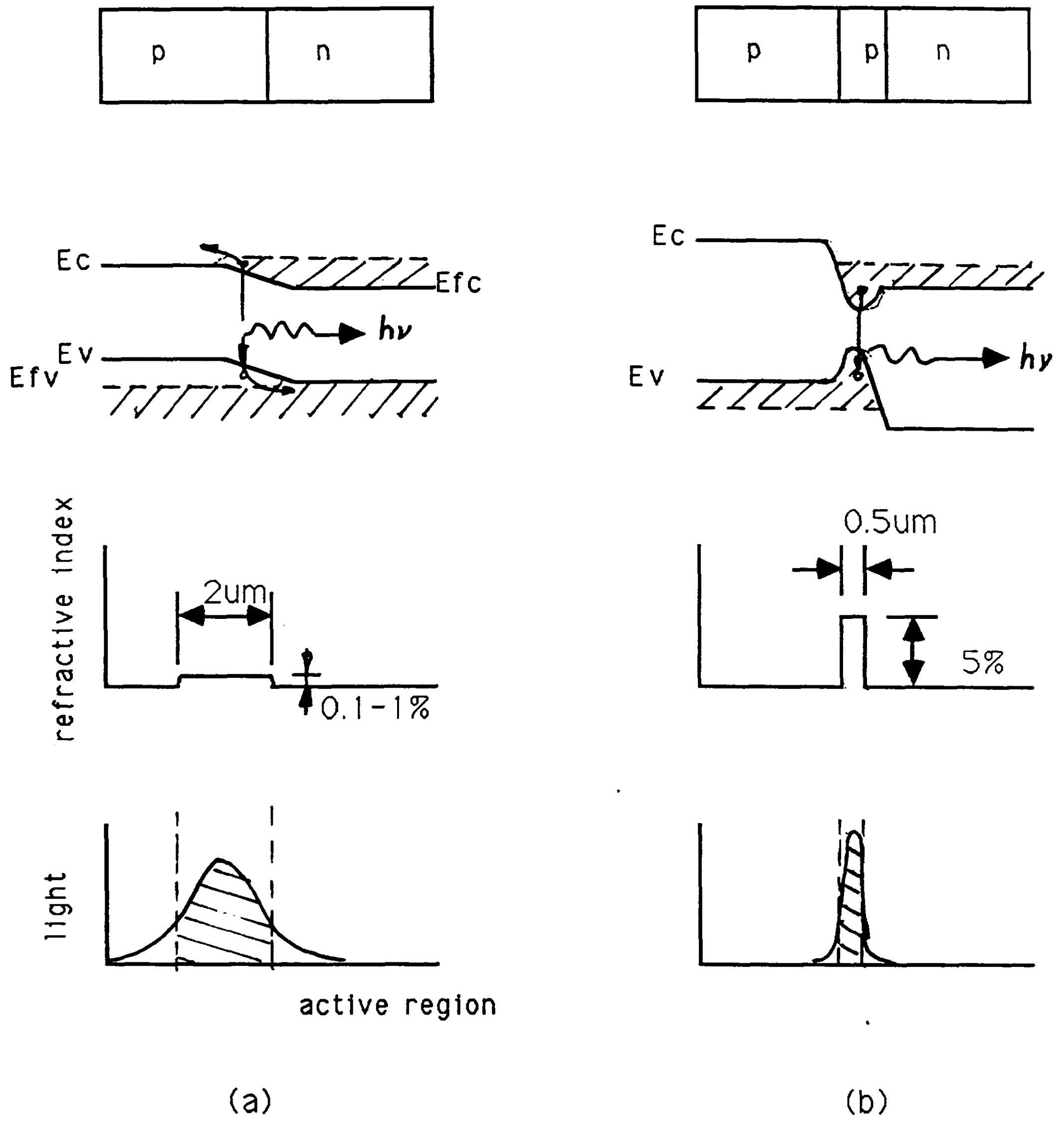

Fig.2.4 Comparision of some characteristics of (a) homojunction laser; (b) double heterostructure laser.

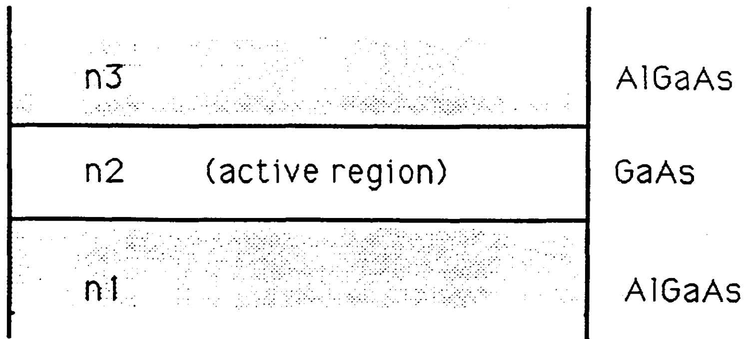

(a)

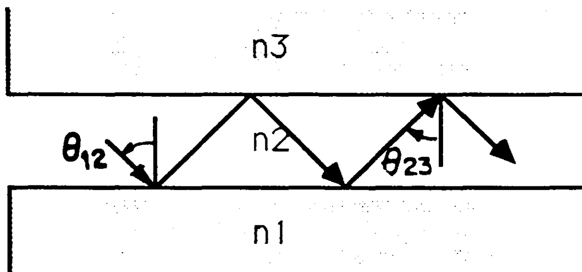

(b)

Fig.2.5 a) Representation of a three-layer dielectric waveguide;
b) ray trajectories of guided wave.

$n_2 > n_1 > n_3$, the ray angle θ_{12} at the layer1/layer2 interface in Fig.(2.5b) exceeds the critical angle given by

$$\sin\theta_C = n_1/n_2$$

A similar situation occurs for θ_{23} at the layer2/layer3 interface. Therefore, when the refractive index in the active layer is larger than the index of its surrounding layers, the propagation of the electromagnetics radiation is guided (confined) in a direction parallel to the layer interface. So, in the thin active region (d= 0.1− 0.5um) a very high concentration of electrons, holes and photons bulids up. Lasing action therefore starts at a much lower threshold current density than in a homojunction laser. Further reduction of current is achieved by using a narrow (20um) stripe contact (Fig.(2.6)) that concentrates the injected carriers under it. Reliable laser diodes that lase continuously at λ =0.85um with I_{th}=10− 20 mA can thus be built.

Because of its properties of small size, spatical coherence, monochromaticity and low threshold current density, high speed modulation, semiconductor DH injection laser have significant applications in many areas of basic research and technology, such as in optical fibre communication, high− resolution gas spectroscopy and atmospheric pollution monitoring.

2.1.4. Temperature dependence of threshold current density

Threshold current density mentioned above is the minimum current density required for lasing to occur. It is a function of temperature. Fig.(2.7) show the temperature dependence of the threshold current in both homostructure and heterostructure laser. It also illustrates that the threshold current density for a

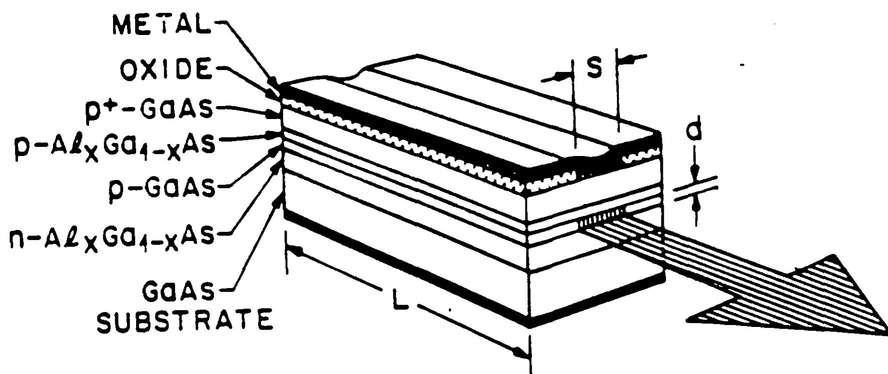

Fig.2.6 Semiconductor double heterostructure stripe laser.

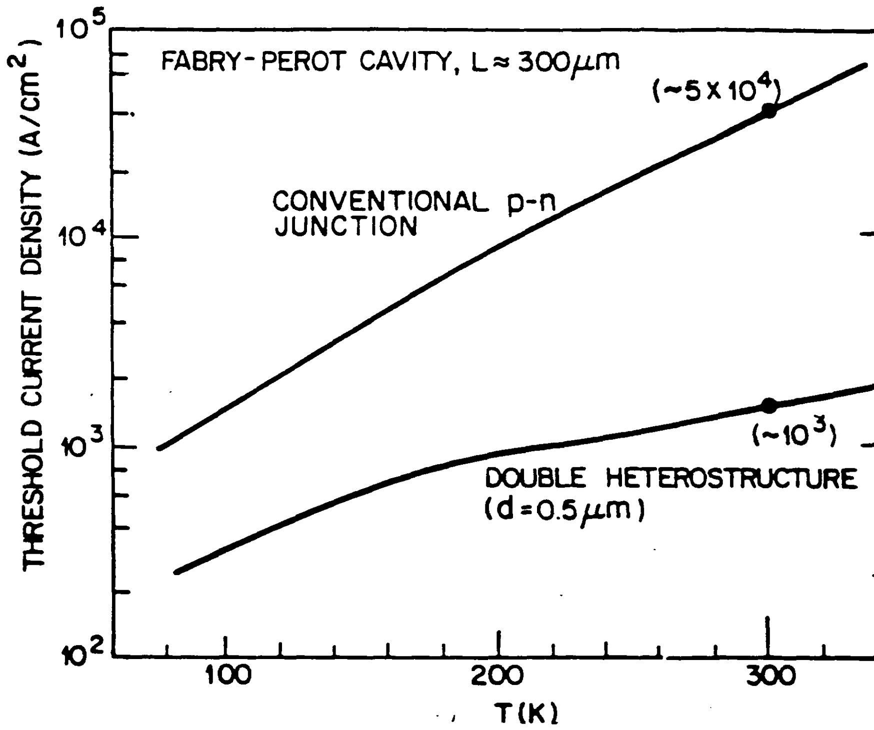

Fig.2.7 Temperature dependendce of threshold current density for the two laser structure [29].

homojunction increases much more quickly than that for the double heterostructure laser (DH laser), and hence CW operation at room temperature for a homojunction laser is impossible.

Threshold current density J_{th} for heterostructure laser can be described by the following equation (4−1)[28]:

$$J_{th}(A/cm^2) = \frac{J_0 d}{\eta} + J_0 \frac{d}{\beta\eta\Gamma} [\alpha + \frac{1}{L} Ln\frac{1}{R_1 R_2}] \qquad (2\text{-}1)$$

where J_0 is the current density for zero gain at room temperature; d is the thickness of the active layer; η is the quantum efficency, that is the number of carriers generated per photon; β is gain factor, which is the representation of the current dependence of gain coefficient; Γ is the confinement factor related to the optical confinement within the active layer; α is the loss per unit length of the cavity and $R_{1,}R_2$ are the reflectances of both ends of the cavity.

It is known that J_{th} is influenced by many factors; including the gain−current density relationship; the degree of carrier and optical confinement; internal absorption and scattering; the internal quantum efficiency and geometrical structure of the device [14].

The threshold current density is dependent on the factors α, η, g which are affected strongly by temperature. Although each of these parameters has a complex temperature variation, a simple approximate exponential relationship has been found [29,30] useful for the DH laser over a moderate temperature range,

$$J_{th} \propto \exp [\frac{T}{T_0}] \qquad (2\text{-}2)$$

here T is temperature, T_0 is an adjustable parameter to fit the measured result. J_{th} increases exponently with temperature. Therefore temperature rise results in J_{th} increasing abruptly which may lead to induced heat dissipation that will destroy the laser device.

2.1.5. Temperature dependence of lasing wavelength

The semiconductor laser emits quasi– monochromatic light. The emission wavelength depends mostly on the energy band gap of the material. The energy band gap E_g is a function of temperature, given by [31] for GaAs:

$$E_g(T) = 1.519 - \frac{(5.405 \times 10^{-4})\ T^2}{207 + T} \qquad (2\text{-}3)$$

The equation for the relevant emission wavelength can be found from Eq.(6.1):

$$\lambda_g(T) = \frac{hc}{E_g(T)} = \frac{1240.6}{E_g(ev)} \ (\mathrm{nm}) \qquad (2\text{-}4)$$

From Eq.(2– 3) and (2– 4), we can draw graphs of the temperature behaviou of E_g and λ_g, shown in Fig.(2.8) and Fig.(2.9). The band gap is getting smaller when temperature rises so that the emission wavelength will shift to longer wavelength.

A typical emission wavelength shift is within the range 0.24 0.30 nm/^{0}C for pure GaAs material at 30 ^{0}C [32].

Fig.2.8 Tepmerature dependence of GaAs energy gap

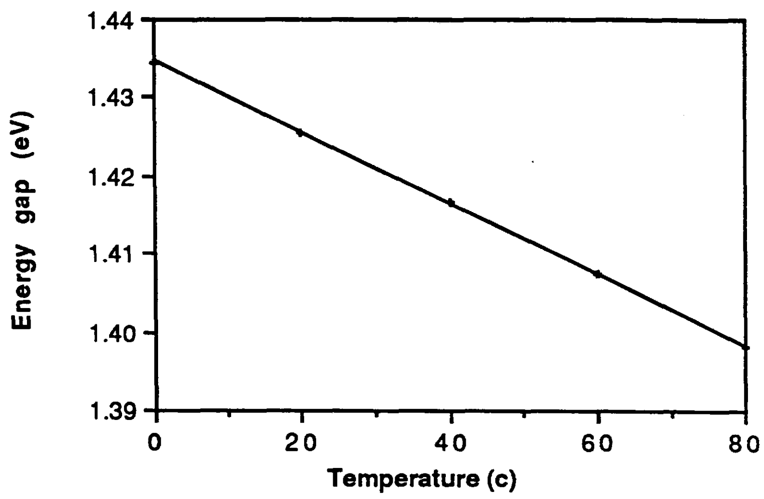

Fig.2.9 Temperature dependence of emit wavelength

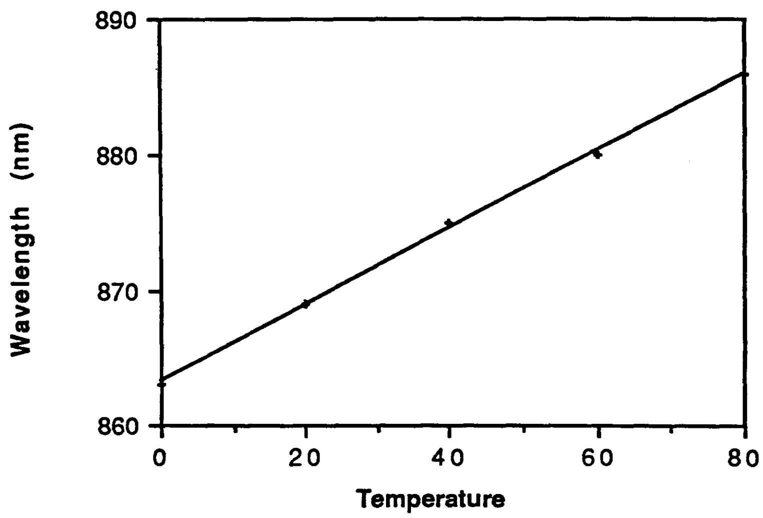

2.2. Semiconductor ring laser

2.2.1. Introduction

Integrated semiconductor ring laser in heterostructure on AlGaAs–GaAs materal are being produced in Glasgow. Considerable attention has been paid to it, because of its simple fabrication process, particular in integrated form and its ring resonant waveguide structure, which is capable of being coupled to other optical devices directly, and its small size (radius) which makes the output mode spacing in longitudinal direction increase so that single–mode operation is possible. However the small ring size can cause more bending loss (discussing in section 2.2.2) and reduce heat dissipation(section 5.5). It seems that there is some conflict between them. therefore, a compromise must be sought and a optimum radius must be determined. In this section, the bending loss and optimum radius will be discussed qualitatively.

2.2.2. Bending loss in ring resonant waveguide

The light wave energy loss when it propagates along a waveguide is generally exhibited by three different mechanisms:

1) scattering loss due to material bulk and surface defects;

2) absorption loss by band edge and free carriers;

3) radiation loss Γ_r, especially when light wave travels along a waveguide bend , due to distortions of the optical field.

The scattering and absorption loss, Γ_{sa}, are approximatly proportional to the distance of light wave propagation. The bending loss will be considered as follows.

Consider the dielectric waveguide with a curved section of radius R, shown in Fig.(2.10) . The wave travelling in direction z is along an axis of the waveguide and

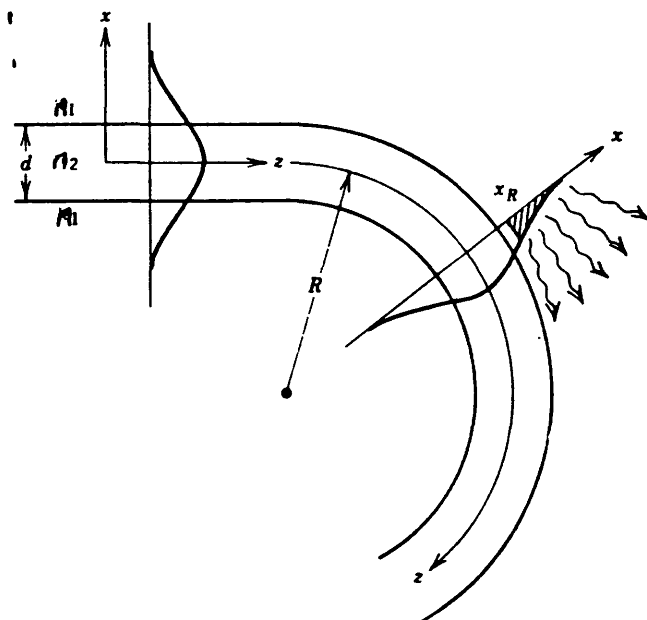

Fig.2.10 Dielectric waveguide with a curved section of radiu R.

E_{en} is the evanescent wave field outside.

The bending radiation loss has been found to be [33,34],

$$\Gamma_r(R) = K \exp[-2\zeta R(\frac{n_e}{n_s} -1)] \qquad (2\text{-}5)$$

where K is an arbitrary constant, ζ is the decay constant of evanescent field, which can be assumed to be independent of the radius R over the range of R of interest; n_e, n_s are the refractive indices in waveguide and surrounding medium respectively. It is important to note that the radiation loss increases exponentially with decreasing bending radius, particularly when the difference of refractive index between the waveguide and the surrounding medium is very small. The smaller the radius, the higher the bending loss. In fact, the minimum allowable curvative radius of a waveguide is generally limited by radiation losses and not by fabrication technigue. Therefore, the radius normally can not be too small. The minimum radius of curvature allowable for radiation loss smaller than 0.1dB/cm has been calculated by Goell[35].

2.2.3. Optimum bend radius in ring resonant waveguide

As discussed above, increasing the ring radius would increase gain, reduce bending loss and improve heat dissipation. On the other hand, a small radius can decrease the internal absorption and scattering loss. There must be a optimum radius.

Our ring laser, shown in Fig.(2.11), is a resonant ring with a Y junction coupling to an output waveguide. The total losses are given by:

$$\Gamma = \Gamma_y + \Gamma_{sa} + \Gamma_r \qquad (2\text{-}6)$$

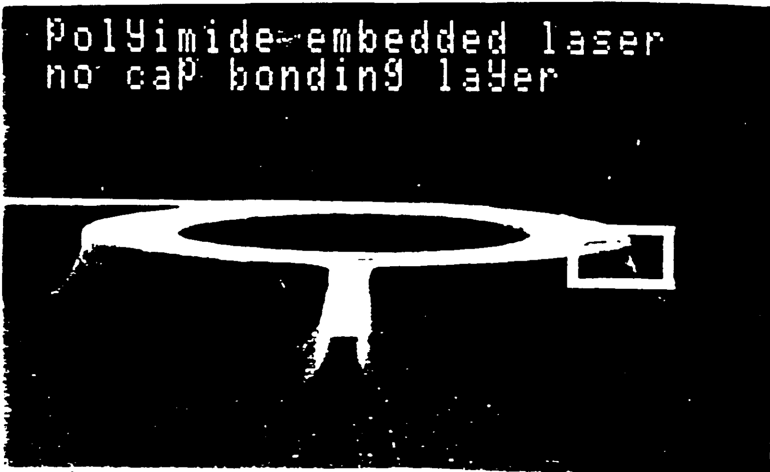

Fig.2.11 Semiconductor ring laser device.

Γ_y is Y junction coupling loss which is about 3dB per circuit for symmetrical Y junction and single mode operation [7].

Γ_{sa} is scattering and absorption loss, $\Gamma_{sa} = \alpha 2\pi R$. α is scattering and absorption loss constant.

Γ_r is bending loss, given by Eq.(2-5).

Therefore,

$$\Gamma \propto \alpha 2\pi R + K \exp[\ -2\zeta R(\frac{n_e}{n_s} -1)] \qquad (2\text{-}7)$$

To optimize the radius , we differentiate Eq.(2-5) with respect to R and set $\partial T/\partial R$ to zero, giveing the optimum value of R_0, (when $R=R_0$, the loss is minimised)

$$R_0 = \frac{1}{2\zeta[(n_e/n_s)-1]} \ln\frac{K\zeta[(n_e/n_s)-1]}{2\pi\alpha} \qquad (2\text{-}8)$$

The bending loss and the optimum radius are discussed only qualitatively here. According to the threshold condition, gain (G) must be sufficient to cancel out the total loss. So choosing the optimum radius, the lower threshold gain can be obtained.

CHAPTER 3

THEORY OF HEAT TRANSFER IN SOLIDS

3.1. Introduction

Heat transfers from the hotter parts of a body to the cooler whenever there is a temperature difference within the body. There are three distinct modes of heat transfer: (1) conduction, in which heat passes through the substance of the body itself; (2) convection, in which heat is transferred by relative motion of portions of the heated body; (3) radiation, in which heat is transferred directly between distant portion of the body by electromagnetic radiation. These three modes will be discussed respectively in the first three section and the temperature distribution equation will be derived in the final section.

3.2. Heat conduction

Heat conduction is an internal energy exchange from one body to another, or from one part of a body to another part by the exchange of the kinetic energy of motion of the molecules by direct communication. This flow of energy passes from high energy molecules to the lower energy ones (i.e., from a high–temperature region to a low–temperature region). The distinguishing feature of conduction is that it takes place within the boundaries of a body, or across the boundary of a body to another body placed in contact with the first, without an appreciable displacement of the matter comprising the body.

Suppose that a temperature gradient $\partial T/\partial X$ exists in a body (Fig.(3.1)). Consider a plate in the body having a surface area A and a very small thickness ΔX. The one side is at a high uniform temperature T_1, and the other side at lower temperature T_2. Let q denote the rate of heat flow through the plate. Experiment has shown that there is an energy transfer from the high– temperature side to the low temperature side and the rate of heat flow per unit area is proportional to the normal temperature gradient,

$$\frac{q}{A} \propto \frac{\partial T}{\partial X}$$

If we define the proportionality constant as K, then the rate of heat energy transfer could be given by,

$$q = -KA\frac{\partial T}{\partial X} \qquad (3\text{-}1)$$

3.2. Heat convection

Heat convection is the process by which heat transfer takes place between a solid surface and the fluid surrounding it. Considering the heated plate shown in Fig.(3.2), the temperature of the plate is T_s and the temperature of the fluid is T_∞ .The velocity of the flow will be reduced to zero at the plate as a result of viscous action. The temperation gradient at the wall is dependent on the rate at which the fluid carries the heat away. A high velocity produces a large temperature gradient and takes more heat away. Newton's law of cooling can be used to describe the heat transfer **q** by convection between the fluid and the boundary surface [36]:

$$q = hA(T_s - T_\infty) \qquad (3\text{–}2)$$

where A is the surface area considered and the quantity h is called the

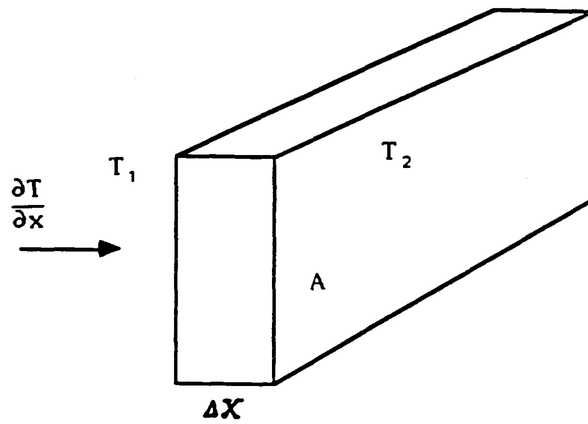

Fig.3.1 Elemental volume for heat conduction analysis.

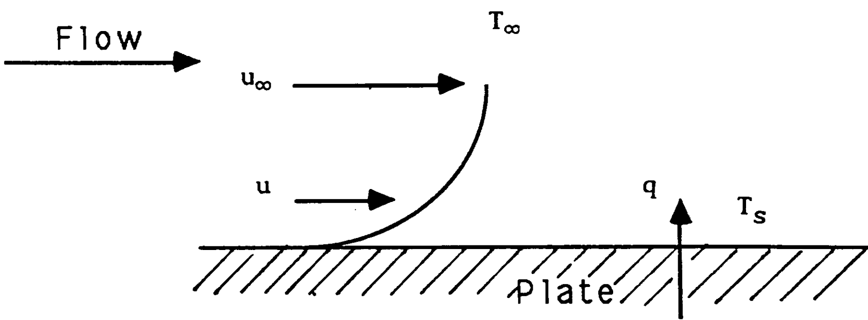

Fig.3.2 Diagram of heat convection.

convection coefficient.

Considering Eq.(3-1) and Eq.(3-2), the heat conducted to the surface can be assumed to be equal to the heat leaving the surface by convection. Therefore, the equation, which is usually considered as the boundary condition of a solid is given by

$$K \left.\frac{\partial T}{\partial X}\right|_{s} = h(T_s - T_\infty) \qquad (3\text{-}3)$$

The convection coefficient, h, is a very complicated function of the fluid flow, the temperature of surface of the solid and the geometrical arrangement of the system. For complex situations, it must be determined experimentally.

For a horizontal solid surface with the cooled side down, the h is given by [37,38]:

$$h = 0.27\left(\frac{\Delta T}{X}\right)^{1/4} \qquad (3\text{-}4)$$

where X is the length of the sample and $\Delta T = T_s - T_\infty$. An approximate range for average surface temperature (30 °C− 70 °C) and dimension 400um is from 1.07 to 1.60W/cm^2 °C.

3.3. Heat radiation

In the case of heat conduction, heat transfer through a material medium is involved. But when two bodies at different temperature are separated by a perfect vacuum, heat transfer between them by conduction and convection is not possible. Heat transfer can take place only by thermal radiation. That is, the radiative energy

emitted by a body because of its temperature is transmitted in the space in the form of electromagnetic waves.

Radiative energy emitted by a body is proportional to the fourth power of its absolute temperature[39]. Consider an ideal radiator, or 'black body', of surface area A, at temperature T. When two such bodies exchange heat by radiation, the net heat exchange is proportional to the difference in T^4, thus

$$q = \sigma A(T_1^4 - T_2^4) \qquad (3-5)$$

where σ is called the Stefan-Boltzman constant with the typical value of $5.6697*10^{-12} W/cm^2 {}^{o}C$.

If the two bodies are not perfectly black, then the equation(3-5) may be modified as

$$q = FA\sigma(T_1^4 - T_2^4) \qquad (3-6)$$

where the factor F is a quantity which is less than unity and accounts for the effects of geometrical arrangement of the surfaces and for bodies not being perfect emitter and absorber.

In general heat transfers within the solid only by conduction. Convection is altogether absent and radiation usually negligible. In the case of the heat transfer across the surface of a solid, the heat conducted through the surface can be considered to be removed from surface by a combination of convection and radiation. An energy balance would be given:

$$KA\frac{\partial T}{\partial X}\bigg|_S = hA(T_S - T_\infty) + FA\sigma(T_S^4 - T_a^4) \qquad (3-7)$$

where T_s, T_a and T_∞ are temperature of surface, surrounding and fluid,respectively.

Eq.(3−3) is usually used as a boundary condition in solid state since the constant σ is [illegible] so small that radiation can be neglected

3.4. Heat distribution equation in the solid

As discussed above, the heat transfer in a solid is dominated by conduction. Now we must find out a basic equation which can describe the heat distribution resulted from conduction in the solid.

Consider the one−dimensional system shown in Fig.(3.3), where the temperature may be changing with time and heat sources may be present within the system. For the element of thickness dx, the following energy balance may be made:

$$\left|\begin{array}{c}\text{energy conducted}\\ \text{in left face}\end{array}\right| + \left|\begin{array}{c}\text{heat generated}\\ \text{within element}\end{array}\right|$$

$$= \left|\begin{array}{c}\text{change in internal}\\ \text{energy}\end{array}\right| + \left|\begin{array}{c}\text{energy conducted}\\ \text{out of right face}\end{array}\right|$$

These energy quantities per unit time are given:

Energy in left face $q_x = -KA \frac{\partial T}{\partial x}$

Energy generated within element $= q^{*}A\ dx$

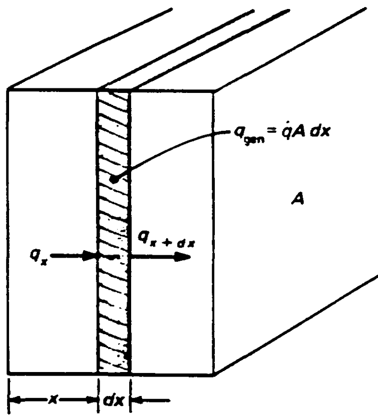

Fig.3.3 Diagram of one-dimensional heat conduction analysis.

Change in internal energy $= \rho CA \frac{\partial T}{\partial x} dx$

Energy out right face $q_{x+dx} = q_x + \frac{\partial q_x}{\partial x} dx$

$$= -A[K\frac{\partial T}{\partial x} + \frac{\partial}{\partial x}(K\frac{\partial T}{\partial x})dx]$$

where q^* is energy generated per unit time per unit volume;

c is spcific heat of material;

ρ is density of material;

t is time.

Combining the formula above,

$$-KA\frac{\partial T}{\partial x} + q^*Adx = \rho cA\frac{\partial T}{\partial t}dx - A[K\frac{\partial T}{\partial x} + \frac{\partial}{\partial x}(K\frac{\partial T}{\partial x})dx]$$

or $$\frac{\partial}{\partial x}(K\frac{\partial T}{\partial x}) + q^* = \rho c\frac{\partial T}{\partial t}$$

This is the one dimensional— heat conduction equation. To treat three dimensional heat flow, we need to consider only the heat conducted in and out of a unit volume in all three coordinate directions, as shown in Fig.(4.4).

The energy balance equation yields

$$q_x + q_y + q_z + q_{gen} = q_{x+dx} + q_{y+dy} + q_{z+dz} + \frac{\partial E}{\partial t}$$

and the energy quantities per unit time are given by

$$q_x = -Kdydz\frac{\partial T}{\partial x}$$

$$q_{x+dx} = -[K\frac{\partial T}{\partial x} + \frac{\partial}{\partial x}(K\frac{\partial T}{\partial x})dX]dydz$$

$$q_y = -K dx dz \frac{\partial T}{\partial y}$$

$$q_{y+dy} = -[\ K\frac{\partial T}{\partial y} + \frac{\partial}{\partial y}(K\frac{\partial T}{\partial y}) dy\ ] dx dz$$

$$q_z = -K dx dy \frac{\partial T}{\partial z}$$

$$q_{z+dz} = -[\ K\frac{\partial T}{\partial z} + \frac{\partial}{\partial z}(K\frac{\partial T}{\partial z}) dz\ ] dx dy$$

$$q_{gen} = q^* dx dy dz$$

$$\frac{\partial E}{\partial t} = \rho c dx dy dz \frac{\partial T}{\partial t}$$

Therefore, the heat conduction equation is

$$\frac{\partial}{\partial x}(K\frac{\partial T}{\partial x}) + \frac{\partial}{\partial y}(K\frac{\partial T}{\partial y}) + \frac{\partial}{\partial z}(K\frac{\partial T}{\partial z}) + q^* = \rho c\frac{\partial T}{\partial t} \qquad (3\text{-}8)$$

For steady state, where there is no time dependence and homogeneous material, Eq.(3−8) may be simplified as:

$$K\frac{\partial^2 T}{\partial x^2} + K\frac{\partial^2 T}{\partial y^2} + K\frac{\partial^2 T}{\partial z^2} + q^* = 0 \qquad (3\text{–}9)$$

For simplicity, two dimensions only are considered, thus Eq.(3.9) can be replaced by:

$$K\frac{\partial^2 T}{\partial x^2} + K\frac{\partial^2 T}{\partial y^2} + q^* = 0 \qquad (3\text{-}10)$$

For some circularly symetrical bodies whose temperature distribution is indenpendent of azimuth, the Eq.(3.10) can be obtained in cylindrical coordinates, r(radius), z(axis):

$$\frac{\partial^2 T}{\partial r^2} + \frac{1}{r}\frac{\partial T}{\partial r} + \frac{\partial^2 T}{\partial z^2} + \frac{q^*}{K} = 0 \qquad (3\text{-}11)$$

Heat distribution can be obtained in steady state within the solid by solving the equation above with certain boundary conditions.

The Eq.(3−11) will be used in ring laser model which is symetrical along the azimuthal direction to get a temperature distribution within the structure of the laser.

CHAPTER 4

NUMERICAL MODELLING OF TEMPERATURE DISTRIBUTION IN RING LASERS

4.1. Introduction

In order to understand thermal behaviour of the ring laser with the aim of improving its heat dissipation system, it is essential to predict temperature distribution within the laser structure. Analytical solutions of the mathematical expressions are possible for very simple cases only. Thermal problems are usually complex and it may be difficult to find their analytical solutions. The numerical method is used extensively in practical applications to determine the temperature distribution and heat flow in solids having complicated geometries and boundary conditions. A commonly used method is based on the representation of the derivatives in the heat distribution equation by a finite difference approximation. Therefore, the partial equation (e.g. Eg.3.9) is approximated by a set of algebraic equations for temperature at a number of nodal points over the region concerned. A brief discussion about the finite difference method will be given in section 2 and a theoretical model of the ring laser substrate in which the effect of lasing rib is not taken into account will be described in section 3. In section 4, some numerical theories about iteration, and rate of convergence is are presented. Errors in this method will be discussed in section 5. Furthermore, the numerical modelling results of laser substrate will be presented in section 6. In section 7, as an extension to the

model above, lasing rib will be specially considered and both results will be combined and discussed. There will be summary in final section.

4.2. Theory for the finite difference method

Consider a two-dimensional body, which is to be divided into equal increment in both the x and y direction, as shown in Fig.(4.1). The $\Delta x, \Delta y$ is mesh size. The symbols i,j are used to indicate the location of a nodal point whose coordinates are $x = i\Delta x$, $y = j\Delta y$. In the numerical method, all differentials are represented by a finite-difference approximation between the nodal points and the continuous partial differential equation is replaced by a set of algebraic equations satisfied only at the points. Therefore, the smaller mesh size can result in better approximation.

$T_{i,j}$ is assumed to be the temperature at node (i,j), as shown in Fig.(4.1). $T_{i+1,j}$, $T_{i-1,j}$, $T_{i,j+1}$, $T_{i,j-1}$ are the temperatures at node (i+1,j), (i-1,j), (i,j+1), (i,j-1), respectively. The temperature differentials can be approximated as [40]:

$$\frac{\partial T}{\partial x} = \frac{1}{\Delta x}(T_{i+1,j} - T_{i,j}), \qquad \frac{\partial T}{\partial y} = \frac{1}{\Delta y}(T_{i,j+1} - T_{i,j}),$$

$$\frac{\partial^2 T}{\partial x^2} = \frac{1}{(\Delta x)^2}(T_{i+1,j} - 2T_{i,j} + T_{i-1,j}), \tag{4-1}$$

$$\frac{\partial^2 T}{\partial y^2} = \frac{1}{(\Delta y)^2}(T_{i,j+1} - 2T_{i,j} + T_{i,j-1}),$$

In cylindrical coordinate, the temperature differentials can also be substituted

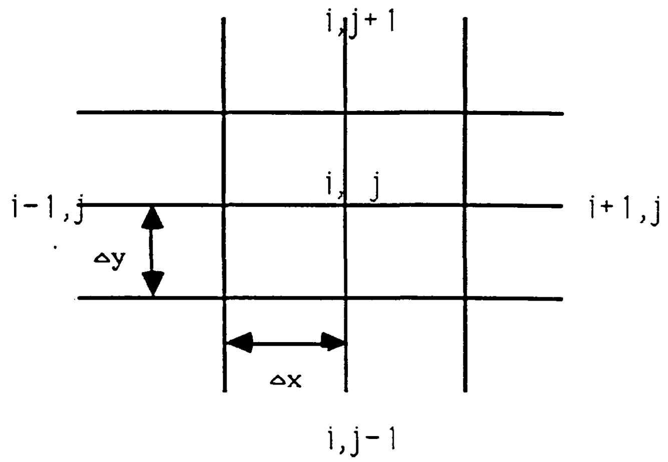

Fig.4.1 Sketch illustrating mesh used in two dimensional numerical analysis.

by the finite differences, as in Eq.(4-1).

For square mesh, $\Delta x = \Delta y = L$, the heat distribution equation Eq(3-10) can be replaced by finite difference form and temperature at nodal point (i,j) is given:

$$T_{i,j} = \frac{1}{4}\left(T_{i+1,j} + T_{i-1,j} + T_{i,j+1} + T_{i,j-1} + \frac{q^{*}L^{2}}{K}\right) \qquad (4\text{-}2)$$

Similarly, in cylindrical coordinate, the Eq(3-11) can be substituted by:

$$T_{i,j} = \frac{1}{4}\left[T_{i,j-1}+T_{i,j+1}+\left(1-\frac{1}{2i}\right)T_{i-1,j}+\left(1+\frac{1}{2i}\right)T_{i+1,j}+\frac{q^{*}_{i,j}L^{2}}{K}\right] \qquad (4\text{-}3)$$

4.3. Theoretical model description

The ring laser chip is placed on the top of a heatsink surrounded with air. The cross section in cylindrical coordinates is shown in Fig(4.2). Consideration of only two dimensions is sufficient, the horizontal and vertical directions corresponding to radius (r) and height (z), respectively, due to symmetry along the azimuthal direction (θ).

There are five assumptions in this model for simplicity:

(1) Only the junction of the laser is assumed to act as a heat source and is near the top of the laser substrate, as the height of the lasing rib ring (6.4um) can be negligible compared to the thickness of laser chip (100um). The influence of the lasing rib will not be considered here. It will be specially discussed in section 4.7.

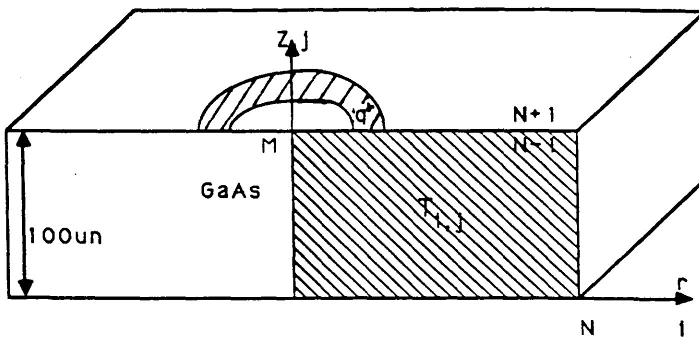

Fig.4.2 The cross section of ring laser chip in cylindrical coordinate

(2) The heat transfer across chip surfaces by conduction through air is neglected because the thermal conductivity of the laser chip material, 0.40W/cm ^{0}c, is much bigger than the thermal conductivity of air, $0.26*10^{-3}$W/cm ^{0}c.

According to Eq(4−1), the boundary condition along z axis is given by:

$$\left.\frac{\partial T}{\partial z}\right|_{s} = 0 \qquad (4\text{-}4)$$

Its finite difference form is:

$$\frac{T_{n+1} - T_{n-1}}{2\Delta z} = 0$$

So,

$$T_{n+1} = T_{n-1} \qquad (4-5)$$

T_n is the temperature on the top surface, T_{n+1} and T_{n-1} are shown in Fig(4.2). The same boundary equation can be obtained on the side surface.

(3) The flow of heat by convection from the top and side surface need not be considered:

Eq.(3−3) describing heat convection can be written in finite difference form as:

$$\frac{T_{n+1} - T_{n-1}}{2\Delta z} = \frac{h}{K}(T_n - T_\infty) \qquad (4\text{-}6)$$

T_∞ is temperature of fluid which is thought as room temperature, e.g.20 ^{0}C,

here. Δr is mesh size which is equal to 2um in the model.

If the surface temperature T_n is 70 ^{0}C and device dimension is 400um, maximum convection coefficient h has been given as 1.60W/cm^2 ^{0}C. Putting all values into Eq.(4−6), we can see that the effect of convection can be neglected, because:

$$T_{n+1} - T_{n-1} \simeq 0.08\ ^0C$$

so
$$T_{n+1} \simeq T_{n-1} \qquad (4-7)$$

(4) Heat loss due to radiation is also negligible.

The radiation power is given by Eq(3−5). If parameters are the same as above, the maximum loss by radiation is about 0.027mW. It is much smaller than total heat power dissipation, which is about 200mW if the supply current is 100mA.

(5) The temperature on the bottom of the chip is forced by a heatsink down to an adjustable temperature, e.g.20 ^{0}C.

From the discussion above, the boundary conditions are given by:

$$\begin{aligned} &\text{AB boundary} && T = 20\ ^0C \\ &\text{BC,CD,DA boundaries} && T_{n+1} = T_{n-1} \end{aligned} \qquad (4-8)$$

Heat distribution can be solved by iteration method using these boundary equations.

4.4. Programme implementation

4.4.1. Solution by iteration

Iteration is one of the important methods in finding solutions of equations in numerical analysis. It starts with an initial guess value and by repeating a number of steps over and over tries to improve the initial guess value until the correct answer is obtained[41].

Assume that x_0 is a root of the equation concerned, x_i is a guess and an arbitrary number ε is as small as wished. To converge x_i to the root x_0, x_i must eventually approach so close to x_0 that the difference $|x_i - x_0|$ is less than arbitrary ε. Supposing M iterations are needed before this requirement is satisfied, the following equation can be written [42]:

$$|x_i - x_0| < \varepsilon \qquad \text{for all } i \geqslant M \qquad (4-9)$$

Eq(4−9) can be replaced by:

$$\lim_{i \to \infty} |x_i - x_0| = 0 \qquad (4\text{-}10)$$

Similarly, x_{i+1} is satisfied by Eq.(4−9), hence

$$\lim_{i \to \infty} |x_{i+1} - x_0| = 0 \qquad (4\text{-}11)$$

Combining Eq.(4−10) and Eq.(4−11):

$$\lim_{i \to \infty} |x_{i+1} - x_i| = 0 \qquad (4\text{-}12)$$

If the difference between any two successive approximations x_i and x_{i+1} is equal to zero when i approaches infinity, x_i can be considered as a root of the equation.

Hence a programme can be written in such a way: firstly, starting with initial guess and iterating until the difference between two successive x_i is smaller than a arbitrary small number ε, then we assume that the correct answer has been found.

The finite difference program used to find the heat distribution within the structure was written in Fortran and run on a IBM 3090 computer with vector facility. The area considered is approximated by 71×51 points. The arbitrary ε is 10^{-6} and the initial guess is chosen according to relative experiment result. The programme contains a procedure to calculate the value at each point over and over again (starting from the left to the right and from the top to the bottom of the area) till the value at each point in two subsequent iterations changes very little (less than ε). Another Fortran programme using the Ghost 80 library on the IBM 3090 was written to draw the contours of the temperature distribution.

4.4.2. Rate of Convergence

Rate of convergence of the result is shown in Fig.(4.3). It illustrates that the program is good because the result can converge to a particular value. In other words, the difference between two subsequent iterations tends to zero when interating a certain amount of times though initial guesses are different. A poor initial guess (e.g. 100 °C) will take more iterations to converge, which needed 35000 iterations. But for 65 °C, only 10000 iterations were needed. Therefore, finding a suitable initial

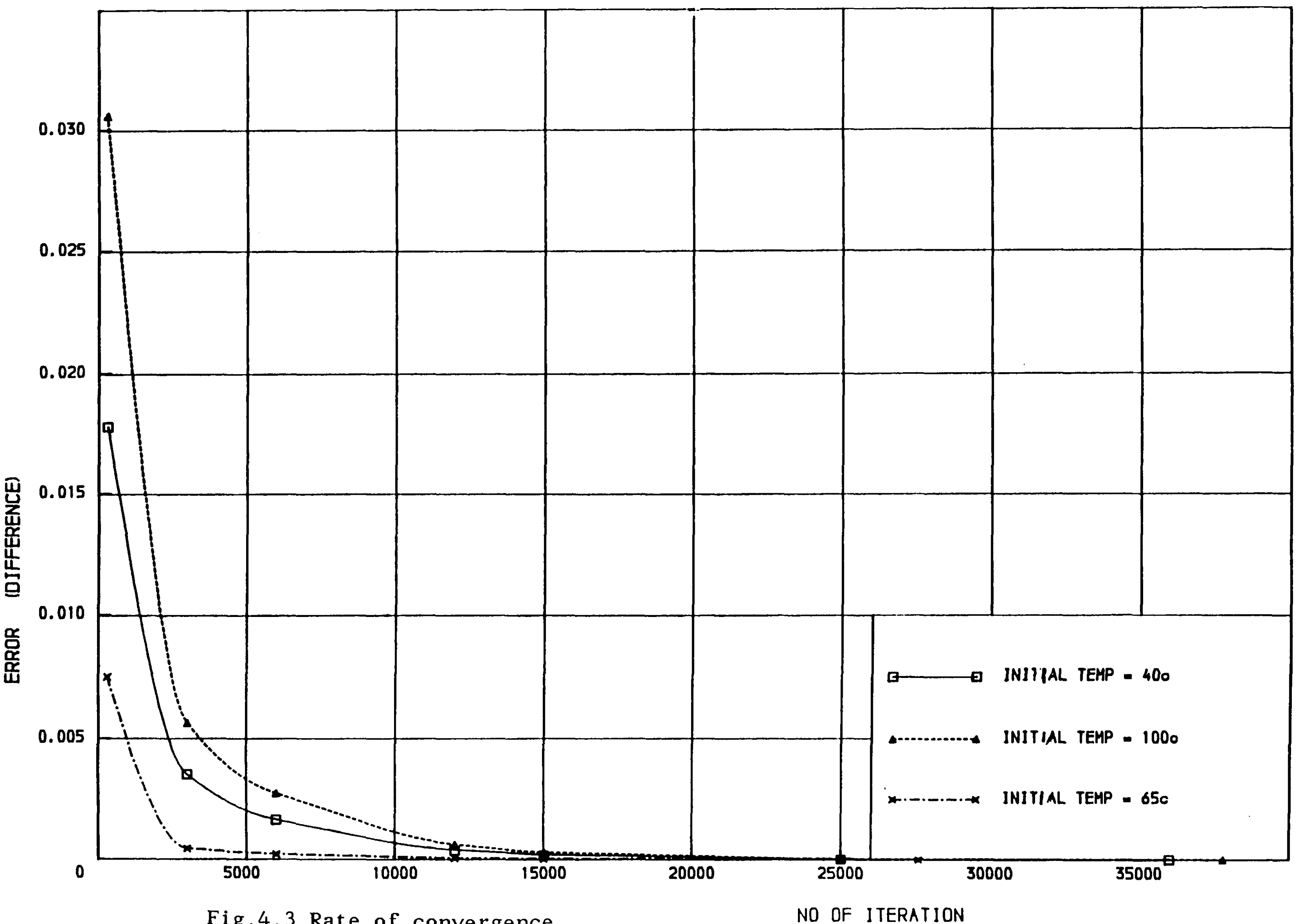

Fig.4.3 Rate of convergence.

(RING LASER, DIAMETER = 40uM, V=51mV, Ts=62c)

guess is quite important for two reasons: firstly a poor initial guess can lead to low convergence, shown in Fig.(4.3), with attendent use of computer time and secondly a poor one may spoil the convergence or cause convergence to the wrong root. Two usual methods of finding a suitable initial guess are given by Jamieson[43]. The initial guess in this program (e.g. 65^{0}C shown in Fig.(4.3)) is chosen by experience.

4.5 Errors in the Numerical Methods [43]

There are three main sources of error as a result of implementing this program on the IBM 3090:

(1) Roundoff error caused by using a number specified by n correct digits (e.g. real number representation) to approximate a number which requires more than n digits for its exact specification. It can be reduced by replacing with double precision numbers and running in IBM3090 mainframe with vector facility.

(2) Truncation error due to the replacement of an infinite process by a finite approximation, e.g. a finite number of iteration and insufficiently small mesh size. This can be reduced by increasing the number of iterations and diminishing the mesh size, which will cause an increase in execution time. In the program used, mesh size Δx= 2um will lead to some error.

(3) Error due to an approximate model and boundary set up. For example, no heat transfers across the surface are considered. The error will be significant especially when temperature is relatively higher. There is no easy way to get rid of this error without improving the model.

4.6. Temperature plots in ring laser substrate

Because of the circular symmetry of the ring laser, it is only necessary to consider a radial section, as shown in Fig.(4.2). The finite difference program takes nearly 30000 interations to converge. It is indeed a slowly convergent program. However, it only took 20 seconds of computer time as the program has been vectorized and runs under the vector facility, which is designed for numerically intensive computing.

The temperature distribution contour plots relating to various diameters of semiconductor ring laser substrate (D=12, 20, 40, 60, 100um) and for the same input power of 200mW are presented in Fig.(4.4)–(4.8). The horizontal and vertical directions correspond to radius and height, respectively, in the ring laser chip. Temperature of the bottom of rectangle is forced down to the adjustable temperature of heat sink, 20 ^{0}C in these graphs. The curves within the structure are isotherms, which correspond to the different temperatures in the table on the right.

A small region on the top of rectangle, where the isothems are more closely spaced, is the ring heat source whose temperature is the highest. Fig.(4.4)–(4.8) show different temperature distributions for different diameter ring lasers under the same power supply of 200mW, that is the power dissipated as heat. It is noted from the graphs that the heat is more concentrated to beneath the junction (lasing rib) and the maximum temperature is higher for a smaller diameter device due to its bigger power density and difficulty of dissipating heat, which is quite in agreement with the discussion before. For example, for a ring diameter of 12um, T_{max}= 128.0 ^{0}C, its temperature drops down 16% from heat source to edge on the top of chip, but for a diameter of 60um, T_{max}= 45.49 ^{0}C and the temperature drops down 47.5%.

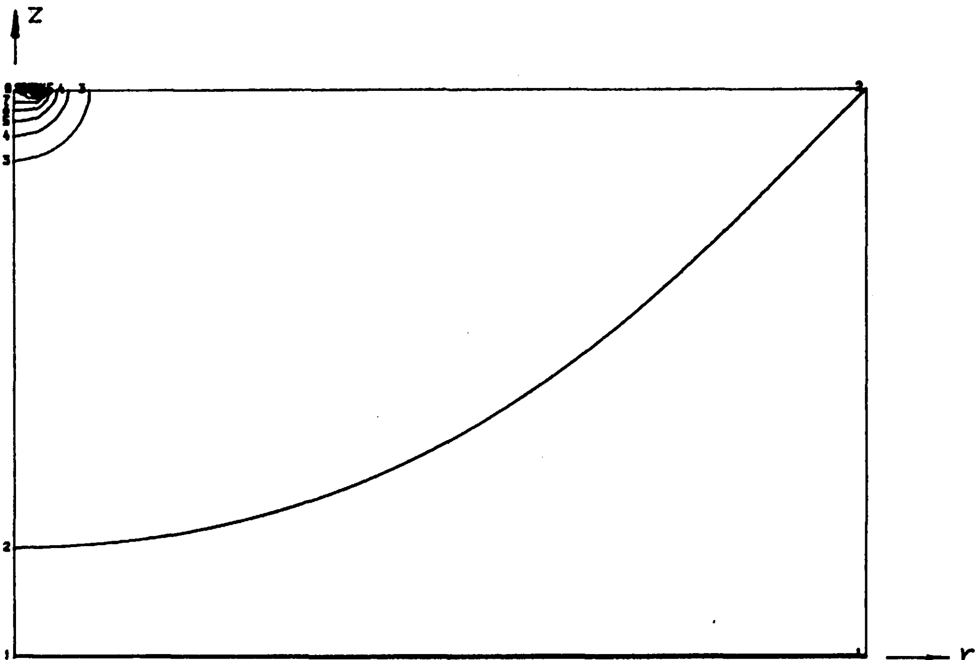

LEVELS	TEMP.
1	20.01
2	21.23
3	42.59
4	53.27
5	63.95
6	74.62
7	85.30
8	95.98
9	106.66
10	117.34
11	128.02

FIG4.4 HEAT DISTRIBUTION WITHIN RING LASER

(DIAMETER=12UM, WIDTH=2UM, POWER=200MW)

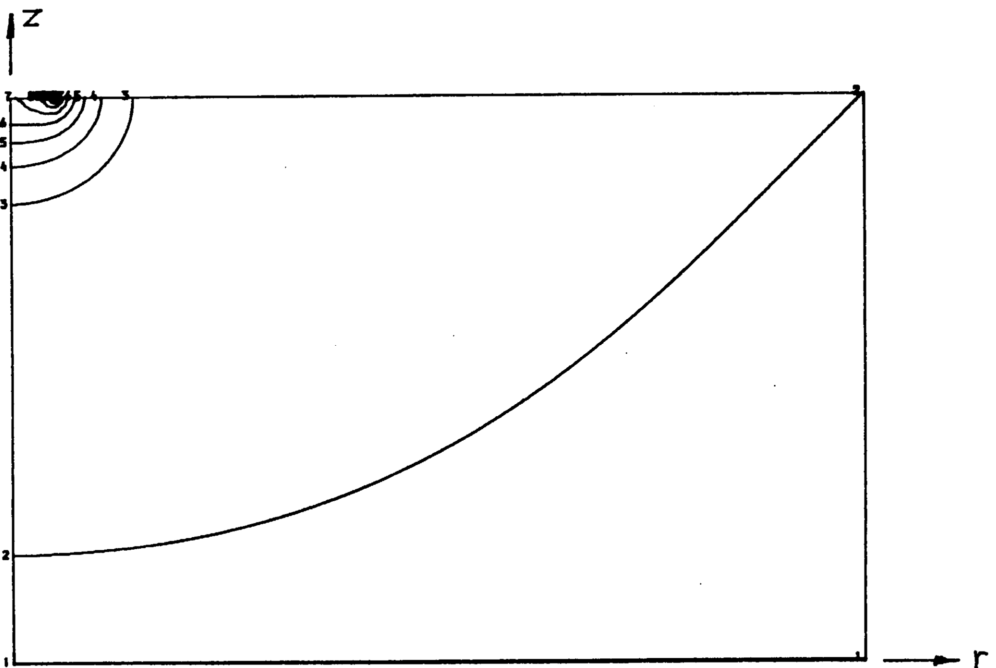

LEVELS	TEMP.
1	20.01
2	21.37
3	34.93
4	41.71
5	48.49
6	55.27
7	62.05
8	68.83
9	75.61
10	82.39
11	89.17

FIG4.5 HEAT DISTRIBUTION OF RING LASER

(DIAMETER=20UM, WIDTH=2UM, POWER=200MW)

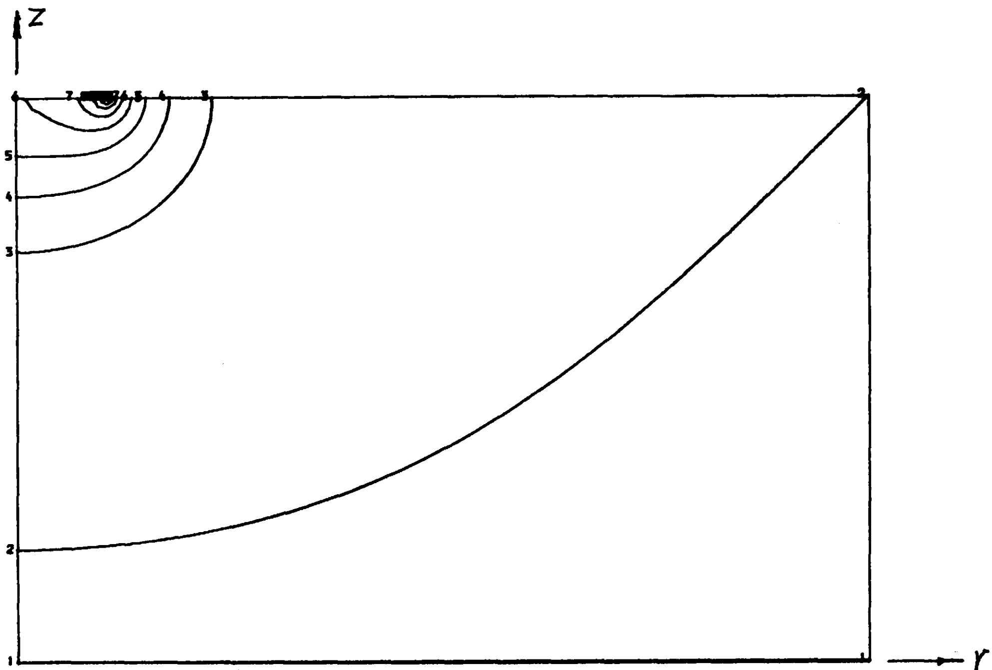

LEVELS	TEMP.
1	20.01
2	21.32
3	28.35
4	31.86
5	35.37
6	38.89
7	42.40
8	45.91
9	49.42
10	52.94
11	56.45

FIG4.6 HEAT DISTRIBUTION OF RING LASER

(DIAMETER=40UM, WIDTH=2UM, POWER=200MW)

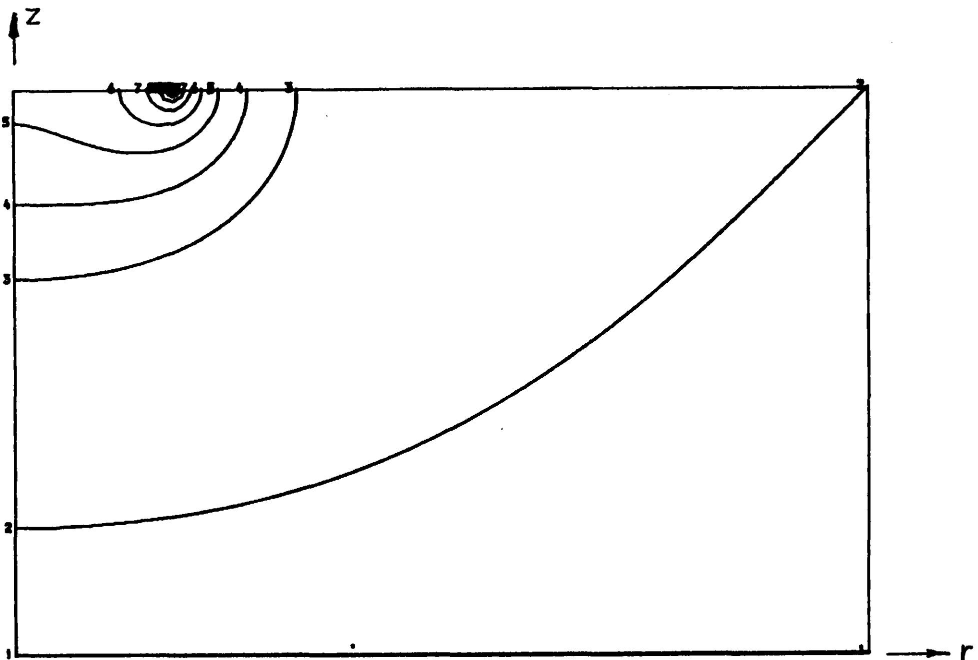

LEVELS	TEMP.
1	20.01
2	21.56
3	26.33
4	28.72
5	31.10
6	33.48
7	35.87
8	38.25
9	40.64
10	43.02
11	45.41

FIG4.7 HEAT DISTRIBUTION OF RING LASER

(DIAMETER=60UM, WIDTH=2UM, POWER=200MW)

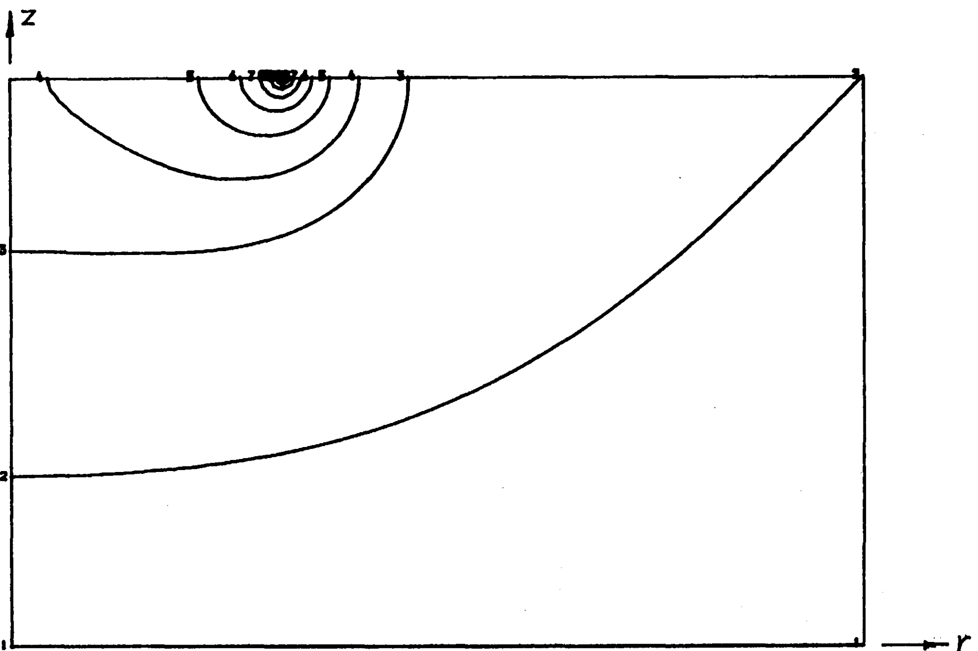

LEVELS	TEMP.
1	20.01
2	22.61
3	26.79
4	28.87
5	30.96
6	33.05
7	35.14
8	37.22
9	39.31
10	41.40
11	43.49

FIG4.8 HEAT DISTRIBUTION OF RING LASER

DIAMETER=100UM, WIDTH=2UM, POWER=200MW)

In addition, the thermal resistance across substrate is described by[44]:

$$R_{th} = \frac{T_{top} - T_{bottom}}{P_{input}} \ {}^{0}C/W \quad (4.13)$$

The thermal resistance vs. different diameter ring can be obtained, shown in Fig.(4.13). It indicates that low thermal resistance can be found for large diameter ring.

Temperature profiles for different input heat powers, 41mW, 100mW and 200mW have been obtained and are shown in Fig.(4.9), (4.10) and (4.6). They illustrate that heat distributions are the same, only the isotherms correspond to different values in the table, e.g. maximum temperature T_{max} is 27.67 ^{0}C for 42mW power supply, T_{max}= 38.75 ^{0}C for 100mW, T_{max}= 56.45 ^{0}C for 200mW. The heat sink temperature was 20 ^{0}C.

The thermal numerical simulation for different temperature of heat sink, T_s= 20 ^{0}C and 60 ^{0}C, under same power supply, 200mW, has been calculated, and is shown in Fig.(4.6) and (4.11). The temperature profiles keep unchanged as expected, only the temperature of the whole chip increases.

Finally, temperature distribution on the top of a 40um diameter ring laser chip under 41mW power supply and 61 ^{0}C heat sink temperature condition is also shown in Fig.(4.12).

It has been found that temperature rise largely for small ring laser, low thermal resistance can be found for large diameter ring laser ,shown in Fig.(4.13) and heat is more concentrated to beneath the lasing rib.

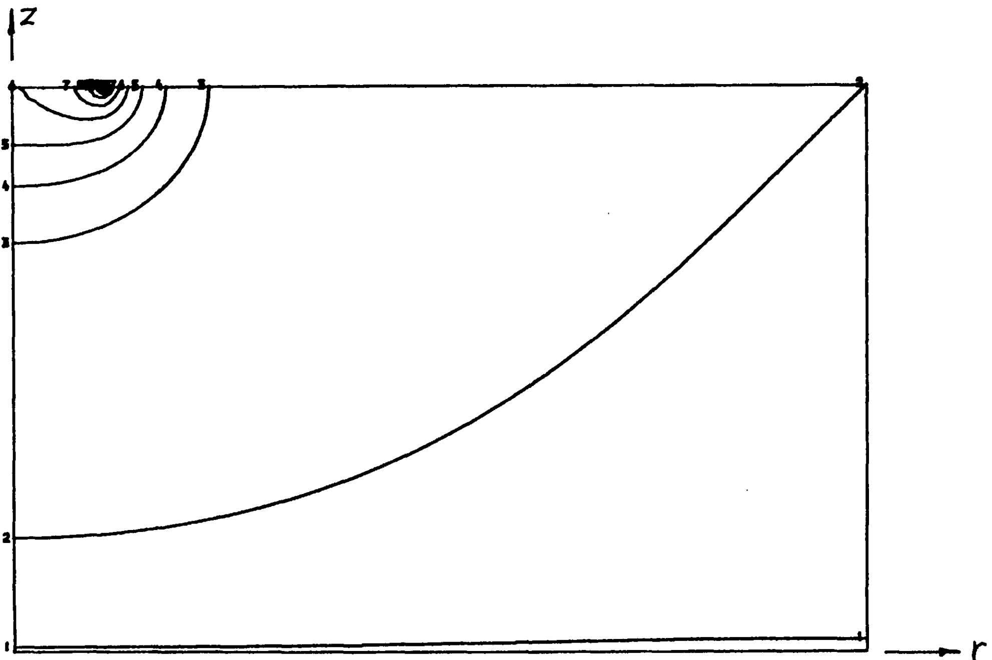

LEVELS	TEMP.
1	20.01
2	20.28
3	21.76
4	22.50
5	23.24
6	23.98
7	24.71
8	25.45
9	26.19
10	26.93
11	27.67

FIG. 4.9 HEAT DISTRIBUTION OF RING LASER

DIAMETER=40UM, WIDTH=2UM, POWER=42MW)

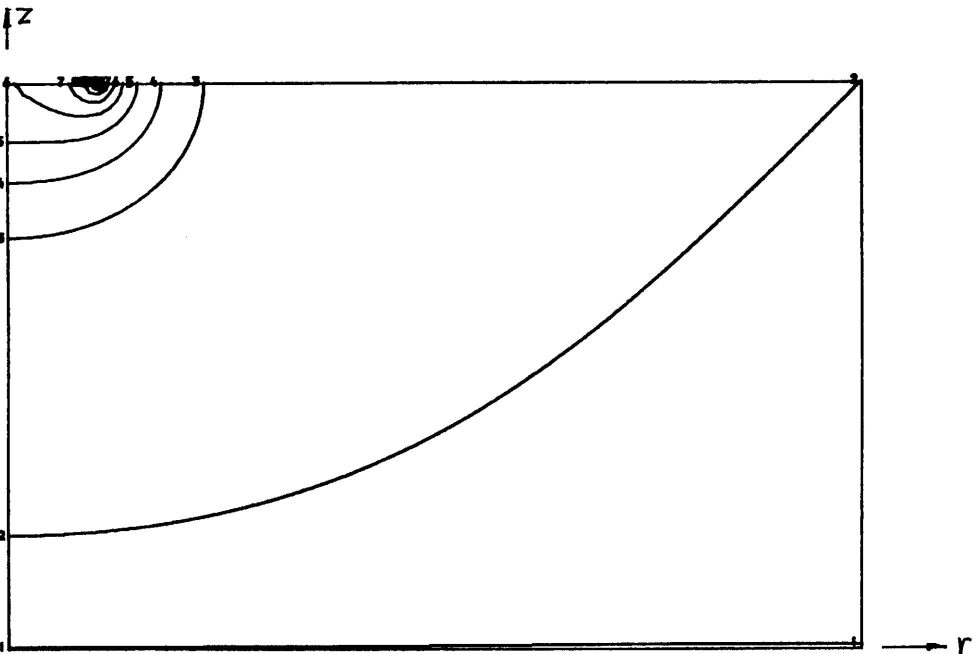

LEVELS	TEMP.
1	20.01
2	20.66
3	24.18
4	25.94
5	27.70
6	29.45
7	31.21
8	32.97
9	34.73
10	36.49
11	38.25

FIG. 4.10 HEAT DISTRIBUTION OF RING LASER

DIAMETER=40UM, WIDTH=2UM, POWER=100MW)

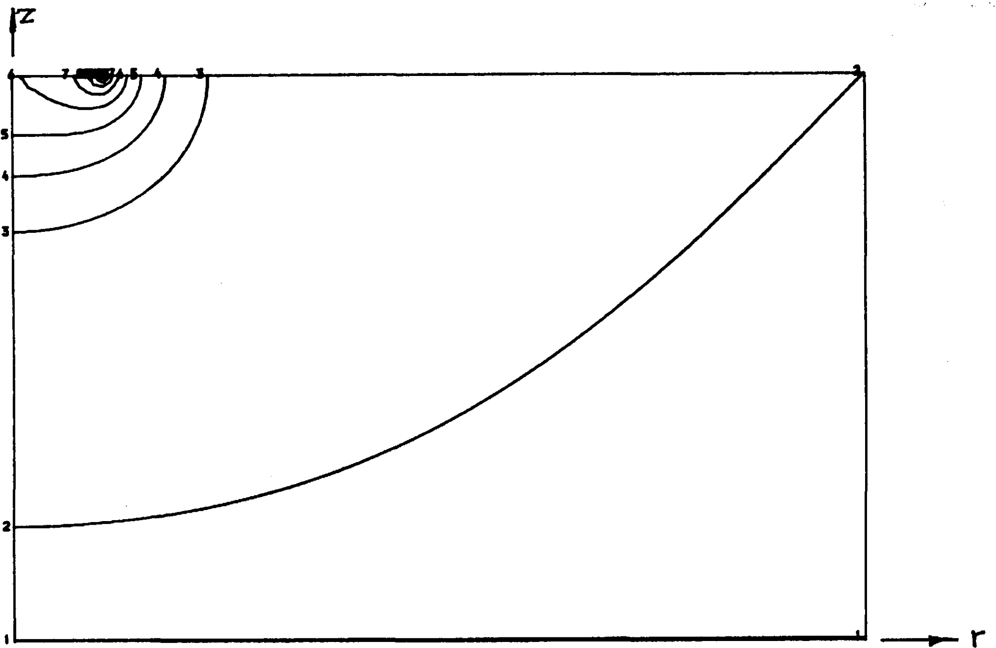

LEVELS	TEMP.
1	60.01
2	61.31
3	68.34
4	71.85
5	75.36
6	78.88
7	82.39
8	85.90
9	89.42
10	92.93
11	96.44

FIG4.11 HEAT DISTRIBUTION OF RING LASER

(DIAMETER=40UM, WIDTH=2UM, POWER=200MW)

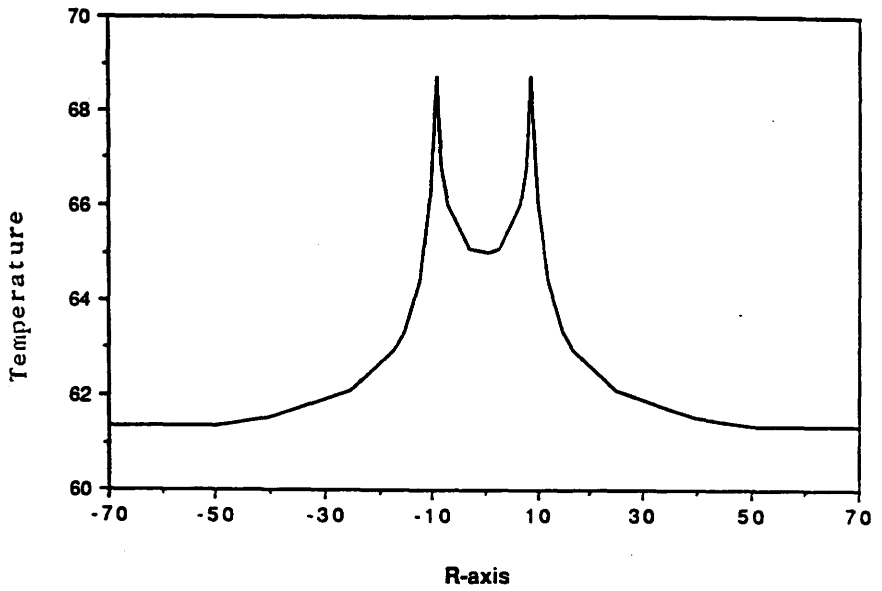

Fig.4.12 Temperature distribution on the top of a 40um diameter ring laser. (power supply=41mw, temp. of heatsink=61°C)

Fig.4.13 Thermal resistance of the ring laser substrate verse ring diameter. (rib width=2um)

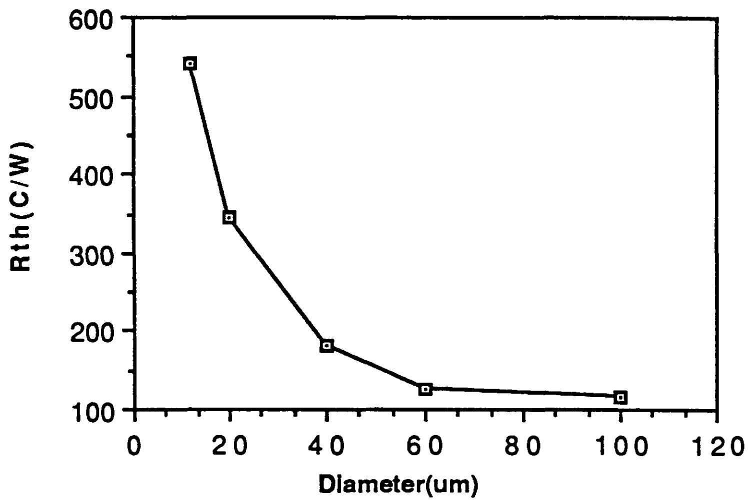

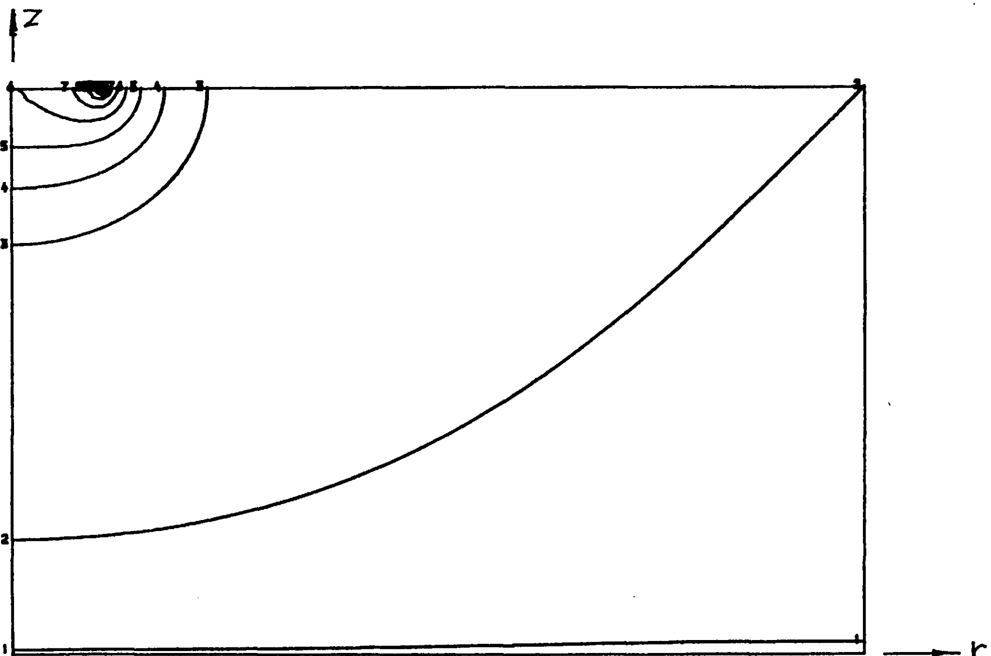

LEVELS	TEMP.
1	20.01
2	20.28
3	21.76
4	22.50
5	23.24
6	23.98
7	24.71
8	25.45
9	26.19
10	26.93
11	27.67

FIG. 4.9 HEAT DISTRIBUTION OF RING LASER

DIAMETER=40UM, WIDTH=2UM, POWER=42MW)

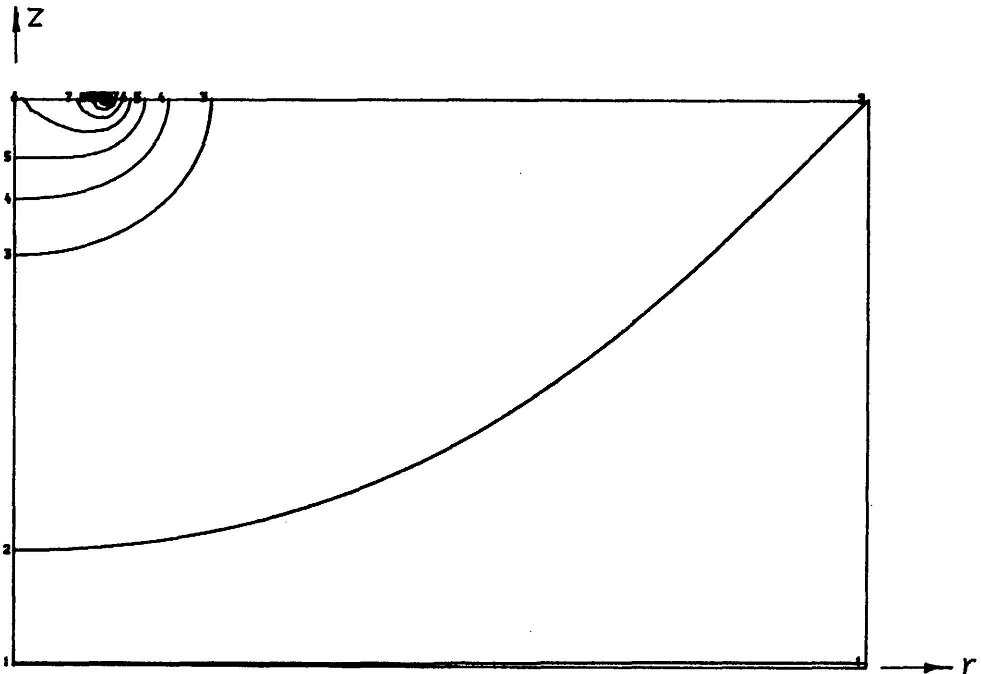

LEVELS	TEMP.
1	20.01
2	20.66
3	24.18
4	25.94
5	27.70
6	29.45
7	31.21
8	32.97
9	34.73
10	36.49
11	38.25

FIG. 4.10 HEAT DISTRIBUTION OF RING LASER

DIAMETER=40UM, WIDTH=2UM, POWER=100MW)

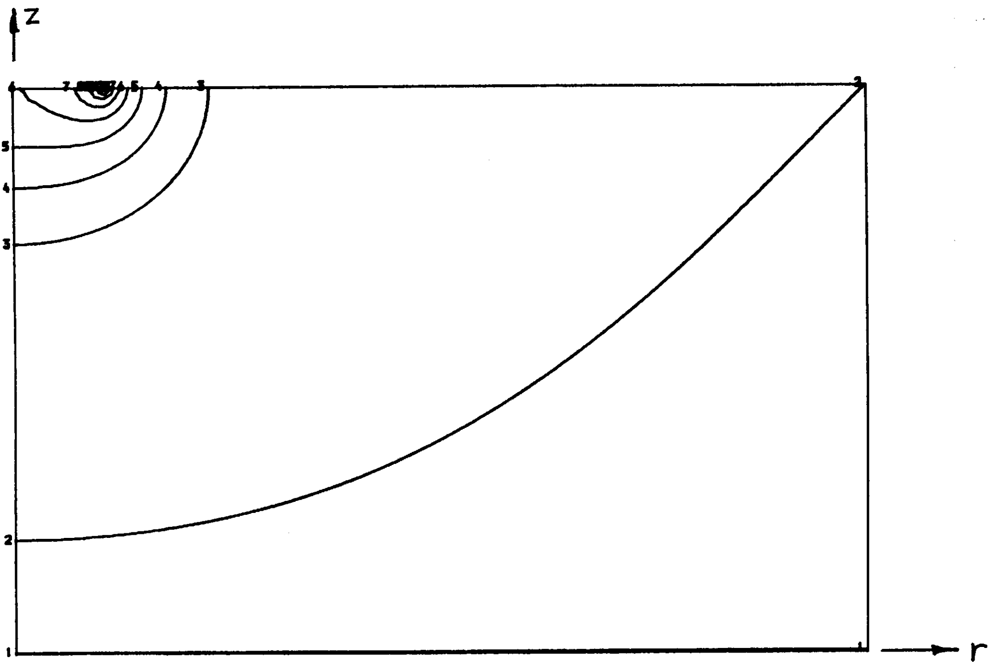

LEVELS	TEMP.
1	60.01
2	61.31
3	68.34
4	71.85
5	75.36
6	78.88
7	82.39
8	85.90
9	89.42
10	92.93
11	96.44

FIG4.11 HEAT DISTRIBUTION OF RING LASER

(DIAMETER=40UM, WIDTH=2UM, POWER=200MW)

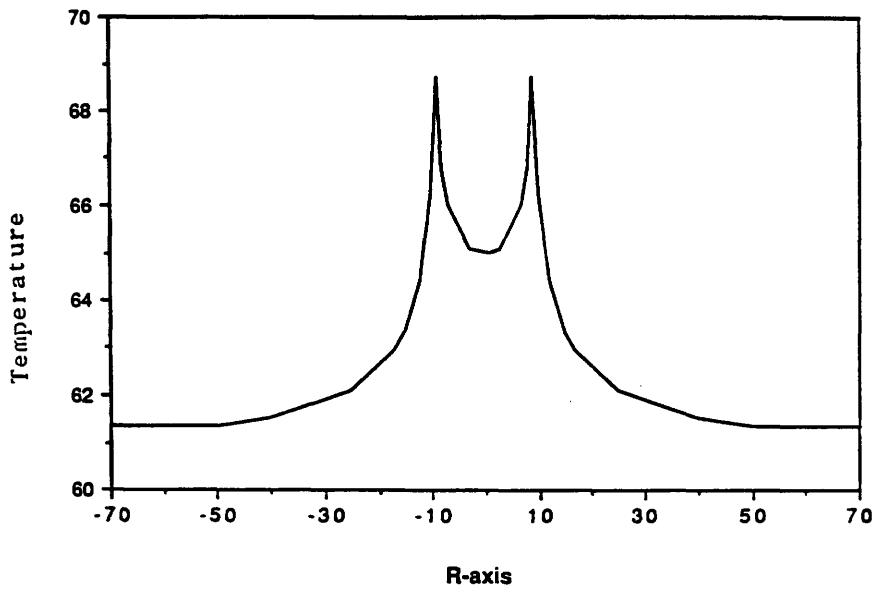

Fig.4.12 Temperature distribution on the top of a 40um diameter ring laser. (power supply=41mw, temp. of heatsink=61^{0}C)

Fig.4.13 Thermal resistance of the ring laser substrate verse ring diameter. (rib width=2um)

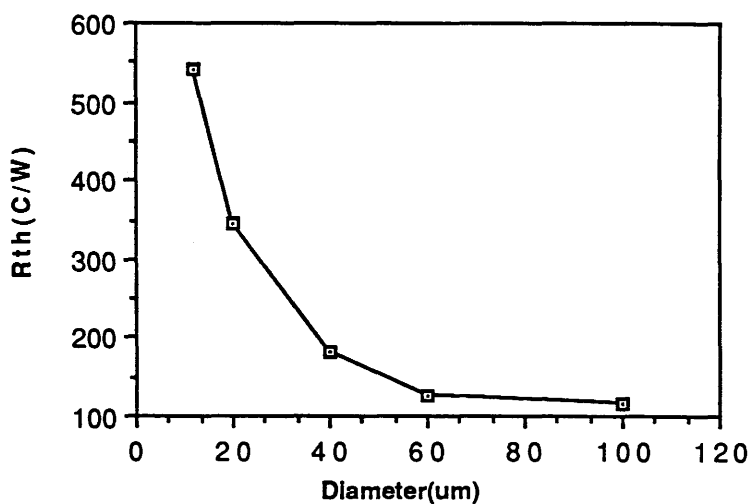

4.7. Temperature distribution across lasing rib

The ring laser chip is shown in Fig.(1.1). It is a ring rib laser of which there is a lasing rib on top of the substrate, as shown in Fig.(4.14). The thermal influence imposed by lasing rib has never been taken into consideration before for simplicity. However, in some case, it cannot be denied and becomes more significant for small rings or very narrow ribs.

Therefore, it is necessary to analyse the temperature drop across the rib. First, let us consider the rib model, as shown in Fig.(4.15) and suppose there is no heat transfer across the side and the top surface. The heat generated in the active layer moves entirely into the substrate so that the top part above the active layer can be neglected. The finite difference technique can be applied in this model. Temperature drop ΔT and thermal resistance R_{th} between the active layer and the top of the substrate can be estimated by using similar methods. Two kinds of ring diameter (40 and 100um) with respective power supply of 42mW and 200mW have been considered. In addition, the temperature drop ΔT_1 and its corresponding thermal resistance R_{th_1} with different rib widths have been calculated and presented in table 1. In comparision, temperature drop ΔT_2 and thermal resistance R_{th_2} between the top and the bottom of the substrate under the same condition are presented in the same table. For 100um diameter ring under 200mW power supply, the temperature drop of the wider rib is smaller than that of substrate. In this case the rib thermal effect can be ignored for simplicity. However, for narrower ribs, the temperature drop of the rib is larger than that of the substrate. In 40um diameter ring, the temperature drop is even more significant.

With reference to their thermal resistances, as shown in Fig.(4.16) and (4.17), obviously, both the thermal resistances of rib (R_{th_1}) and substrate (R_{th_2}) increase with decreasing widths and R_{th_1} increases more quickly than R_{th_2}. Fig.(4.17) shows

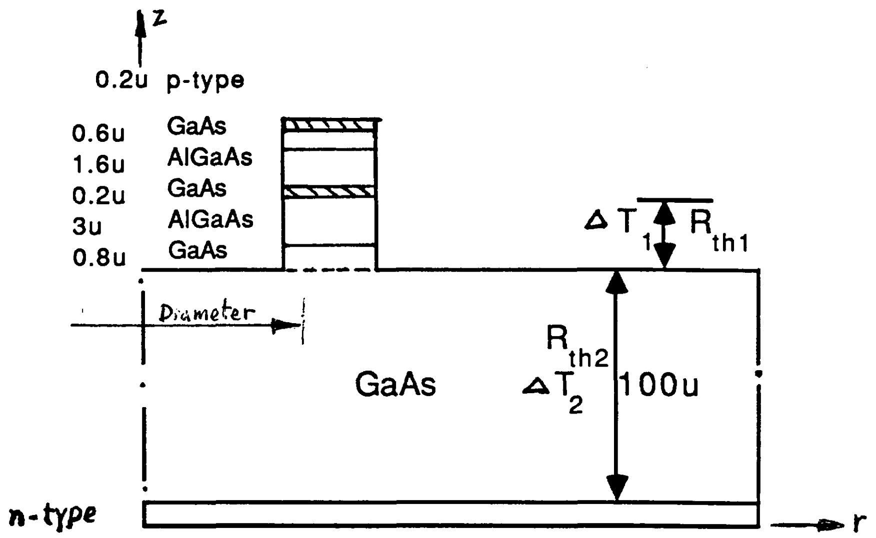

Fig.4.14 Cross section of ring laser chip in cylindrical coordinate. (rib+substrate)

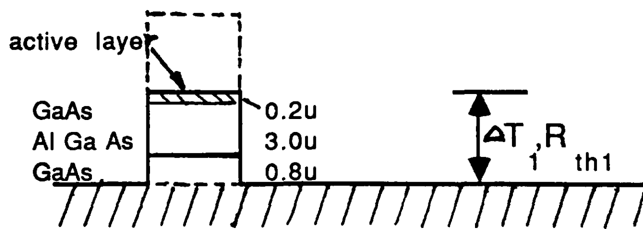

Fig.4.15 The lasing rib model for simplisity

diameter(um) \ width(um)			2	4	8	10
40 power=42mw	rib	$\Delta T1$(C)	8.79	4.64	2.61	2.22
		R1(C/W)	209.2	110.5	62.14	52.86
	substrate	$\Delta T2$(C)	7.72	7.0	6.73	6.53
		R2(C/W)	183.8	166.7	160.2	155.5
100 power=200mw	rib	$\Delta T1$(C)	16.24	8.29	4.32	3.54
		R1(C/W)	81.2	41.45	21.6	17.7
	substrate	$\Delta T2$(C)	23.5	14.0	12.96	12.6
		R2(C/W)	115.0	70.0	64.8	63.0

Table1. Comparision of the temperature drop and thermal resistance between lasing rib and substrate of the ring laser

Fig.4.16 Thermal resistance of lasing rib and substrate verse rib width

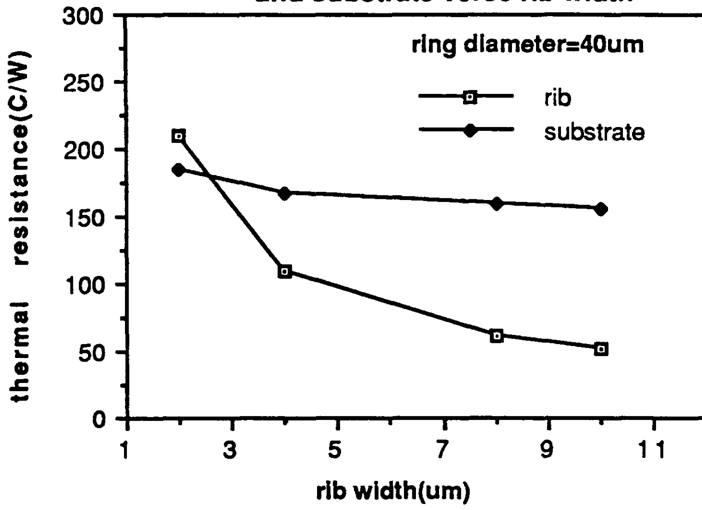

Fig.4.17 Thermal resistance of lasing rib and substrate verse rib width

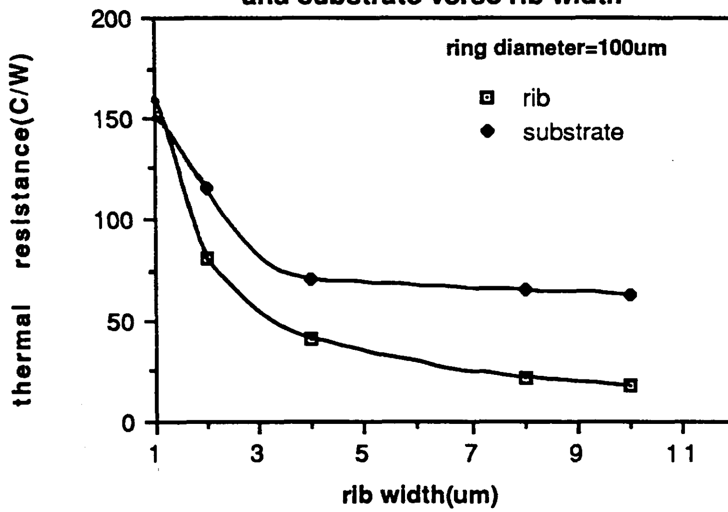

that for wider ribs (more than 7um), $R_{th\,2}$ is three times larger than $R_{th\,1}$. The total thermal resistance (rib+ substrate) is less than 100 ^{0}C/W when the rib width is larger than 6um. However, when the rib width is less than 4um, $R_{th\,1}$ increases more quickly than $R_{th\,2}$ and eventually it is bigger than $R_{th\,2}$. In Fig.(4.16), 40um diameter ring laser has relatively big thermal resistances for both the substrate and the rib. The thermal resistance of the rib ($R_{th\,1}$) increases sharply with increasing rib width. When the width is less than about 2.5um. $R_{th\,1}$ is bigger than $R_{th\,2}$.

As a result, not only the thermal influence by lasing rib cannot be ignored but also more attention should be paid to small rings or narrow lasing rib. This is because of the difficulty in heat dissipation in small sized area. In addition, a shallower and wider lasing rib can be of advantage because the thermal resistance of the rib is proportional to its height.

4.7. Summary

Temperature distributions of substrate and lasing rib in a variety of conditions have been successfully found. The thermal model fits the experimental device fairly well although the cylindrical-symmetry model is used and no account is taken of convection or radiation which are estimated to be small. The results obtained show large temperature rises in the laser, which are more severe for smaller rings and smaller width rib, and heat dissipation would be decreased.

The isotherms in the substrate model are concentrated close to the heat source, which means the temperature gradient is strongest just beneath the rib, the temperature of which does not depend on the thickness of the substrate. The isotherm distribution is the same for increases in input power or in heatsink temperature, but the temperature corresponding to each isotherm also increases, as

would be expected.

Thermal effect of the lasing rib is significant for small ring or narrow width rib. Therefore, large ring and wide width rib structure would be better for heat dissipation. Fig.(4.18) shows the thermal resistance of the whole ring laser chip. It suggests that for 100um diameter ring laser, thermal resistance of only the structure in which the rib width is more than 6.0um can be less than 100 ^{0}C/W, which may be thought of as a device with acceptable thermal characteristics.

The simulation results indicate that for a semiconductor ring laser structure with good thermal characteristics, which it is possible to run in CW operation, one or both of the following factors must be taken into consideration:

(1) a large diameter ring;

(2) a shallower and wider rib.

Fig.4.18 Thermal resistance of whole ring laser chip (rib+substrate)

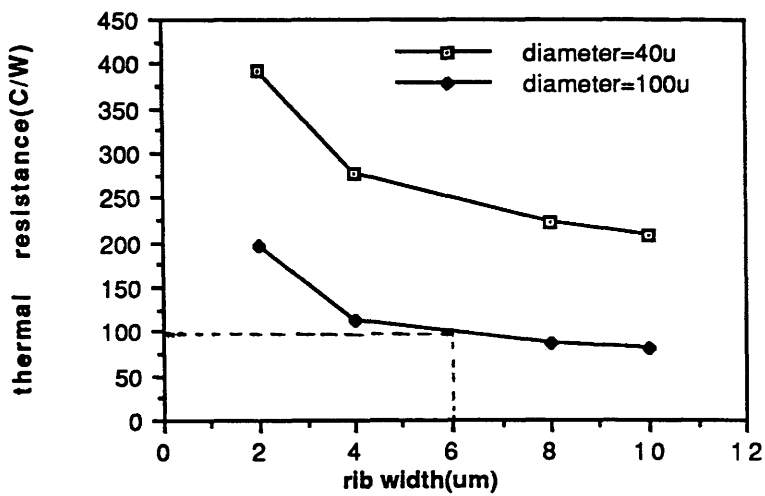

CHAPTER 5

TEMPERATURE MEASUREMENT BY THERMAL IMAGING

5.1 Introduction

The measurement of temperature distribution in a semiconductor laser device is of vital importance for designing and running the device. Especially, direct observation of temperature profile on the top of semiconductor laser device is most significant. A very convenient way of measuring the thermal map is to use some temperature sensitive feature of the material of the device structure concerned. For example, infrared thermal images of the laser surface may be used. Infrared thermal maps of the semiconductor ring laser were obtained by using a Barns RM50 Infrared Micro Scanning Imager in the Wolfson semiconductor laboratory at the University of Birmingham. A brief account of the infrared imaging technique will be given first and the equipment will be described in section 5.3. Attention must be paid to sample preparation, which will be discussed in section 5.4. Finally, thermal mapping of the top surface of the ring laser under a variety of power supplied and different heatsink temperatures has been carried out, and will be presented and discussed in section 5.5.

5.2. Principle of infrared thermal imaging

The infrared is that region of the electromagnetic spectrum which lies

between the visible and microwave regions, i.e. between wavelengths of about 800nm and 1mm. Its importance arises from the fact that every material object emits infrared radiation in a characteristic manner depending upon the surface temperature. It can be used to distinguish a body from its surroundings or to identify an unknown material, also to obtain the temperature profiles of the body from a study of the intensity and wavelength distribution of the radiation [45].

The radiation intensity and wavelength distribution are strongly influenced by surface temperature, as shown in Fig.(5−1). The energy intensity per unit wavelength interval $\lambda \rightarrow \lambda + \Delta\lambda$ radiated from a object at an absolute temperature T is given by the Planck radiation equation [46]:

$$\psi = \frac{K_1}{\lambda^5[\exp(K_2/\lambda T)-1]} \qquad (5\text{-}1)$$

Here K_1 and K_2 are constants. This equation only holds when the heated body is "black". The black body is defined as one which absorbs all radiation falling on it whatever the wavelength is. Fig.(5.1) shows the temperature dependence of the relationship between radiation energy and wavelength. It is noted that energy is very small for large and small λ. The maximum energy is emitted at a peak wavelength, and will increase and move to a shorter wavelength by increasing temperature. Conversely, temperature of a body can be obtained by measuring its radiation energy intensity in a certain wavelength interval $\lambda_1 \rightarrow \lambda_2$, as shown in Fig.(5.1).

A thermal image map of the sample can be recorded by scanning and measuring the intensity of radiation from point to point on the sample.

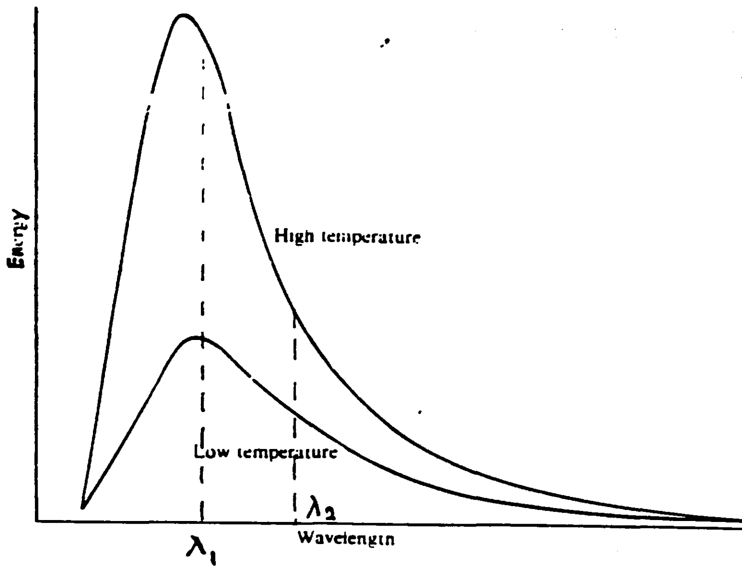

Fig.5.1 Radiation energy intensity verse wavelength.

5.3. Experimental equipment

A RM–50 Scanning Infrared Micro Imager was used through out this work, shown in Fig.(5.2). It is interfaced to a DEC 11/34A computer, which handles any digital processing and has a colour monitor display. This microscanner combines the features of an infrared microscope with those of a real–time thermal graph. It employs advanced electro–optical techniques to scan all portions of the target, measure the temperature of each resolution element, and produce a continuous magnified thermal image on the colour monitor display[47].

Fig.(5.3) is a micro imager optical schematic diagram. The optical system consists essentially of detector, optical chopper and 2–axis scanning system. The system uses a indium–antimonide detector cooled by liquid nitrogen, for the purpose of increasing the resolution. The sensitive range $\Delta\lambda$ of the InSb detector is between 2 and 5 um. The temperature measuring range is ambient to 200 ^{0}C with sensitivity of 0.1 ^{0}C at 30 ^{0}C. The chopper is an electromechanical device which periodically interrupts the infrared radiation reaching the detector and target scanning is accomplished by torque–motor driven mirrors. One mirrors scans in the X direction at a rate of 60Hz, while the other mirror scans in the Y direction at a rate of 1 or 2 Hz. This produces an image composed of a raster of 64 horizontal lines at a rate of 1 frame per second. As a result, it will take 1–2 second to scan one thermal map.

There is a heater which is used to raise and accurately hold the specimen holdertemperature constant. The visual display can be photographed by an special camera with push–button control.

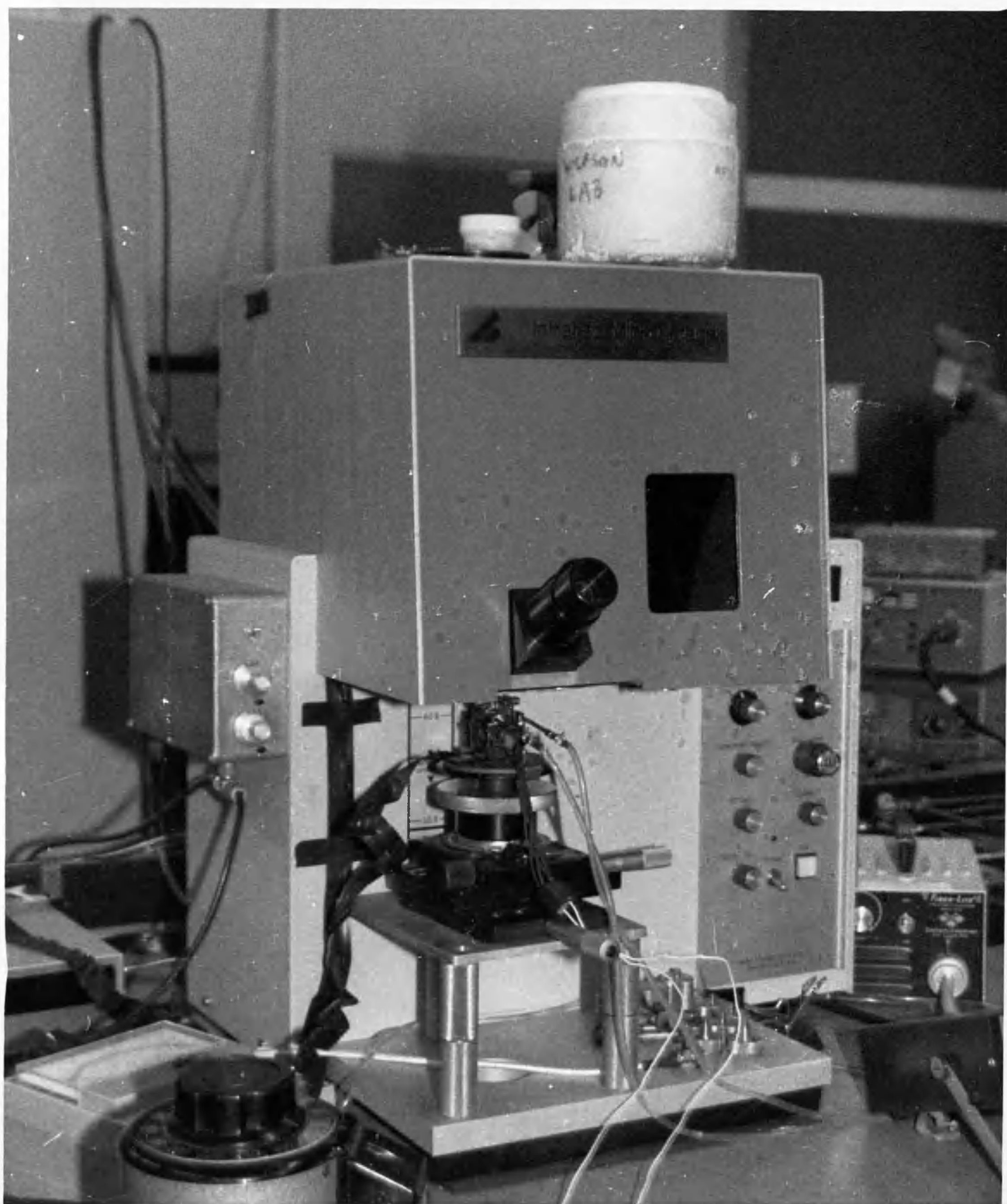

Fig.5.2 A RM-50 Scanning Infrared Micro Imager.

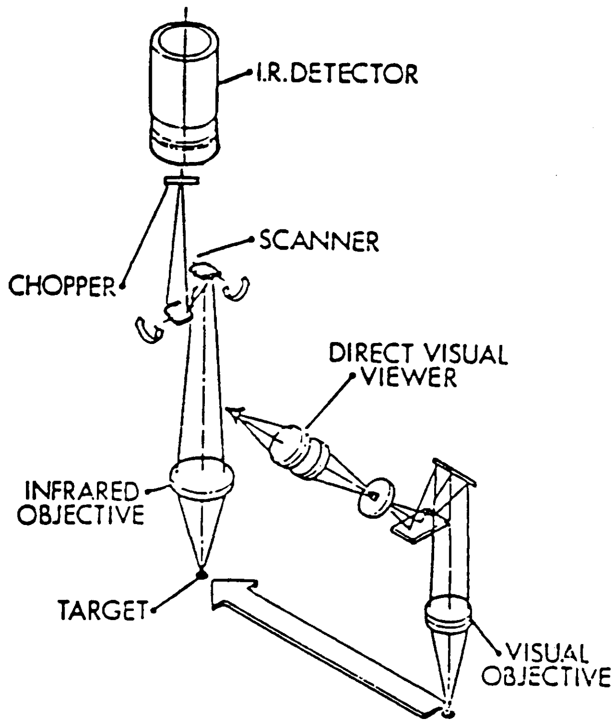

Fig.5.3 Micro imager optical schematic diagram.

5.4. Description of the sample

The dimension of the ring laser chip used in this experiment is about 450um square by 100um thick. The diameter of the laser ring is 100um . The chip is mounted onto a copper block by silver epoxy, and is placed on the top of the heater in the system.

The electronics measurement circuit is shown in Fig.(5.4). Supply current I_d and voltage across the laser diode V_d were measured at the same time while thermal maps on the top of sample were being recorded. Resistance R_2 is for current limitation and supply current I_d was given by measuring voltage V_d divided by resistance R_1, in case the laser diode is damaged when an autoranging ammeter changes range by chance.

The problem which always arises in this experiment is that lower material emissivity makes measurement difficult, especially for this sample which has low supply current (10mA–120mA). A solution to the problem has been made by using a coating of known high thermal emissivity, such as various polymers, paints or lacquers, or silicon monoxide [48], which increase the minimum emissivity up to values exceeding 0.4 and do not require any correction to be used on the recorded data. In practice, each sample needs to be treated as an individual problem, i.e. the type of coatings described do not represent a general solution, and whether this type of approach is suitable depends on what information is sought. For temperature mapping, the coating layer has to be thin and uniform and to have good thermal contact. A better coating material for the sample in this experiment is silicon monoxide (SiO), which was deposited on the top of sample, about 3um, under 10^{-5} torr pressure. Even where the low emissivity problem was solved, the accuracy in this experiment was about $2\,^{o}C$.

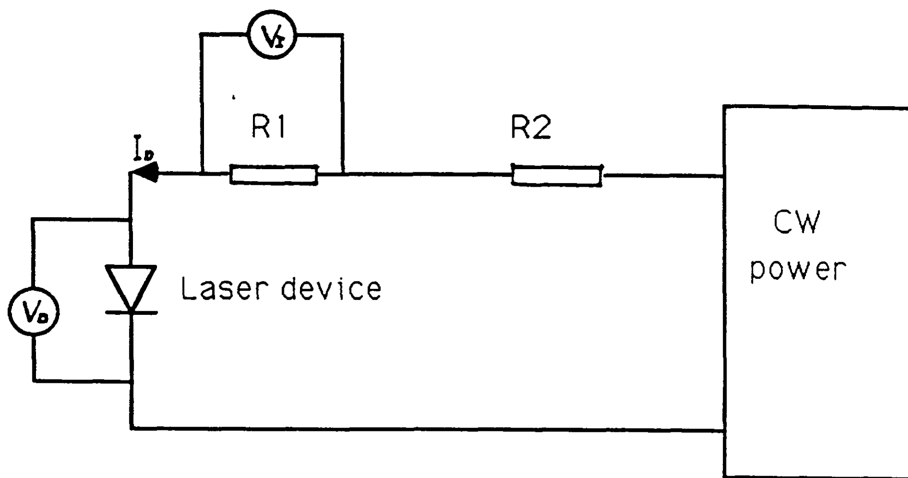

Fig.5.4 Electric measure circuit for
the infrared imaging experiment.

5.5. Result and discussion

Some results will be presented for two different ring diameter laser, 100um and 40um various supplied power and base temperatures. Fig.(5.5) shows the 100um diameter laser configuation and Fig.(5.6) shows the laser emits ring light.

The emissivity map, as shown in Fig.(5.7), was determined from observations of radiant energy by heating the sample (temperature of the heatsink is 57.2 ^{0}C). The shape of the sample on the map fits the configuration of the laser in Fig.(5.5) and it seems that the emissivity of the material of the sample is not quite uniform. However, the infrared scanner automatically adjusts its resulting temperature profile calculation to allow for the measured various in emissivity [47,49].

Increase of power supply on the laser device will make it not only emit more light, also generate more heat. 100um diameter ring laser was used with 100, 50, 30, 2mA supply current, with the different base temperatures (heatsink temperature) of 57.0, 57.1, 57.6, 61.0 ^{0}C, respectively. Their thermal maps are presented in Fig.(5.8)–(5.11).

The thermal maps clearly illustrate the temperature distributions on the top of the sample and it is hotter in the ring region than that outside the ring. Different colours on the maps correspondsto different temperatures which are shown on the right–hand side. It is clear from the photos that the temperature on the top of the ring is not uniform. For example, in Fig (5.8), there is a hottest point, 102 ^{0}C, at the Y junction and the left half of the ring is hotter than the right half. The average temperature on the ring can be estimated roughly to be about 92 ^{0}C. It is not easy to explain the nonuniform temperature distribution because it depends on many factors, e.g. low resolution of instrument, emissivity, non–uniformity of the material and its surroundings. The reason for the higher temperature in the left half

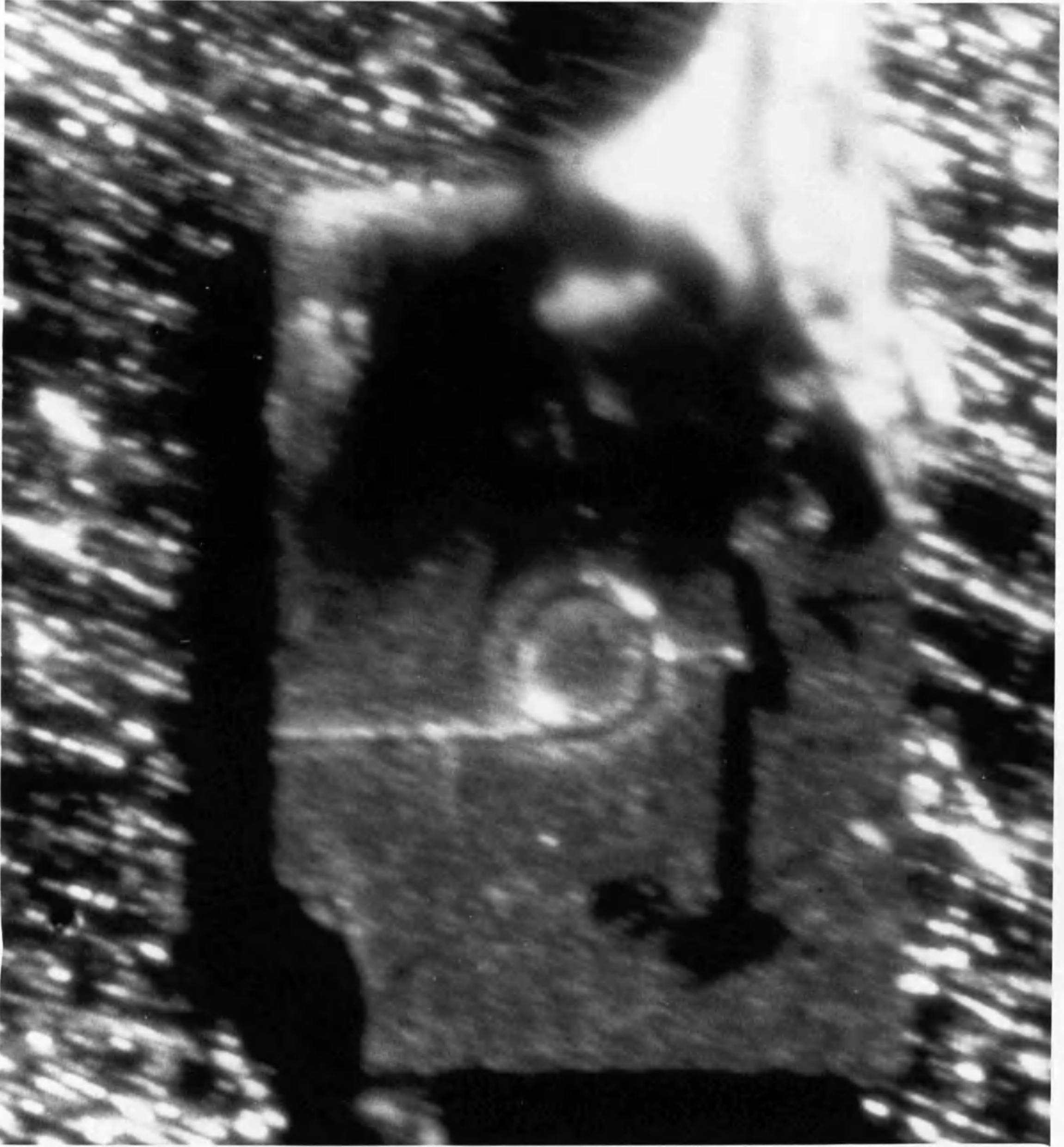

Fig.5.5. 100um diameter ring laser configuation.

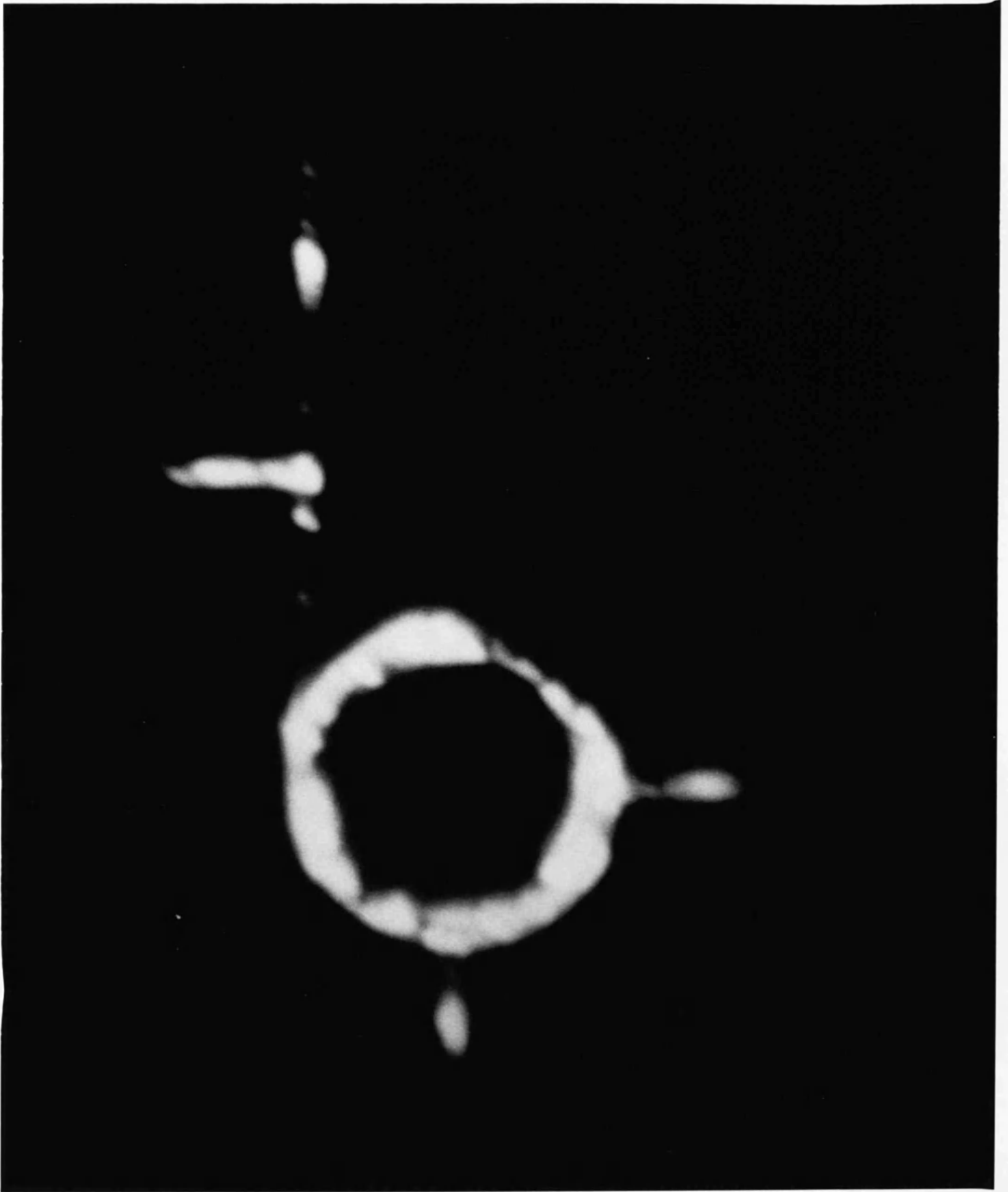

Fig.5.6 Ring light picture emitted by 100um diameter ring laser.

RING LASER 100UM 57.2C

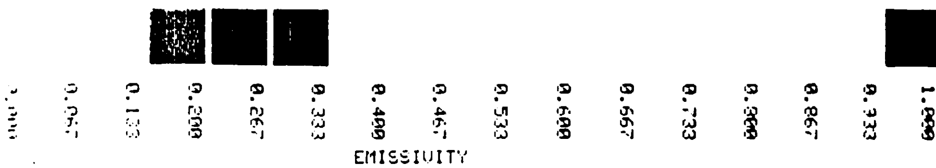

Fig.5.7 Emissivity map of 100um diameter ring laser.

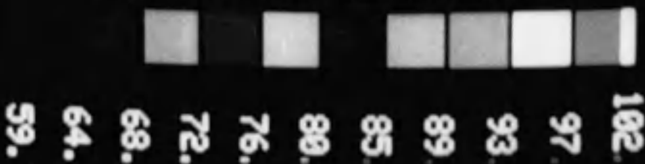

Fig.5.8 Infrared temperature map
(Average temperature on the top of ring is 92^{0}C)

Fig.5.9 Infrared temperature map.

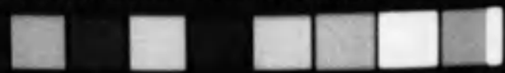

Fig.5.10 Infrared temperature map.

RING LASER 100UM 2MA
SIZE= 0.32mm

Fig.5.11 Infrared temperature map.

of the ring may be explained by the fact that there is a big drop of epoxy, conductivity of which is $0.02W/cm\,^0C$ and is much smaller than that of GaAs, $0.44W/cm\,^0C$, on the top left corner of the chip. As a result, heat is more difficult to dissipate in the left half of the ring. The hottest point is due to Y junction coupling where more current is concentrated.

Fig.(5.8) and Fig.(5.12) show temperature distributions for different base temperatures, T_S = 22.5 ^0C and 57.0 ^0C under the same 200mW power supply. It is clear that the results obtained are quite in agreement with the theoretical simulation results in chapter 4, i.e. the temperature profiles keep unchanged, only temperatures in the Table shift to higher temperatures. For example, the difference between maximum and base temperatures in Fig.(5.8) is about 45 ^0C, which is nearly equal to the equivalent difference, 43.3 ^0C, in Fig.(5.13).

In the numerical modelling discussed in chapter 4, only average of the maximum temperature on the top of ring was taken into account. However, from the thermal map, we can find the temperature is not uniform. In order to compare with experimental results, the experimental average maximum temperature has to estimated. In Fig.(5.12), it is about 54.5 ^0C (the temperature drop is 32.5 as temperature of the heatsink is 22.0 ^0C here).

The thermal image maps for diameter 40um ring under 42mW (25mA) and 51mW (30mA) power supply are demonstrated in Fig.(5.13) and (5.14). The maximum temperatures shown in each temperature table are also the average temperature of the whole ring, because the ring is too small to be distinguished between different temperatures on the ring.

Table 2 shows the comparision of temperature drop and thermal resistance in theory and experiment. It illustrates that the theoretical results are bigger than the

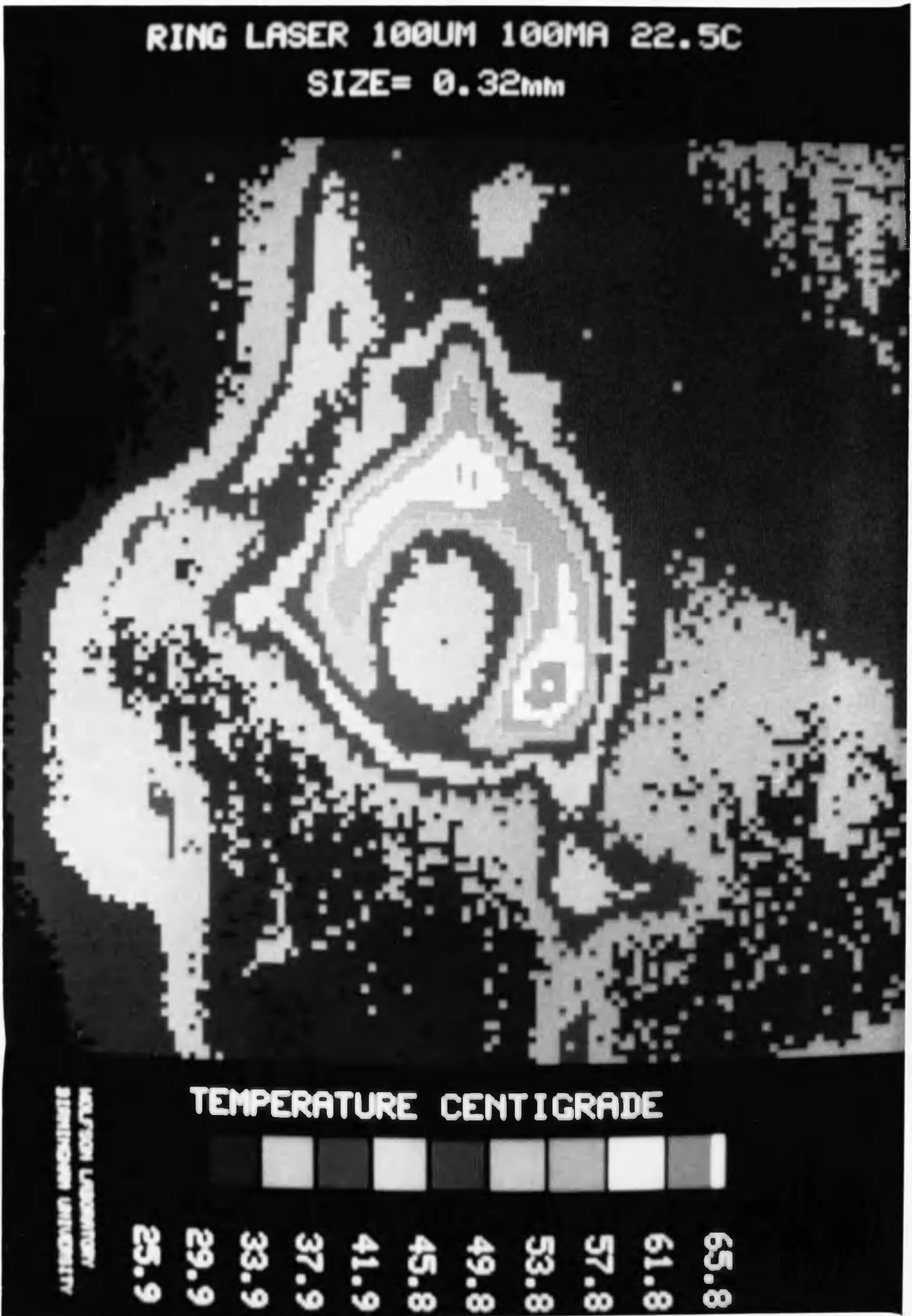

Fig.5.12 Infrared temperature map.
(Average temp.on the top is 54.5^{0}C)

25MA
SIZE=0.635mm

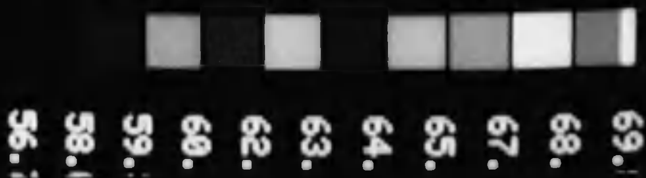

Fig.5.13 Infrared temperature map.
(Diameter=40um,power=42mw, T_s=61°C)

Fig.5.14 Infrared temperature map.

values obtained experimentally. These differences between theoretical model and experiment can be explained by noting that the resolution of the infrared scanner is 10um at best which is larger than the width of the lasing rib. Therefore, the temperature of the ring shown in the thermal maps is actually the average temperature of the rib and surrouding substrate, see table 2. Where the rib is widened, for example at a y– junction, the scanner will indicate a higher temperature.

5.6. Summary

Temperature distributions on the top of the sample have been obtained by using infrared image scanner. The thermal maps show the temperature distribution so obviously and directly that we can say it is a good method to observe the thermal behaviour of the device. Although it can not indicate rib temperature well due to the results much affected by low resolution of the apparatus, it does give some idea of the temperature distribution of the device which is in broad agreement with theoretical expectation.

Table 2. Coparision of temperature drop and thermal resistance of the ring laser in theory and experiment

	diameter=100um power=200mw	diameter=40um power=42mw
theoretical		
substrate	ΔT=23.5 C, R=115.0 C/w	ΔT=7.72 C, R=183.0 C/w
rib+sustrate	ΔT=39.74 C, R=198.7 C/w	ΔT=16.51 C, R=393 C/w
experiment	ΔT=32.5 C, R=162.6C/w	ΔT=9.8 C, R=209 C/w

CHAPTER 6

SEMICONDUCTOR LASER TEMPERATURE CONTROL SYSTEM

6.1. Introduction

Semiconductor lasers are known to be adversely affected by heat which is generated at the active junction. This heat may degrade the laser, which reduces its useful lifetime and the junction temperature rise will lead to a deterioration of laser operating characteristics: an increase in threshold current, a shift in the output wavelength and a decrease in the output power.

These effects will limit the use of the lasers, particularly for optical– fiber communication applications. So great attention has been paid to finding a method which can remove heat generated at the junction efficiently and achieve a stable and long lived operation. Thermoelectric (Peltier) cooling device has been used intensively to provide a simple, reliable solution to precise temperature control in many applications of optoelectronic device. In this work a small Peltier cooler, which is 8mm long, 10mm wide and 2.7mm high and nominal voltage of 3.5V, is used to cool a semiconductor laser chip. Its operating principle will be briefly discussed in section 2.1. The Peltier cooler must be driven by a electrical control system, which will be described in section 2.2. The temperature dependence of threshold current and lasing wavelength were measured by using this system, which will be presented in section 3,4. Finally conclusions will be drawn.

6.2. Temperature control system

6.2.1. Peltier effect and Peltier cooler

The thermoelectric (peltier) cooling device is based on the thermoelectric effect or Peltier effect which was discovered by Jean.C.Peltier[50] in 1834. This effect, in Fig.(6.1), shows that an electric current passing through a junction of two dissimilar conductors can either cool or heat this junction depending on the direction of current. Heat generated or absorbed is proportional to the current.

Generally, the peltier device is made from two heavily doped semiconductor blocks (usually bismuth telluride), which are connected electrically in series and thermally in parallel, as shown in Fig.(6.2). When current goes in a clockwise direction, i.e. metal → n−type → metal → p−type → metal, the electrons in n−type and holes in p−type will carry heat from heat souce to heatsink. If the current is changed, the carriers will move the heat up to heat source. Overall, changing the direction of current can heat or cool the top of the device. A conventional Peltier device often contains dozens of semiconductor block to increase the efficiency of heat transfer. Total heat transfered is easily multiplied by increasing the number of blocks.

6.2.2. Laser temperature control system

A laser temperature control system is presented in Fig.(6.3). The laser chip is mounted on a copper block which is placed on the peltier cooling device. Then the Peltier device is soldered onto a I−C header. In the metal block, there are two holes near the bottom of sample which contain a thermistor, that measures the

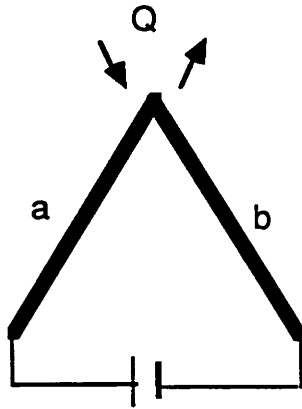

Fig.6.1 Schematic diagram of the Peltier effect.

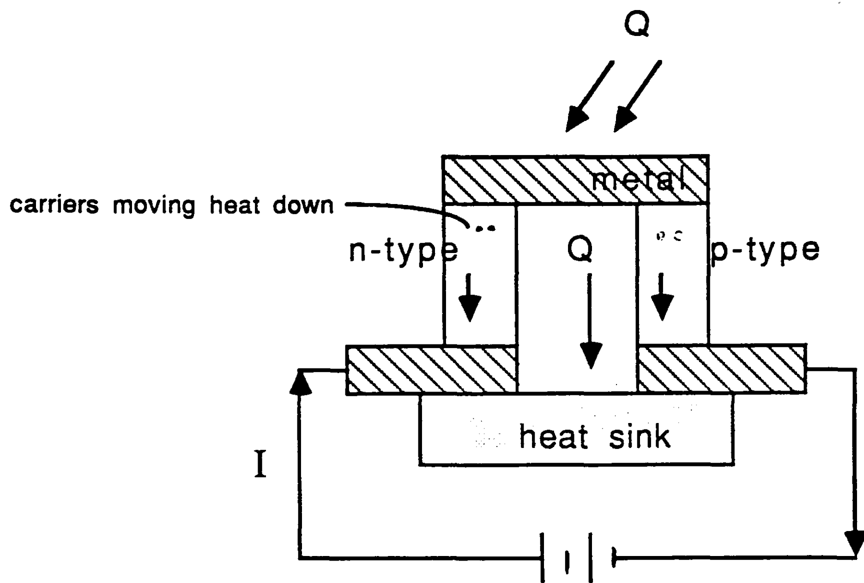

Fig.6.2 Principle diagram of a Peltier cooler device.

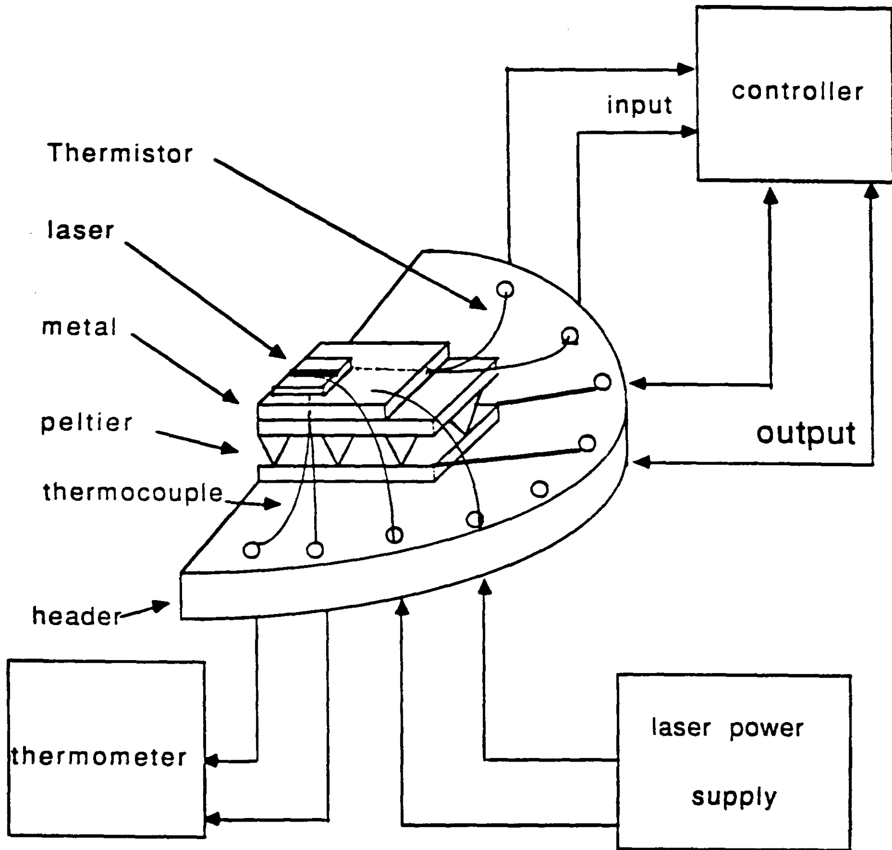

Fig.6.3 Schematic diagram of a laser temperature control system.

temperature of the bottom of the laser chip and sends it to the controller, and a thermocouple that indicates the temperature.

Fig.(6.4) is a diagram of the feedback control system. The metal block temperature is measured by a thermistor. This temperature is then compared to a set point temperature (reference temperature), to produce an error signal proportional to the temperature difference. The error signal processor produces an output based on the error signal. The output controls a bipolar output driver, which supplies the Peltier cooler. Therefore, when the temperature on the bottom of the sample changes, the error signal processor will produce an output to drive the Peltier cooler which control the block temperature. As a result, this system can keep the temperature of the bottom of the sample (called the heatsink temperature) at a particular value.

6.3. Temperature dependence experiment of semiconductor stripe laser

One of the applications of the laser temperature control system is to change the heatsink temperature T_S to a certain value and measure temperature dependence of the laser operating characteristics, e.g. threshold current, lasing wavelength and optical output power.

6.3.1. Temperature dependence of threshold current

A very narrow stripe (1 um) DH laser, on a chip 400um×400um square, was mounted in the system. It was pumped by a pulsed current supply, with pulse width = 0.06us and interval = 30us. Its optical power output characteristic as a function of current supply at room temperature (15 ^{0}C) is shown in Fig.(6.5), illustrating that

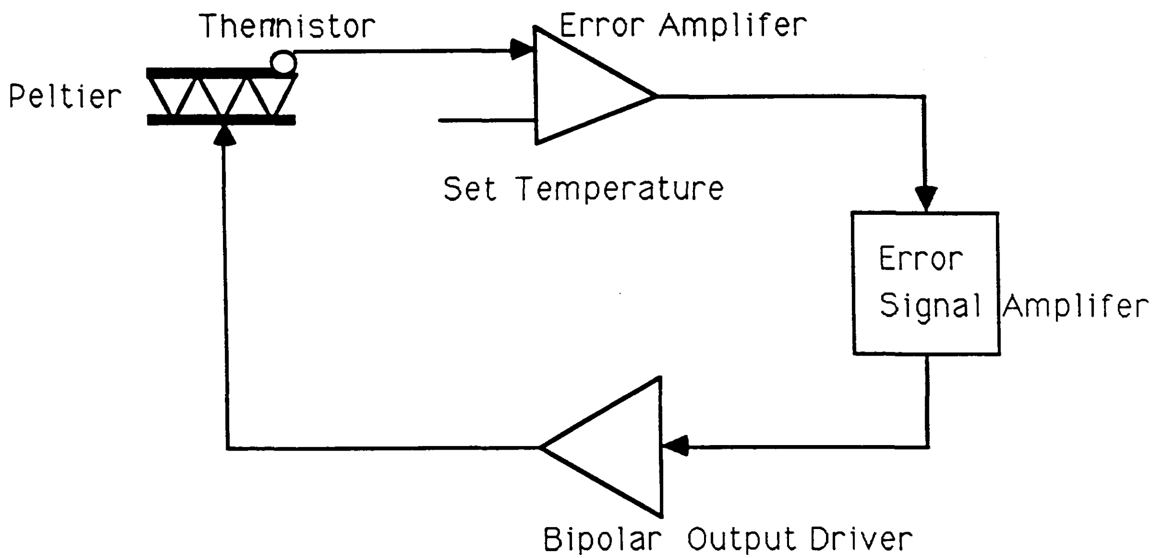

Fig.6.4 Diagram of the feedback control system.

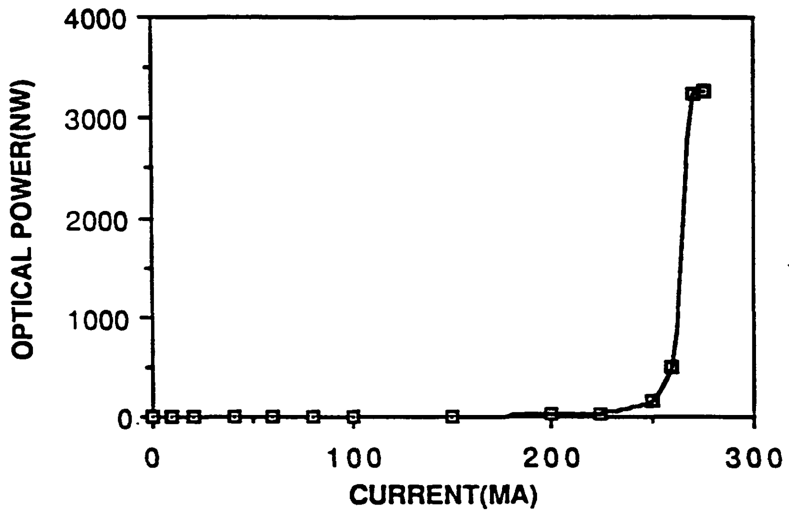

Fig.6.5 Optical output power with current supply.

the threshold current is about 240mA.

The temperature of the heatsink can be changed by adjusting a reference resistance in the controller and the threshold current as a function of heatsink temperature was obtained, shown in Fig.(6.6). The following point can be noted from this figure. The threshold current increases exponentially with heatsink temperature rise. It is quite in agreement with Eq.(2−2). In order to obtain laser action, the threshold gain must be sufficient to overcome sources of loss in the device. When temperature rises, internal absorption and scattering loss α increase significantly and quantum efficency η decreases. Clearly, the threshold current must be high enough to produce a gain which satisfies the oscillation condition.

6.3.3. Temperature dependence of emission wavelength

Fig.(6.7) shows the system for measuring the optical spectrum of the stripe (1um)laser with varying temperature of the heatsink. The optical spectrum for different temperatures was measured by changing the heatsink temperature and adjusting pulse current supply (t= 0.06, T= 30us) up to threshold value and shown in Fig.(6.8). The following points can be obtained from Fig.(6.8): threshold current increases, shown in Fig.(6.6) and emission wavelength shifts to longer wavelength as discussed in chapter 2, shown in Fig.(6.9), with temperature rise. This is because the energy band gap is getting smaller when temperature increase (Fig.(2.8)). The emission wavelength shifted an average of 0.26nm/^{0}C from the experimental result which is near the value mentioned in [51].

In Fig.(6.9), the experimental emission wavelength varies with heatsink temperature and in Fig.(2.9), the calculated emission wavelength increases with junction temperature. Therefore, the temperature drop between junction and heatsink

Fig.6.6 Temperature dependence of threshold current

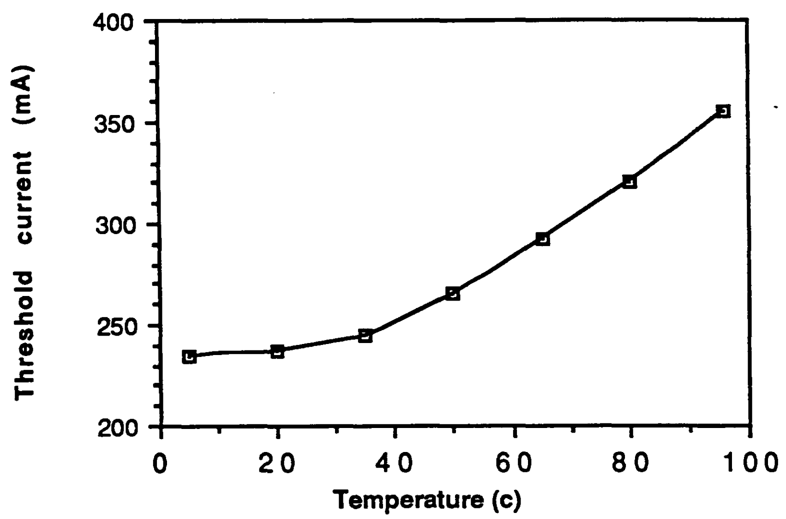

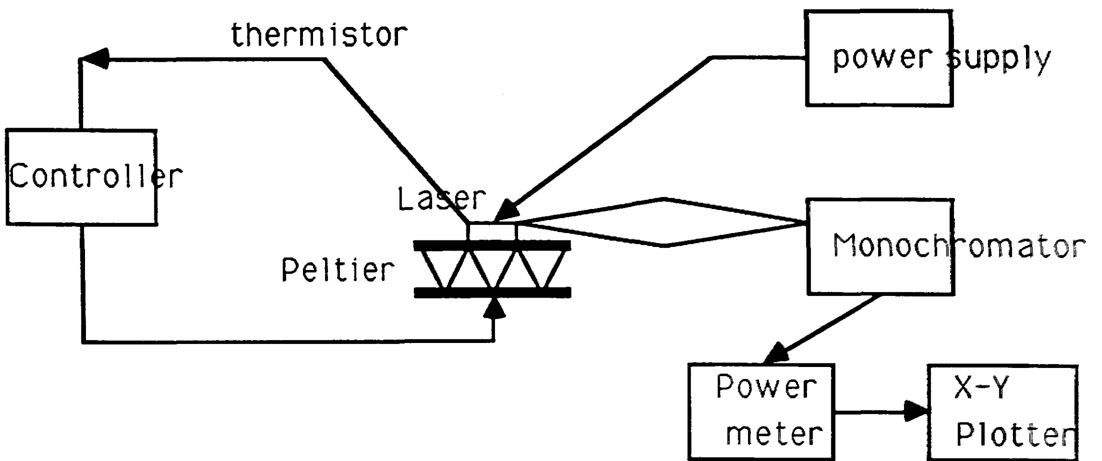

Fig.6.7 Optical spectrum measure system.

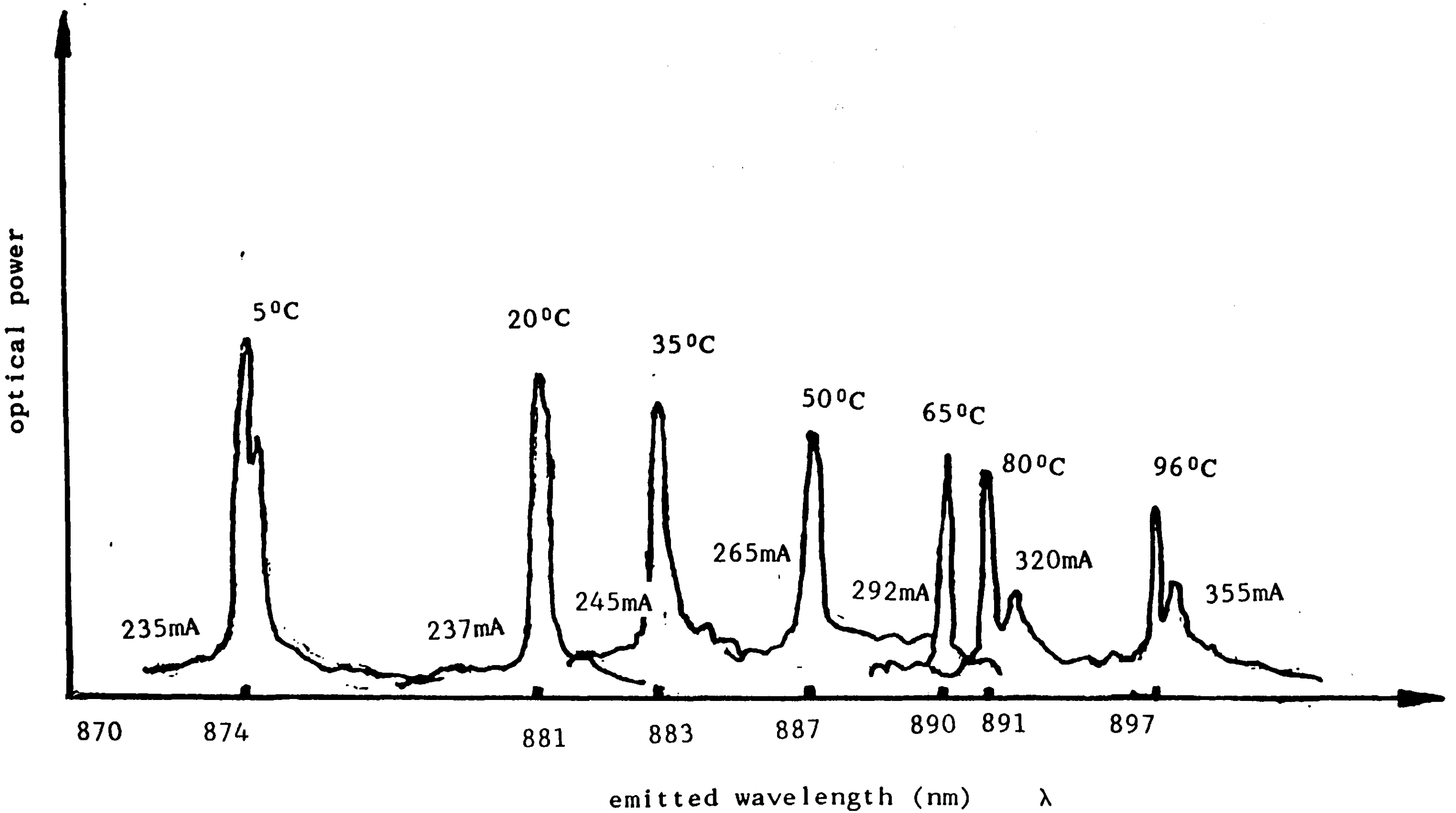

Fig.6.8 Temperature dependence of optical spectrum.

Fig.6.9 Temperature dependence of lasing wavelength

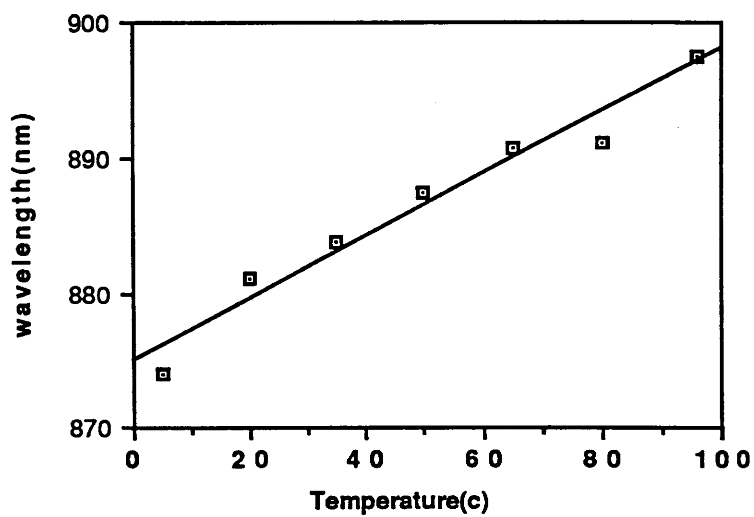

can be determined from both graphs. For threshold current I_{th}= 245mA, choosing emission wavelength λ_p= 883nm, the related heatsink temperature is 35 ^{0}C from Fig.(6.9) and using λ_p= 883nm, the related junction temperature is 72 ^{0}C from Fig.(13). As a result, the temperature drop between them is about 37 ^{0}C. Furthermore, the thermal resistance for this stripe laser is 75 ^{0}C/W [52].

6.4. Summary

The semiconductor laser temperature control system has been set up. It was used successfully to control the bottom temperature of the laser chip. The temperature control range can be 0 ^{0}C – 100 ^{0}C for this particular Peltier and maybe be reduced below 0 ^{0}C. This system is suitable for various types of laser, including ring laser, although it was only used for stripe laser in this experiment.

Two experiments concerned with temperature dependence of threshold current and lasing wavelength were demonstrated. From the result obtained, the temperature drop across the device and thermal resistance for this stripe laser have been calibrated. In addition, temperature rise actually degrades the characteristics and stability of the devices: thershold current increases and emission wavelength shifts. Therefore, it is better to run the laser at as lower temperature as possible.

CHAPTER 7

TEMPERATURE SENSING SYSTEM

7.1. Introduction

Stability of laser oscillations is improved with increased heat transfer away from the junction, which may be achieved using the laser temperature system described in chapter 6. The controller is driven by a thermistor placed near a laser chip. This will result in two problems: firstly, the large size of the thermistor, compared with the laser chip dimension, introduces big error in temperature sensing and secondly, it does not indicate the temperature of the active layer of the laser, placed near its top surface. So a very small temperature sensor which can indicate the top temperature of the laser is essential.

For this purpose, a small Al– Au thermocouple has been successfully investigated, and will be presented in section 2. The fabrication of a broad area laser with an additional thermocouple pad has been carried out, which will be demonstrated in section 4. In section 5, a final measurement system will be described. The experimental results will be presented and discussed in section 6 and will be concluded in the last section.

7.2. Investigation of Al– Au thermocouple

The thermocouple is based on Seebeck effect that is the other sort of thermoelectric effect. Consider a conduction path consisting of two different materials a and b, as shown in Fig.(7.1). If the two junctions are at different temperature, this will produce a voltage difference ΔV between them, which is proportional to temperature difference ΔT:

$$\Delta V = \alpha \Delta T$$

where α is called Seeback coefficient. Therefore, the temperature on one junction can be obtained if the voltage difference is measured and the temperature on the other junction is considered as a reference.

The electronic industry often uses either gold or aluminium connecting wires. The possibility of using both materials to form a small thermocouple has been successfully demonstrated. The thermocouples (Fig.(7.2)) used small diameter (25um) Al and Au wires or evaporated films. In the first case, the wires are bonded onto a gold dot on the top surface of a silicon chip, by using a Model– 4123 ultra– sonic bonder, shown in Fig.(7.3), for the purpose of checking if it is possible to form a thermocouple on the top of the laser. In the second case, the evaporated Al–Au films are connected with Al and Au wires respectively to the output circuit, to check if it is possible to measure the temperature on the bottom of the laser properly.

The above thermocouples have similar thermoelectric properties and their voltage versus temperature characteristics are presented in Fig.(7.4). The characteristics are linear with a slope of about 3.5uV/^{0}C and cross 0v at room temperature, which means the voltage will change 3.5uv when temperature increases 1 degree centigrade. As a result, Fig.(7.4) can be use to calibrate the temperature

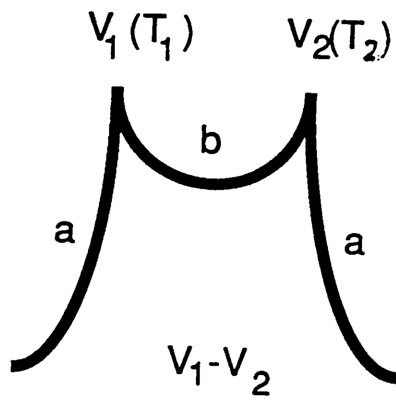

Fig.7.1 Diagram of Seeback effect.

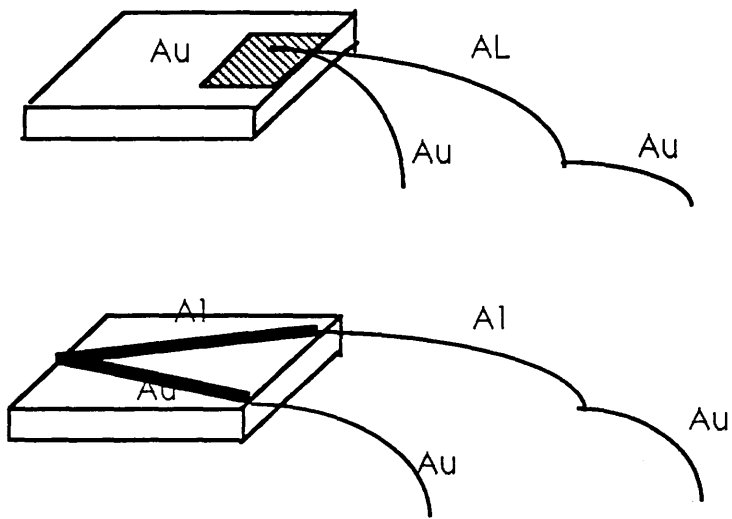

Fig.7.2 Investigation of Al-Au thermocouple.

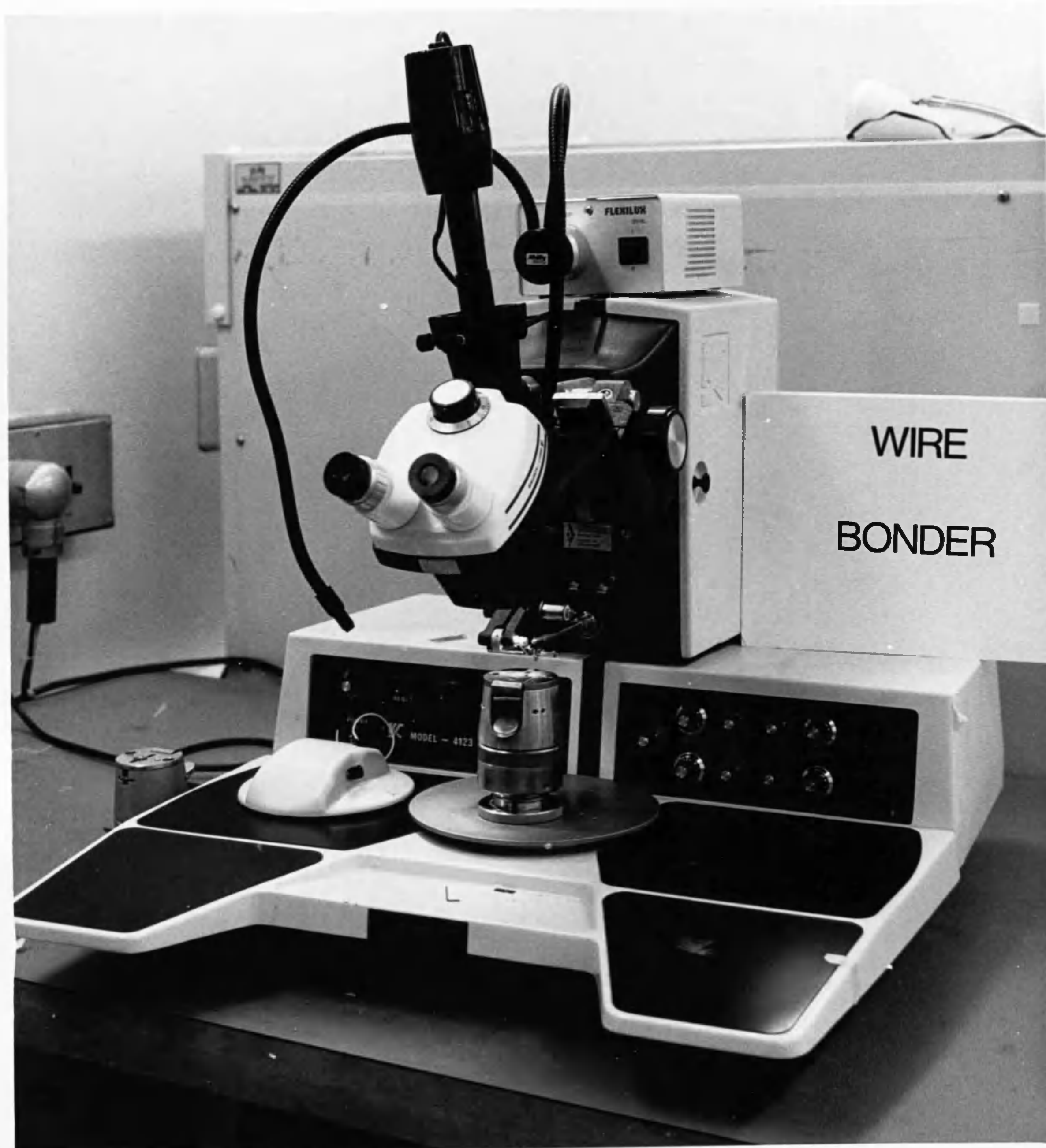

Fig.7.3 Model-4123 Ultra-Sonic Bonder.

Fog.7.4 Thermoelectric voltage vs temperature

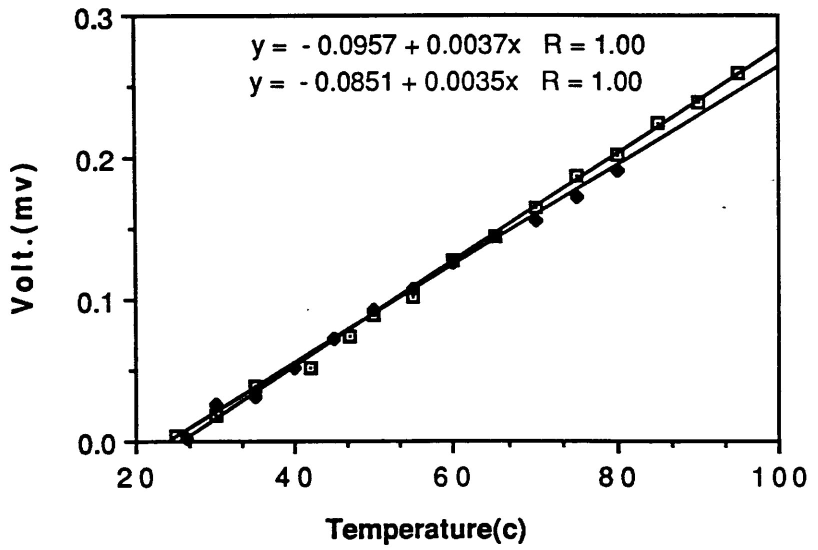

when the voltage of the thermocouple is measured.

7.3. Production of a broad area laser with thermocouple pad

It was found necessary to use an electrically– insulated bonding pad on which to locate the thermocouple when measuring the temperature of the top surface of a broad area laser chip.

The fabrication process for producing a broad area laser with thermocouple pad structure shown in Fig.(7.5), which is insulated from power supply pad, has three main steps:

(1) surface preparation (clean);

(2) photoresist pattern;

(3) evaporation.

The properties of a device are critically dependent on the quality of each step, especially evaporation. The first two steps were carried out in clean room which is equipped with filtered reduced osmosis water, analar grade solvents, ultrasonic baths, filtered nitrogen and mask aligner. The third was done in a Model 12E3/1526 evaporator, shown in Fig(7.6).

The fabrication process is as follows:

(1) *surface preparation*

a. removal contaminants by organic solvents;

(i) methanol, 15sec, rinse, for precleaning and drying the sample;

(ii) trichloroethylene, 5min.+ u/s (ultrasonic agitation), to remove

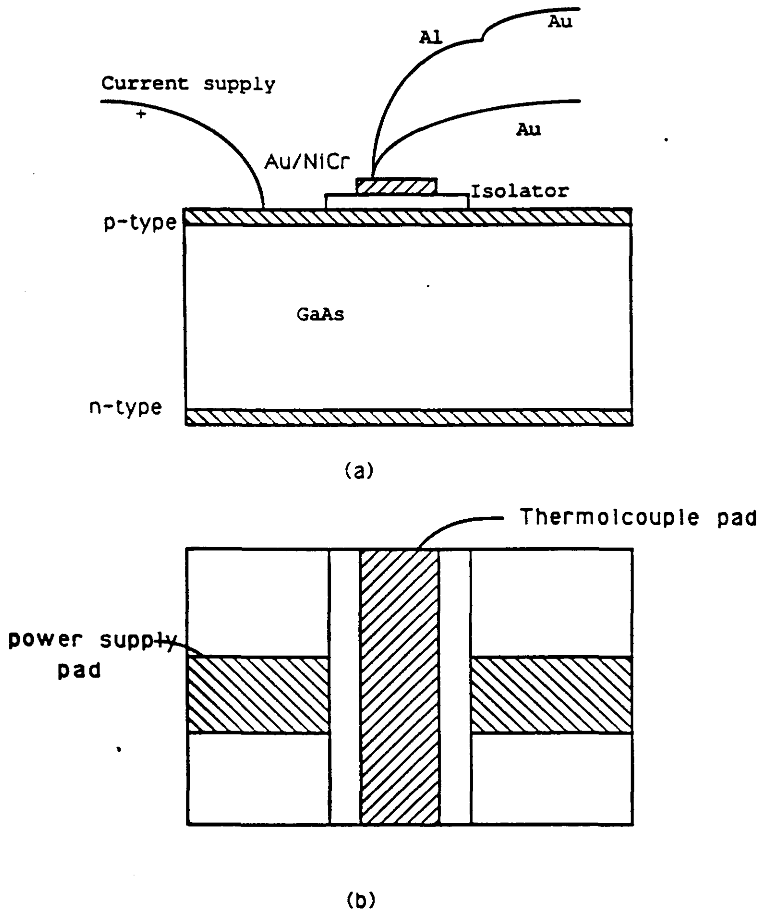

Fig.7.5 a) Cross section and b) top view of a broad area laser device with thermocouple pad.

Fig.7.6 Model-12E3/1526 Evaporator.

contaminants (e.g. grease);

(iii) methanol, 30sec.+ u/s, to dissolves trichloroethlene;

(iv) acetone, 5min. u/s, 2−3 changes;

(v) methanol, 5min. u/s, 2 changes;

(vi) reduced osmosis water(R.O.water), 5min. u/s, 2 changes;

b. oxide reduction for GaAs

(i) 30% NH_4OH : R.O.water – 1:1, 5min., to reduce oxide;

(ii) R.O. water, 2min., rinse;

(iii)IPA, 5min., rinse, 2 changes;

(iv) blow dry with N_2.

(2) *first photoresist pattering*

a. photoresist coating

(i) putting the sample in cabinet for drying, 2min.;

(ii) placing the sample on spinner chuck and then spinning at 8000rpm, 20sec, for cleaning;

(iii) deposition of the AZ1350J photoresist (positive);

(iv) spinning at 4000rpm, 40 sec.;

(v) baking photoresist in oven at 75 ^{0}C, 15min.;

b. exposure with a Mask Aligner, 6 sec.

c. developing of photoresist

(i) chlorobenzene, soak, 15min., to modify the surface, which will result in

an undercut profile of the further developed resist;

(ii) blow dry with N_2;

(iii) development, developer : R.D.water – 1:1, about 1 min.;

(iv) R.O.water, rinse;

(v) blow dry with N_2;

(vi) checking a quality of the pattern under a microscope. Unsatisfactory pattern could easily be removed by rinsing the sample in acetone, methanol and R.O.water;

(vii) etching of GaAs , 1ml potassium chlorate solution ($KClO_3$ 10g + H_2O 100ml) : 50ml HCl;

(3) <u>*first evaporation* of the contacts *for power supply pad (p–type contact)*</u>

a. prior to loading of the sample, bell jar of the evaporator is cleaned of metal with a mixture of HCl:Nitric acid –3:1, then rinsing with water and IPA, baking for 30min. in a vaccum over at 12°C;

b. pumping down to 2×10^{-2} torr atmosphere by a rotary pump, shown in Fig.(7.7);

c. switching on diffusion pump to 5×10^{-6} torr pressure;

d. R.F.sputter cleaning in Ar atmosphere at a presure of 10^{-4} torr, 100W, for 15min.;

e. slow evaporation at a rate of 0.2nm/s of subsequent layers of Au (30nm), Zn (30nm) and Au (200nm). The thickness of the material was monitored using an Intellemetrics Thickness Monitor (Model– IL100). The system uses a crystal oscillator at a frequency depending on evaporated materal thickness; and is calibrated by specifying the material properties of the metal being evaporated;

f. cooling down for 40min and removing the sample from the vacuum system;

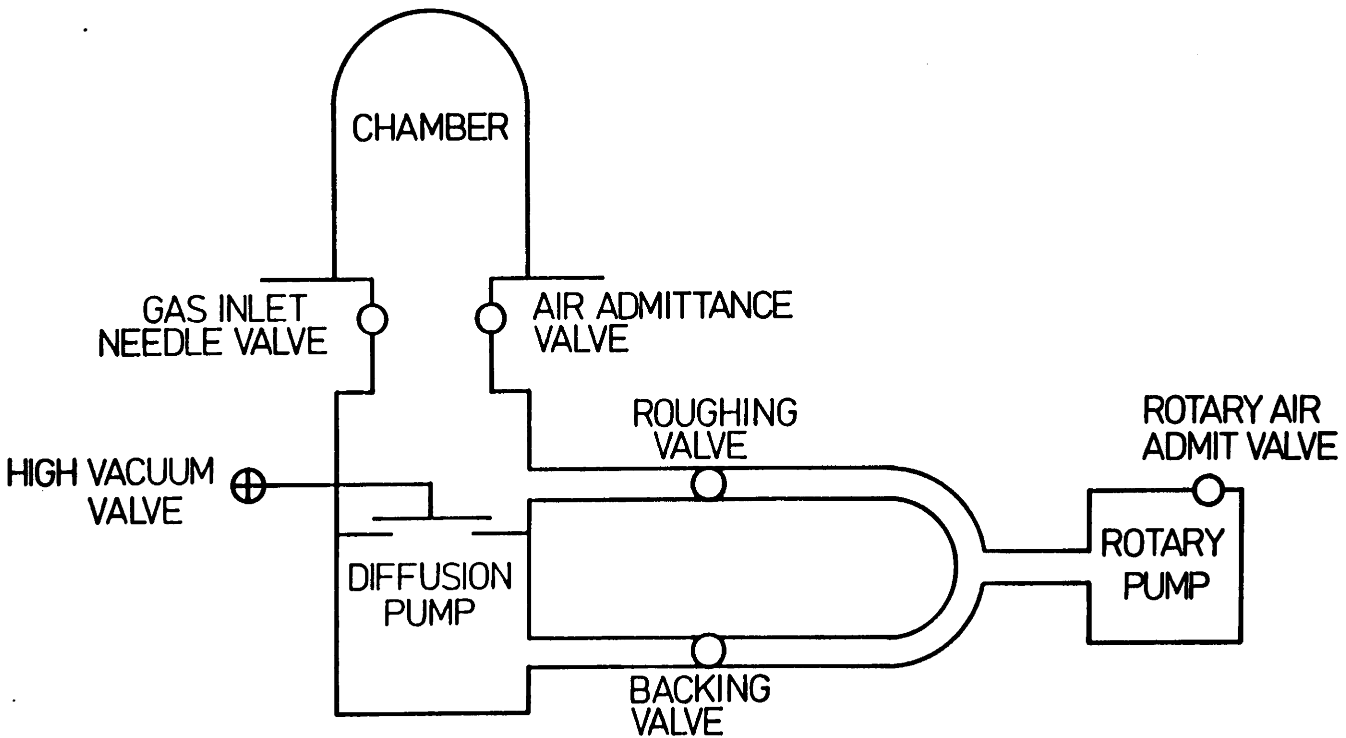

Fig.7.7 Schematic diagram of model-12E3/1526 Evaporator.

(4) *lift off*

a. removing unwanted metal which lay on the top of photoresist with acetone about 1min. with 1sec. u/s agitation;

b. checking the quality of deposited metal under microscope;

(5) annealing

annealing of the sample in an annealing oven, shown in Fig.(7. 8), 400 ^{0}C, 10sec.under Ar atmosphere for getting a good ohmic contact;

(6) *second photoresist patterning*

making pattern for SiO_2 insulator, same process as in (2);

(7) *second evatoration* of the insulating *SiO_2*

as in (3), very slow evaporation of SiO_2 up to 100nm thick layer, cooling the system down for 20min.and continuation of evaporation up to 200nm thick layer;

(8) *lift off*, as in (4);

(9) *third photoresist patterning*

producing a pattern for thermocouple pad, as in (2);

(10) *third evaporation*

evaporation of NiCr (50nm) and Au (200nm) for thermocouple pad which is insulated from power supply pad, as in (3);

(11) *lift off*, as in (4);

Fig.7.8 Annealing machine.

(12) *annealing*, as in (5);

(13) *back polishing of the sample*

reducing the thickness of the sample to 100um. This was a ccomplished with a polishing of the back surface of the GaAs sample using alumina powder (12.5um) and water mixture. The sample thickness was measured with clock gauge (accurate to 2um);

(14) *fourth evaporation* for n-type ohmic contact

evaporation of the subsequent layers of Ge (50nm), Au (60nm), Ni (30nm) and Au (200nm) on the back of the sample for producing n-type ohmic contact, as in (3);

(15) *annealing*, as in (5);

(16) *sample cleaving*

the sample was scribed using a scribing maching, shown in Fig.(7.9) and cleaved into a small chip (400um×400um);

7.5. Temperature measurement system

The temperature sensing system is shown in Fig.(7.10) and Fig.(7.11). It is connected to a temperature control system as described in chapter 6. A laser chip is mounted by using conductive epoxy onto a metal block which is placed on the top of a Peltier cooling device. The Peltier is epoxied onto an I-C header. Next to the laser chip there is a thermistor (as decribed before) which will drive the temperature controller. The temperatures are sensed using Al-Au thermocouples. The first one senses the temperature of a thermocouple pad placed near laser junction. The

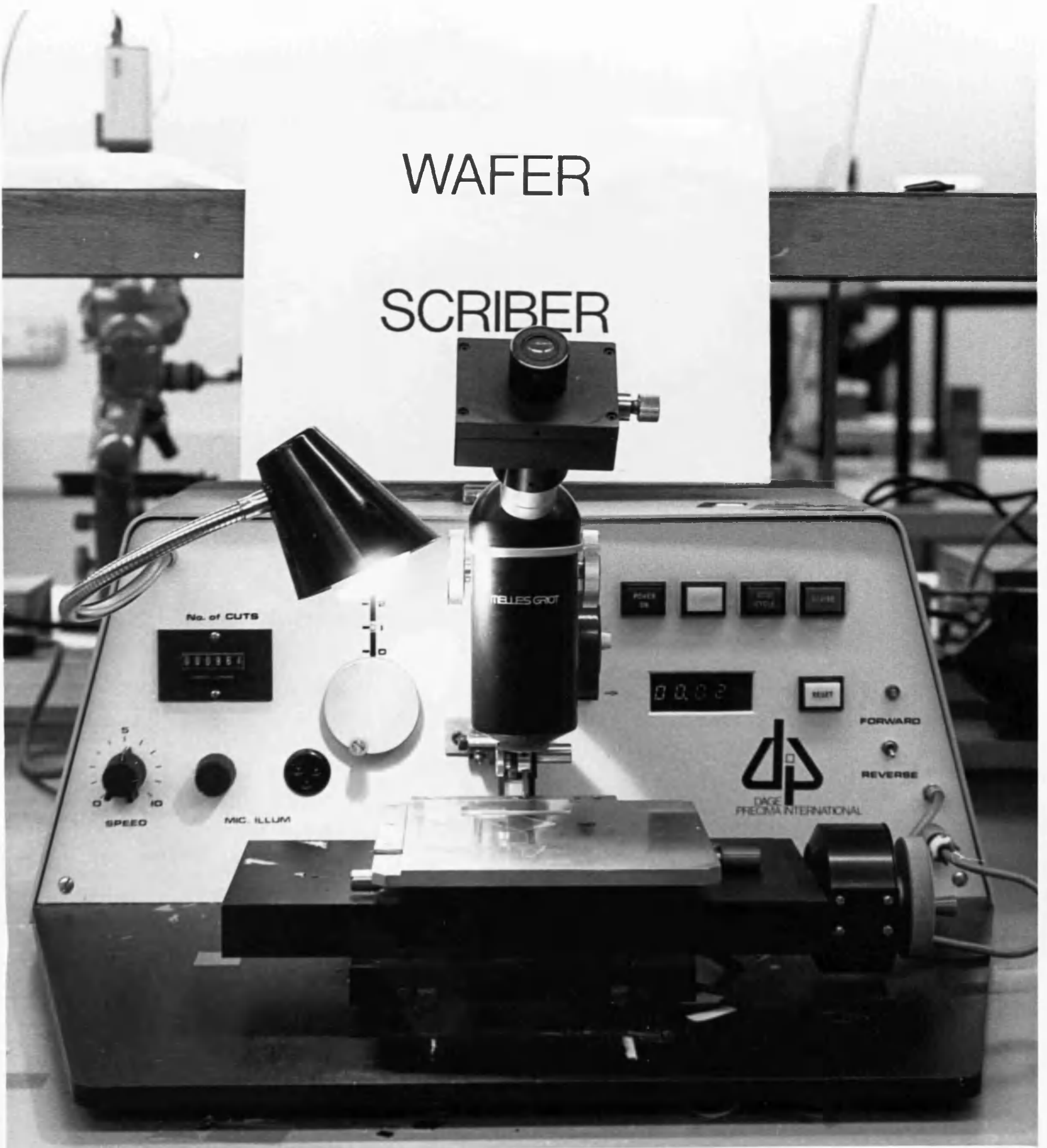

Fig.7.9 Scribing machine.

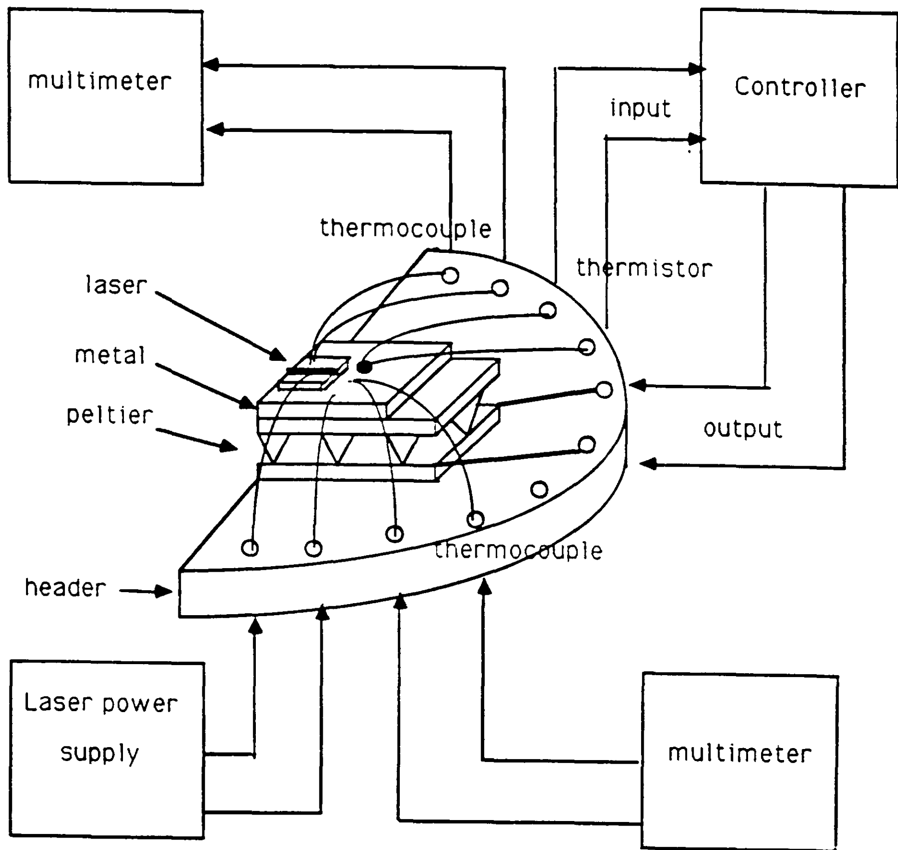

Fig.7.10 Temperature sensing system.

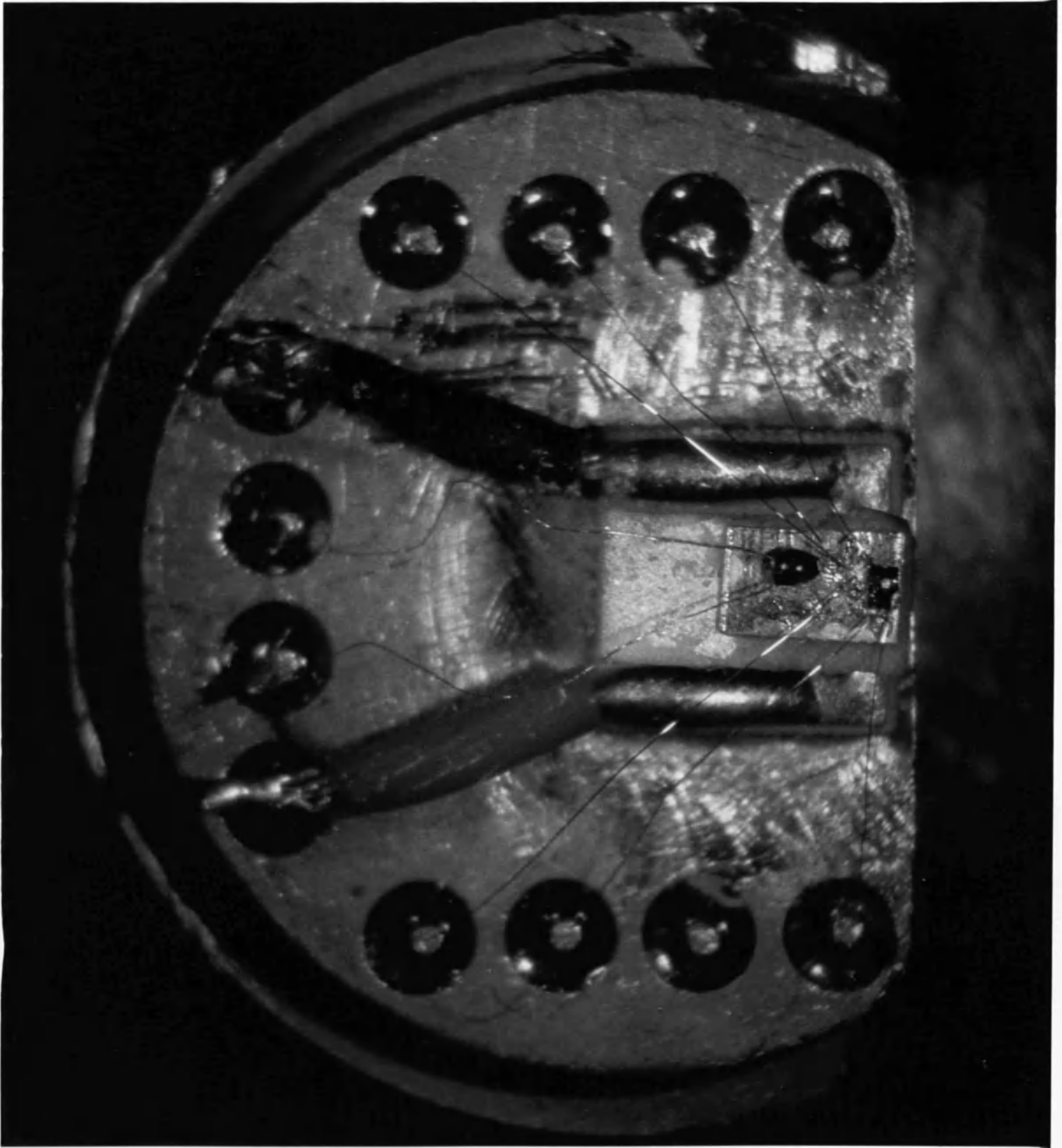

Fig.7.11 Temperature sensing system.

second thermocouple senses the temperature of the bottom of the sample (approximately heatsink temperature).

7.6 Measurement and result discussion

The purpose of this experiment is to check the possibility of producing a thermocouple to measure the temperature on the top and bottom of the laser chip. For some reason, in this experiment, the thermocouple was only bonded on the point which is 100um away from the junction, shown in Fig.(7.12).

The laser was pumped by CW current supply. The voltage (V_d) aross the laser diode and two thermoelectric-voltage were measured by 7045 multimeters. The temperatures Ta and Tb can be obtained from the thermoelectric-voltage measured by using the calibration curve in Fig.(7.4). The temperature difference between top, T_a, and bottom, T_b, vs. CW current supply are calibrated and presented in Fig.(7.13). Temperature drops ($T_a - T_b$) under certain current are nearly the same for various bottom temperature T_b kept by Peltier cooler. However, the current can not be increased over 30mA because the pumping capacity of the Peltier used is too small (0.32mW). The temperature difference between top of junction T_t and thermocouple T_a can be estimated from the isotherm diagrams,usually 80% of the total temperature drop. For example, I=25mA, V_d=4.25V, T_b=17 °C, T_a=23.5 °C, the temperature on the top of junction is approximately 29.4 °C. As a result, the temperature drop between top of the junction and between ($T_t - T_b$) is about 12.43 °C. The thermal resistance of this broad area laser can be obtained:

$$R_{th} = \frac{T_t - T_b}{I \times V_d} = 116.9\,^{\circ}C/W$$

Because T_t was estimated very approximately, the R_{th} obtained is not a good

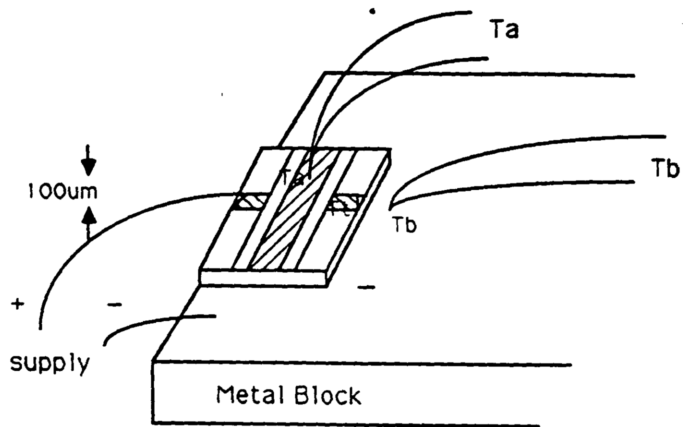

Fig.7.12 Zoom picture of temperature sensing system.

Fig.7.13 temperature difference (Ta-Tb) vs current supply

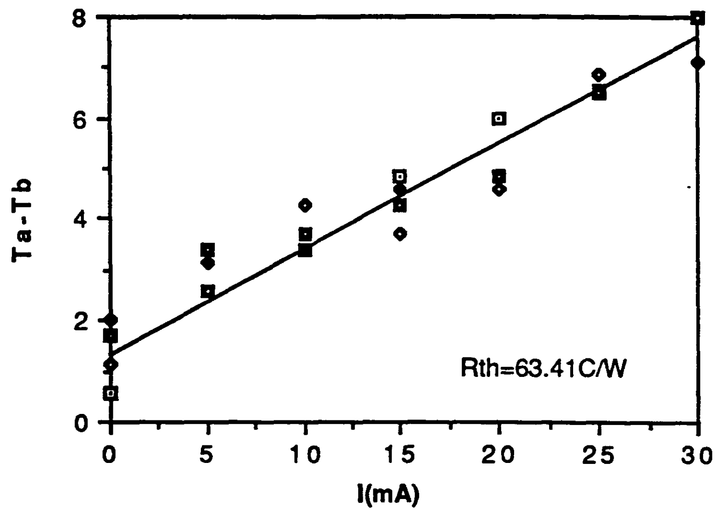

result. The result just shows that it is possible to use the Al– Au thermocouple as a temperature indicator.

7.7. Summary

The small Al– Au thermocouple has been investigated and shown promise as a temperature sensor. The temperature drop across the substrate has been obtained and the thermal resistance for this particular laser is 116.9^{0}C/W. The thermocouple must be attached onto an electrically– insulated bonding pad. The bonding process must be undertaken carefully, as it is easy to damage the insulated layer and ohmic contact layer. In this experiment, the thermocouple only was produced on the side of top surface. However, it can be clearly found that it is possible to make a thermocouple for measuring directly the temperature on the top of junction and bottom of the laser. If this thermocouple is used as a sensor to drive the controller, the junction temperature of a laser will be possibly controlled more directly.

CHAPTER 8

CONCLUSION

8.1 Conclusion

This work has dealt with the theoretical analysis and thermal measurement of temperature distributions in semiconductor ring and stripe lasers, improvement of the laser temperature control system and study of a laser temperature sensing system.

The theoretical thermal modelling of the ring laser device was based on the finite difference technique. Two thermal models have been set up — ring laser substrate and lasing rib models. The temperature distributions in them have been sucessfully obtained which fit the experimental device fairly well, although a cylindrical—symmetry model was used which assumed that all the heat was considered to be transferred to the heatsink. For simplicity, no convection or radiation have been taken into account. The results obtained indicate that for smaller rings and narrower ribs, temperatures rise and the increase in the thermal resistance of the laser is more severe. Furthermore, the drop in temperature in the sustrate is concentrated beneath the rib. Finally, more attention should be paid to the influence of the thermal behaviour imposed by the lasing rib.

The simulation results suggest that in a successful operation of the ring laser for lasing the following factors have to be considered:

(1) shallower and wider sandwich rib structure;

(2) larger diameter laser ring (for 100um diameter, if rib width>6um, R_{th}<100 °C/W);

(3) lower threshold current;

(4) pulse operation(although only CW has been analysed);

(5) lower heatsink temperature;

(6) sample placed up side down (i.e. top surface of the device attached on the heatsink, allowing the heat generated in the junction to be transferred to the heatsink directly rather than passing through the substrate);

The infrared thermal image scanning technique has been utilized to explore the surface temperature distribution of the ring laser. The thermal maps taken from RM−10 infrared image scanner show the surface temperature distribution so clearly and directly. Although the scanner can not provide very good quantitative results which could be readily used to compare with the theoretical results, mainly due to low resolution of the apparatus(10um), it can still give a fair qualitative assessment of the thermal behaviour of a ring laser.

The semiconductor temperature control system which was driven by a temperature sensor — thermistor has been set up. Two experiments which were concerned with the temperature dependence of the threshold current and the lasing wavelength of a stripe laser were demonstrated by using this system to control the temperature of the heatsink. Two points can be drawn from the experimental results: (1) temperature rise strongly affects the characteristics and stability of the device, e.g. such a rise causes an increase in the threshold current and a shift in emitted wavelength; (2) temperature drop ΔT between the top and the bottom of the laser and the thermal resistance of the laser has been calibrated by using both the experimental and theoretical results.

The final part of this work was about the investigation of a miniature

thermocouple which could measure the temperature on the top of the laser device directly. The broad area laser with a electrially— insulated bonding pad on the top of the laser has been fabricated and the thermocouple has been formed by Al— Au small diameter wire attached to the bonding pad. The temperature drop across the device has been measured by two thermocoples which were bonded onto the top and near the bottom of the laser chip. Although the thermocouple did not give an accurate indication of the temperature distribution, it is shown however that it can be used as a temperature sensor in driving the temperature control system.

8.2 Suggestions for further work

Further investigations are recommended as follows:

(1) setting up a theoretical model in which the thermal behaviour of the substrate and the lasing rib are taken into consideration at the same time and compared with the results above;

(2) investigation into the thermal transient problem of the ring laser. It is more practical as at the monment the ring laser only can lase under pulse operation;

(3) improvement of the temperature sensing system and to design a new controller circuit which can be driven by the thermocouple.

(4) designing a new ring laser which has less etched rib and charasterics its thermal behaviour. This laser can reduce the thermal effect imposed by lasing rib as discussed in chapter 4;

(5) running the lasers on a heatsink cooled by liquid nitrogen to obtain CW operation.

REFERENCE

[1] PANISH,M.B.
Heterostructure injection lasers, Proc. IEEE, 64, 1512–1540, (1976).

[2] HALL,R.N., FENNER,G.E., KINGSLEY,J.D., AND CARLSON,R.O.
Coherent light emission from GaAs junctions, Phys.Rev.Lett., 9, 366–368, (1962).

[3] NATHAN,M.I., DUMKE,W.P., BURNS,G., DILL,F.H., AND LASHER,G.J.
Stimulated emission of radiation from GaAs p–n junctions, Appl.Phys.lett., 1, 62–64, (1962).

[4] QUIST,T.M., REDIKER,R.H., KEYES,R.J., KRAG,W.E. AND ZEIGER,H.J.
Semiconductor maser of GaAs, Appl.Phys.Lett., 1, 91–92, (1962).

[5] HOLINYAK,N. AND BEVACQUA,S.F.
Coherent (visible) light emission from GaAsP junctions, Appl.Phys.Lett., 1, 82–83, (1962).

[6] LIAO,A.H. AND WONG,S.
Semiconductor injection lasers with a circular resonator, Appl.Phys.Lett, 36, 801–803, (1980).

[7] JEZIERSKI,A.F. AND LAYBOURN,P.J.R.
Integrated semiconductor ring lasers, IEE Proc., Pt.J, (1987).

[8] WONG,S.,CHOI,H.K. AND FATTAH,I.H.A.
Studies of semiconductor lasers of the interferometric and ring types, IEEE J.Q.E., 18, 610–617, (1982).

[9] AUSTIN,M.W.
GaAs/GaAlAs curved rib waveguides, IEEE J.Q.E., 18, 795–800, (1982).

[10] THOMPSON,G.H.B.
Physics of semiconductor laser devices, New York, 1980, John Wiley & Sons

[11] HARTMAN,R.
Reliability of DH GaAs lasers at elevated temperature, Appl.Phys.Lett.,26, 239–241, (1972)

[12] ETTENBERG,M., NUESE,C.J. AND KRESSEL,H.
The temperature dependence of threshold current for double heterojunction lasers, J.Appl.Phys., 50, 2949–2950, (1979).

[13] HESS,K., VOJAK,B.A. AND CHIN,R.
Temperature dependence of threshold current for a QW heterostructure laser, 23, 585–589,(1980).

[14] JUNG,H., GOBEL,E., ROMANEK,K.M. AND PILKUHN,M.H.
Temperature dependence of optical gain spectra in GaInAsP/InP double heterustructure lasers, Appl.Phys.Lett., 39, 468–470, (1981).

[15] DYMENT,J.C., CHENG,Y.C. AND SPRINGTHORPE,A.J.
Temperature dependence of spontaneous peak wavelength in GaAs and GaAlAs electroluminescent layers, J.Appl.Phys., 46, 1739–1743, (1975).

[16] KITAMURA,M., YAMAGLCHI,M. AND MITO,I.
Low–threshold and high–temperature single–longitudinal mode operation of 1.55um–band DFB–DC–PBH LDs, Electr.lett., 20, 595–596, (1984).

[17] CHINONE,N.,ITO,R. AND NAKADA,O.
Limitation of power outputs from continuesly operating GaAs–GaAlAs double heterostructure lasers, J.Appl.Phys., 47, 785–786, (1976).

[18] GOOCH,C.H.
Gallium Arsenide laser, New York, 1969, Macmillan Publishing Co..

[19] JOYCE,W.B. AND DIXON,R.W.
Thermal resistance of stripe lasers, J.Appl.Phys, 46, 855–862, (1975).

[20] NEWMAN,D.H.
Thermal resistance models for proton–isolated DH lasers, IEE Solid–state & Electron Device, 2, 41–46, (1978).

[21] DUKA,E.
Thermal resistance and temperature distribution in DH lasers: calculation and experimental results, IEEE J.Q.E., 15, 812–817, (1979).

[22] BUUS,J.
A model for the state properties of DH lasers, IEEE J.Q.E. 15, 734–749, (1979).

[23] LAFF,R.A.
Thermal performance and limitations of silicon substrate packaged GaAs laser arrays, Appl.Opt., 17, 778–784, (1978).

[24] NAKWASKI,W.
Simple formulas giving temperature profiles in active layer of stripe–geometry laser diode without oxide barriers, Electr.lett., 19, 368–370, (1983).

[25] NAKWASKI,W.
Dynamical thermal properties of stripe–geometry laser diodes, IEE Proc., 131, 49–102, (1984).

[26] CORTES,C.M.
efects of contact resitance and dopant concentration in metal–semiconductor thermoelectric coolers, IEEE E.D., 27, 521–525, (1980).

[27] HAVA,S.and HONSPERHER,R.G.
Monolithically peltier cooled laser diodes, J.Lightwave.Tech., 2, 175–180, (1984).

[28] CASEY,H.C. AND PANISH,M.B.
Heterostructure lasers, Part A, New York, 1978, Academic Press.

[29] SZE,S.M.

Semiconductor device, New York, 1985, John Wiley & Sons.

[30] ETTENBERG,M., NUESE,C.J. AND KRESSEL,H.

The temperature dependence of threshold current for double heterojunction lasers, J.Appl.Phys., 50, 2949–2950, (1979).

[31] BLAKEMORE,J.S.

Semiconductor and other major properties of GaAs, J.Appl.Phys., 53, R123–181, (1982).

[32] DYMENT,J.C., CHENG,Y.C. AND SPRINGTHORPE,A.J.

Temperature dependence of spontaneous peak wavelength in GaAs and GaAlAs electroluminescent layers, J.Appl.Phys., 46, 1739–1743, (1975).

[33] WALKER,R.G. AND WILKINSON,C.D.W.

Integrated optical waveguiding structures made by silver ion–exchange in glass. 2: Directional coupler and bends, Appl.Opt., 22, 1929–1936, (1983).

[34] WALKER,R.G. AND WILKINSON,C.D.W.

Integrated optical waveguiding structures made by silver ion–exchange in glass. Appl.Opt., 22, 1029–1035, (1983).

[35] GOELL,J.E. AND STANDLEY,R.D.

Loss mechanicsms in dielectric waveguides, Bell syst.Tech.J.,3445–3448, (1969).

[36] CHAPMAN,A.J.

Fundamentals of heat transfer, New York, 1987, Macmillan Publishing Co..

[37] RAMAMURTHY,V. AND KAKATI,D.

Computer–aided thermal analysis of reverse–biased PIN diodes, IEE Proc., Pt.I, 3, 82–86, (1984).

[38] RAMAMURTHY,V., CHATURVEDI,P.K. AND KAKATI,D.

Temperature rise in PIN diodes–A computer–aided analysis, Solid–State Elect., 24, 445–453, 1981

[39] DUSINBERRE,G.M.

Heat transfer calculations by finite differences, Pennsylvania, 1960, International Textbook Co..

[40] CHAPMAN,A.J.

Fundamentals of heat transfer, New York, 1987, Macmillan Publishing Co..

[41] STARK,A.

Introduction to numerical methods, New York, 1970, Macmillan Poblishing Co..

[42] SCRATON,R.E.

Basic Numerical methods, London, 1984, Edward Arnold.

[43] JAMIESON,M.J.

Elementray numerical methods, Britain, 1983, Biddles Ltd..

[44] CASEY.H.C.

Heterostructure lasers, Part B, New York, 1978, Academic Press.

[45] WRIGHT,H.C.

Infrared techniques, Oxford, 1973, Clarendon Press.

[46] HOUGHTON,J.T. AND SMITH,S.D.

Infrared Physiscs, Oxford, 1966, Clarendon Press.

[47] WEBB,P.W.

Measurement of thermal transients in semiconductor power devices and circuits, IEE Proc. Pt.I, 130, 153–159, (1983).

[48] PETERMAN,A.P.

Thermophysics of Si power transistors, Texas instruments internal report, 99, 278–298, (1966).

[49] LIDBACK,C.A.

On the determination of infrared emissivity of semiconductor devices, 3rd biennial conference on infrared information exchange proceedings, Aug.1969, Missouri, USA.

[50] JOHNSON,L.A.

Controlling temperatures of diode lasers and detectors thermoelectrically, Lasers & Opt., 109–113, Apr. (1988).

[51] DYMENT,J.C., CHENG,Y.C. AND SPRINGTHORPE,A.J.

Temperature dependence of spontaneous peak wavelength in GaAs and GaAlAs electroluminescent layers, J.Appl.Phys., 46, 1739–1743, (1975).

[52] PAOLI,T.L.

A new technique for measuring the thermal impedance of junction lasers, IEEE J.Q.E., 11, 498–503, (1975).

GLASGOW
UNIVERSITY
LIBRARY